Axial capacity of piles in sand

A field investigation using distributed fibre optic sensing

Kevin Duffy

Axial capacity of piles in sand

A field investigation using distributed fibre optic sensing

Axial capacity of piles in sand

A field investigation using distributed fibre optic sensing

Dissertation

for the purpose of obtaining the degree of doctor
at Delft University of Technology
by the authority of the Rector Magnificus, Prof.dr.ir. T.H.J.J. van der Hagen,
chair of the Board for Doctorates,
to be defended publicly on Tuesday 13th May 2025 at 10:00

by

Kevin DUFFY

Master of Science in Civil, Structural and Environmental Engineering
University College Dublin, Ireland
born in Drogheda, Ireland

This dissertation has been approved by the promotors.

Composition of the doctoral committee:

Rector Magnificus	chairperson
Prof.dr. K.G. Gavin	Delft University of Technology, *promotor*
Dr.ir. M. Korff	Delft University of Technology, *copromotor*
Independent members:	
Prof.dr. P.J. Vardon	Delft University of Technology
Prof.dr. M.J.Z. Brown	University of Dundee, United Kingdom
Prof.dr. B.M. Lehane	University of Western Australia, Australia
Dr.ir. R. Spruit	Gemeente Rotterdam, The Netherlands
Prof.dr.ir. T.J. Heimovaara	Delft University of Technology, *reserve member*

Keywords: Cone penetration testing, axial pile design, pile testing, fibre optic sensing

Printed by: Gildeprint

Cover photo: Ries van Wendel de Joode

Email: k.duffy@tudelft.nl; kevinjamesduffy@gmail.com

ISBN 978-94-6384-769-8

An electronic version of this dissertation is available at
https://doi.org/10.4233/uuid:33133873-380d-4873-8643-63fe9955b632

Contents

Summary

This dissertation presents axial compressive load tests where the pile base and shaft resistances were measured with distributed fibre optic sensors. Two test sites were established: one at Amaliahaven in the port of Rotterdam, and another in Delft. At Amaliahaven, the performance of three different pile types was compared in very dense sand: driven precast, driven cast-in-situ and a screw displacement pile type known as a screw injection pile. The screw injection piles were further investigated in the medium dense sand of Delft, comparing screw injection piles installed with a removable casing to screw injection piles installed with sacrificial casings. With these tests, the influence of installation method on the axial pile capacity was examined, and the results were considered in the context of design methods which use the cone penetration test to predict the axial pile capacity.

The piles at Amaliahaven reached very high base and shaft resistances, up to 30 MPa and 600 kPa respectively. These values are nearly three times greater than limiting resistances in design standards, suggesting that limiting resistances lead to excessive conservatism in dense to very dense silica sands. On the contrary, the screw injection piles at Amaliahaven mobilised much lower base capacities than anticipated. This became the focal point for the tests at Delft, and likewise, the piles at Delft also mobilised much lower base capacities than forecasted.

The influence of different installation methods on the pile base resistance was then examined in a review of other instrumented load tests—a review extending beyond screw injection piles and to screw displacement piles overall. The analysis confirmed that the installation of a screw displacement pile leads to little soil improvement around the pile base. In other words, a screw displacement pile tends to mobilise base resistances comparable to a soil-replacing (bored) pile rather than a soil-displacing (driven) pile.

A larger database of both instrumented and uninstrumented test records was then used to consider the implications of these findings. To do so, the base, shaft, and total capacity of each pile was compared to design methods from Belgium, France, the Netherlands and the USA. These design methods tended to overestimate the pile base contribution yet underestimate the shaft contribution, especially at cone resistances greater than the limiting resistances. A best-fit to the measured base and shaft resistances gave the best agreement on average to the measured total capacity. Nevertheless, there is room for improvement with this new formulation, particularly for the shaft resistance of screw displacement piles with an enlarged displacement body.

From the findings in this dissertation, a series of adjustments have been proposed for the Dutch pile design standard NEN 9997-1. The tests presented in the dissertation are also the first set of pile tests to be incorporated into the Dutch national pile test database, with the findings also being used to refine and optimise quay wall design across the port of Rotterdam.

Samenvatting

Dit proefschrift beschrijft axiale drukbelastingsproeven waarbij de paalpunt- en schachtweerstanden werden gemeten door gedistribueerde glasvezelsensoren. Er zijn twee proeflocaties opgezet: één in Amaliahaven in de haven van Rotterdam en één in Delft. In Amaliahaven werden de draagvermogens van drie paaltypen vergeleken in zeer dicht zand: (i) heipalen, (ii) vibropalen en (iii) schroefinjectiepalen. Deze schroefinjectiepalen werden verder onderzocht in dicht zand in Delft. Alle resultaten werden beschouwd in de context van de invloed van de installatiemethode op de axial paaldraagvermogen en in de context van ontwerpmethoden die de sondering gebruiken om de draagvermogen te voorspellen.

De palen in Amaliahaven bereikten hoge punt- en schachtweerstanden, tot respectievelijk 30 MPa en 600 kPa. Deze waarden zijn bijna drie keer groter dan de limietwaarden in de ontwerpnormen. Dit suggereert dat limietwaarden leiden tot overmatig conservatisme in dicht tot zeer dicht silica zand. De schroefinjectiepalen bij Amaliahaven mobiliseerden echter veel lagere puntweerstanden dan verwacht. Dit werd het aandachtspunt voor de paalproeven in Delft. De metingen van Delft lieten wederom zien dat schroefinjectiepalen veel lagere puntweerstanden mobiliseerden dan voorspeld.

De invloed van verschillende installatiemethoden op de paalpuntvermogen is vervolgens onderzocht in een review van andere geïnstrumenteerde paalproeven. Deze review focust niet alleen op schroefinjectiepalen, maar op schroefverdringingendepalen in het algemeen. De analyse bevestigde dat de installatie van een schroefverdringendepaal leidt tot weinig bodemverbetering rond de paalpunt. Met andere woorden, schroefverdringendepalen mobiliseren doorgaans puntweerstand die vergelijkbaar zijn met een grondvervangende boorpaal in plaats van een grondverdringende heipaal.

Naar aanleiding van de review is vervolgens een grotere database van zowel geïnstrumenteerde als niet-geïnstrumenteerde testgegevens gebruikt om de implicaties van deze bevindingen te overwegen. Hiervoor werden de punt, schacht en totale draagvermogen van elke paal vergeleken met ontwerpmethoden uit België, Frankrijk, Nederland en de Verenigde Staten. Het bleek dat deze ontwerpmethoden de neiging hadden om de bijdrage van de paalpunt te overschatten, maar de bijdrage van de schacht te onderschatten, vooral bij conusweerstanden die groter waren dan de limietewaarden. Een best-fit voor de gemeten punt en schacht draagvermogen bleek nauwkeuriger in zijn voorspelling van de paaldraagvermogen. Verbeteringen zijn ook voorgesteld, met name in de voorspelling van het draagvermogen van schroefverdringendepalen met een verdikt deel.

Op basis van de bevindingen in dit proefschrift is enkele aanpassingen voorgesteld voor de Nederlandse norm NEN 9997-1. De paalproeven in het proefschrift zijn ook de eerste paalproeven die zijn opgenomen in de Nederlandse nationale database voor paalproeven. De bevindingen worden tevens gebruikt om het ontwerp van kademuren in de haven van Rotterdam te optimaliseren.

Acknowledgements

I firmly believe that a PhD's quality of life is largely dependent on their support team: their supervisors, their colleagues, their friends and their family. I count myself incredibly fortunate to have all of these. It has really helped me to enjoy what I'm doing, not just the PhD itself, but in my day-to-day life in the Netherlands and beyond.

First and foremost, I'd like to extend my utmost thanks to Ken, the person who brought me here. Your unwavering support, feedback and openness have been instrumental in how I've developed both as a researcher and a person.

To Dirk, who has dedicated so much time in helping me with the pile tests, I am eternally grateful. Your friendliness and engineering brilliance is truly admirable, and it has been an honour to work with you.

Mandy, your kindness and support is also hugely appreciated, especially when the going got tough. And I know that I share this admiration with many of the students and employees at TU Delft and Deltares.

There's an infinite number of colleagues I could thank in the Geo-Engineering section and TU Delft, particularly when it came to getting quick bits of advice and socialising inside and outside work. To the colleagues I've had weekly meetings with—Fei, Fengwen, Na and Sara—it has been pleasure working with you and I look forward to our continued collaboration. I've also had the privilege to work with many Bachelors and Masters students, which has been an enjoyable and insightful experience each and every time. Thank you.

To the people outside of TU Delft who've supported my work, I am deeply appreciative of the time you have given me. I would like to extend a special thanks to Gust from Buildwise; Rodriaan and Willem from Gemeente Rotterdam; all the technicians from Deltares; and to everyone at APTS, De Klerk, Fundex, Mariteam, Plump, Vroom and the *InPAD* project partners. Your contributions have been invaluable.

Outside of TU Delft, much of my free time was spent either playing or socialising with the people of Rotterdam tag rugby, especially in the throes of the COVID-19 pandemic. I cannot thank this group enough for giving me treasured memories and friends for a lifetime. The same goes for those at bouldering, golf, frisbee and god knows what other sport I took up—thanks everyone for keeping me sane.

Also to those back in Ireland, especially my friends from Drogheda and UCD. As the popular saying goes "far away hills are green" and damn, you guys have kept the hills of Ireland a very, very luscious green.

Lastly to my girlfriend Anna and family—Mam, Dad, Conor, Dervla, Kathleen and Gerry, the extended family and the Lotz family—your love and support mean the world to me and it has shaped me into the person I am. I can only hope that I return the same and I look forward to a lifetime of shared memories with you all.

Kevin Duffy
Delft, 13th May 2025

1

Introduction

1

1.1. Introduction

For centuries, piles have played an intrinsic role in Dutch construction, enabling millions of people to live in unfavourable geological conditions. Soft clay and peat soils envelope much of the country, rendering it nearly impossible to use shallow foundations. Instead, piles are used to bypass these soft layers, transferring the building's weight to a dense sand formation deeper down. In the big cities of the western Netherlands, such as Amsterdam (Figure 1.1), this sand was deposited by rivers some tens of thousands years ago, in an geological epoch known as the Pleistocene. Because of a much smaller, looser sand layer that's often present at shallower depths, the deeper sand layer is colloquially named *de tweede zandlaag*—the second sand layer.

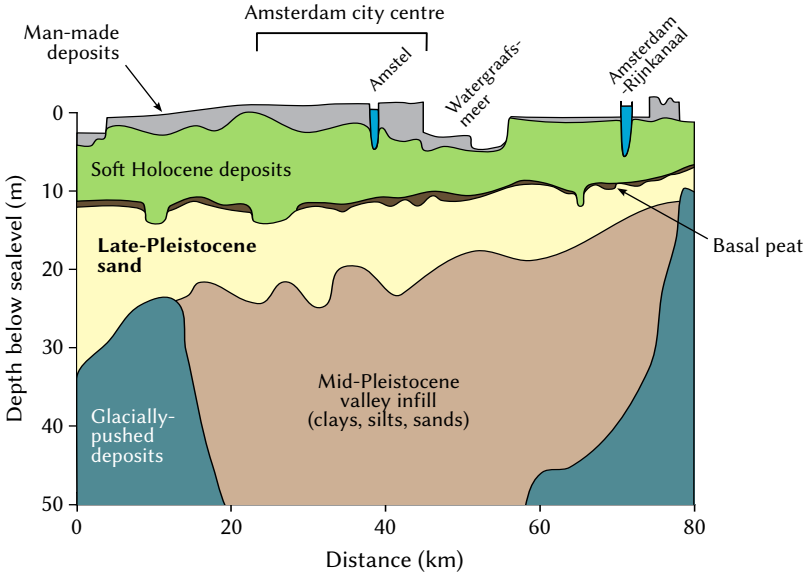

Figure 1.1: West-east cross-section of Amsterdam. Most piles go down to the top part of the late-Pleistocene sand (adapted from Schokker et al., 2015).

To get the pile down to this layer as efficiently as possible, engineers can choose from a range of installation methods. Prefabricated concrete or steel piles are common; piles that are then driven or vibrated into place on-site. Alternatively, reusable drilling tools can bore a hole into the ground (Figure 1.2), a hole that is then filled with concrete and left to harden. Whatever the installation method, the process starts a series of stress changes in the soil which affects the amount of load a pile can transfer from the overlying structure to each soil layer. For example, hammering a prefabricated pile simply pushes the soil aside, densifying the soil and increasing the stresses acting on the pile. By contrast, bored piles remove the soil directly, putting much less stress on the surrounding soil. Essentially, these two mechanisms define the upper and lower bounds of a classification spectrum, that is, a spectrum ranging from soil-displacing piles to soil-replacing piles.

Choosing whether to go for a soil-replacing pile or a soil-displacing pile (or somewhere in between) is seldom a one-size-fits-all approach. Engineers need a reliable pile, both

Figure 1.2: Installation of a screw injection pile at the Amaliahaven test site.

geotechnically and structurally speaking, without affecting the local environment or nearby buildings. The Dutch industry have been creative in meeting these challenges, with over one hundred different pile types in use across the country (SBR, 2010). This innovativeness and experience with piled foundations is highly regarded worldwide and many of the top research symposiums have taken place in the Netherlands in recent years, such as CPT'18, SW22, TISOLS2023 and ECPMG 2024. The rapid growth of offshore wind means the demand for research and development is also as high as ever, with research focussing on improving the installation efficacy of large offshore piles whilst reducing the effect of noise on marine wildlife (Kementzetzidis, 2023; Konstadinou et al., 2023; Quinten et al., 2023).

However, accelerating urbanisation in the midst of global climate change has brought the sustainability of the construction sector into question. The sector is the single largest producer of CO_2 emissions worldwide, amounting to 37 % of all global emissions (United Nations Environment Programme, 2024). Most of these emissions come from operational energy demands, although ongoing research and development is continuing to reduce this amount—engendered by numerous certifications and directives both regionally and internationally (de Klijn-Chevalerias and Javed, 2017). By comparison, little attention has been paid to a building's construction, maintenance, and end-of-life phases. During these phases, a sizeable amount of energy is sequestered in the building, otherwise known as embodied carbon.

Depending on the structures being built, foundations can contribute substantially to the CO_2 emissions produced (Sandanayake et al., 2016; Pujadas-Gispert et al., 2020). On a national level for example, around 525,000 m^3 of precast concrete piles were installed in the Netherlands in 2020 (NVAF, personal communication, 2021). Considering the emissions

from concrete production alone, this figure translates to 210 kilotonnes of CO_2—equal to the annual energy consumption of 140,000 Dutch households. Emissions from transporting and installing the foundations increase this figure even more, depending on the installation equipment and the location of the site.

Moreover, many existing foundations have already reached the end of their theoretical design lifetime. Recent failures in the quay walls along Amsterdam's historic canals have raised concerns about the reliability of the timber piles underneath (Korff et al., 2022; Hemel, 2023; Pagella et al., 2024). Furthermore, many port authorities are also seeking to readapt and reuse existing foundations to accommodate for growing ship sizes and traffic volumes (Roubos, 2019). In both scenarios, a complete infrastructural overhaul would have significant economic, environmental and social effects on the surrounding area.

Geotechnical engineers are therefore tasked with understanding how a foundation's reliability is affected by long-term loading changes and structural degradation, along with anticipating how these will change in the future. In this regards, being precise and accurate in estimating the capacity of an existing foundation is a good first step in making a targeted rehabilitation or upgrading approach.

1.2. Pile design and the need for pile testing

Design standards provide a reliable and consistent means of designing structures, albeit limiting some of the flexibility engineers may have. Since 2012, geotechnical design in the Netherlands has followed Eurocode 7, presented in NEN 9997-1 (NEN, 2017b) along with additional stipulations in the National Annex. The pile design method in NEN 9997-1 predicts the pile's capacity using measurements from the cone penetration test (CPT). A CPT is a small probe (Figure 1.3) which can infer the strength and stratigraphy of the soil by measuring the resistance acting on the cone tip q_c, the friction acting on the probe's sleeve f_s and the porewater pressure u_2 (although measuring u_2 is done somewhat sparingly in the Netherlands). With these measurements, the pile base resistance q_b and shaft resistance q_s can by inferred through the factors α_p and α_s respectively. The magnitude of α_p and α_s is dependent on both the pile type and soil type.

Crucially, a review of previous pile load tests (van Tol et al., 2013; Stoevelaar et al., 2014) concluded that the pile design method in NEN 9997-1 was too optimistic. As a result, the 2017 update of NEN 9997-1 reduced α_p by 30 % across all pile types. However, this change was met with resistance from the industry, with many believing that the update would create overly conservative designs. Essentially, these conservative designs would lead to greater financial and environmental costs, whilst also making installation of these larger piles exceedingly difficult.

Nevertheless, the review also cited the low number of fully instrumented static load tests in the database, particularly since most tests are already hamstrung by the cost and time constraints of just a single full-scale test. Indeed, piles can be tested at a smaller scale in the laboratory or even numerically simulated. Both methods have been influential in helping the mechanistic understanding of pile response, for instance, with respect to the influence of weak zones on the pile base resistance (de Lange, 2018; Tehrani et al., 2018; Yost et al., 2022) or with how persistent hammering leads to a reduction in the radial stresses acting on the pile, a phenomenon known as friction fatigue (White and Lehane, 2004; White and Bolton, 2005).

Figure 1.3: An example of a cone penetrometer (CPT) and the measurements it collects.

Yet extrapolating the results of physical models or numerical simulations to full-scale piles is confounded by a variety of factors. For example, it is difficult to scale the large deformations and dynamic effects of pile hammering, along with translating installation-induced stresses from small-scale conditions to full-scale conditions (Paik et al., 2003). Cast-in-situ piles have their own modelling obstacles, particularly with concrete casting and casing withdrawal—both of which may affect the capacity of cast-in-situ piles (Lam et al., 2015; Flynn and McCabe, 2016; Li et al., 2017; Siegel et al., 2019; Sharif, 2024). Ultimately, harmonising mechanistic insights from laboratory and numerical models with field test measurements is necessary for developing an efficient design method.

1.3. Distributed fibre optic sensing (DFOS)

To determine a pile's base and shaft resistance during a pile load test, the strain in the pile needs to be measured. Luckily, strain can be measured in many different ways (Flynn and McCabe, 2022): such as mechanical methods (e.g. telltales), electrical methods (resistivity or vibrating wire gauges) or fibre optic methods (Faby-Perot sensors or Fibre Bragg Gratings). Most of these gauges are called 'point sensors', since they give a single value of strain between two fixed points, separated by a distance ranging from a few millimetres to a couple of metres.

Yet point sensors have a couple of downsides when it comes to pile load tests. Firstly, several sensors are needed to measure the pile resistance with any sort of statistical certainty, especially in very variable soils. While these sensors are often quite cheap, more sensors creates more complexity and congestion in the reinforcing cage and at the pile head. Secondly, a sensor measures both the structural and geotechnical response of a pile. Imperfections in the concrete, like cracks or bulges, can make it difficult to infer the pile's geotechnical response—again reducing the statistical certainty in the findings.

Distributed fibre optic sensing (DFOS) combats the downsides of point sensors by

measuring the strain across every single part of a fibre optic cable. DFOS uses the principle of light scattering: when light propagates through a medium (like the glass of an optical fibre), small changes in the medium's properties creates a scattering of light photons. By looking at the wavelength of the backscattered light, the returning photons can be grouped into three different types (Figure 1.4). Some photons return at the same wavelength as the input wavelength, known as Rayleigh scattering. Other photons return at completely different wavelengths, known as Raman or Brillouin scattering. Strain and temperature variations also affect the intensity of this backscattered light. For instance, the intensity of Raman scattered light is only affected by changes in temperature. The wavelength of Brillouin scattered light, on the other hand, is affected by both strain and temperature.

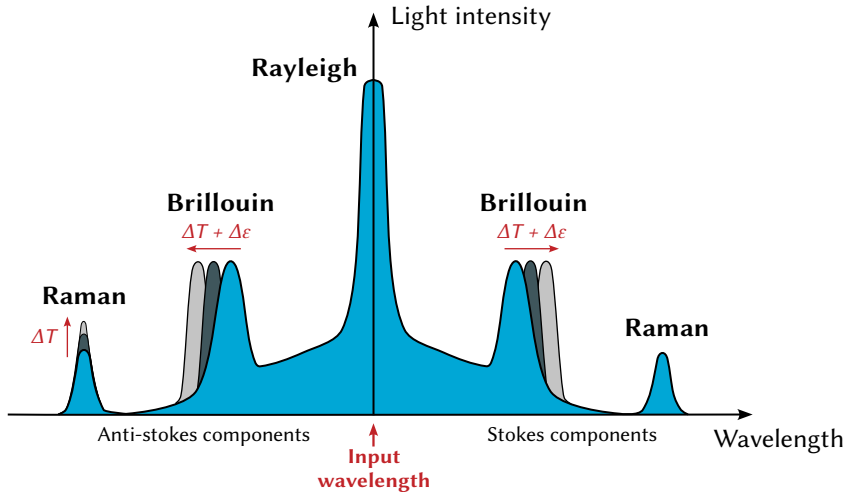

Figure 1.4: Different types of backscattered light in a fibre optic cable and their response to a change in temperature ΔT and change in strain $\Delta\varepsilon$.

Just like point sensor interrogators, DFOS interrogators are classified by the accuracy and frequency at which they can make measurements. Yet some specifications are also unique to DFOS interrogators, such as the *sensing length* and *spatial resolution*, the former describing the maximum length of cable that can be interrogated and the latter describing the smallest distance within which an interrogator can fully detect a change in strain or temperature. In terms of strain sensing, Rayleigh-based systems usually provide a finer spatial resolution compared to Brillouin-based systems, although this comes at the cost of sensing length—and often prohibitively so for full-scale piles.

To date, DFOS systems have performed well in axial load tests on piles (Klar et al., 2006; Kechavarzi et al., 2019; Kania et al., 2020). The technology also continues to improve, with current systems reaching spatial resolutions of the order of several centimetres, with a sensing length of 20 km. For piles embedded only a few pile diameters into the main load-bearing layer—that is, most Dutch sites—improved spatial resolutions can be a particularly useful characteristic to have, giving as much information as possible into how the load is transferred to the load-bearing layer through the pile shaft and pile base.

1.4. Research aim

Through an analysis of static load tests on piles instrumented with distributed fibre optic sensors, this research aims to improve the understanding and design of axially loaded piles in sand. Three pile types were tested: driven precast piles, driven cast-in-situ piles and a screw displacement pile type known as a screw injection pile. The results of these tests were considered in the context of the primary research question:

How does the installation method affect the axial response of piles in sand and what aspects should be considered for design?

As part of this research question, several sub-questions were considered and are presented on a chapter-by-chapter basis:

- Should limiting values be applied to pile base and shaft resistance? (Chapter 2)
- How does the installation method of a screw displacement pile affect its base response? (Chapter 3)
- How should CPT-based design methods for screw displacement piles be improved? (Chapter 4)

When it comes to answering these research questions, full-scale field testing has several advantages over laboratory and numerical modelling: (i) all phases of pile installation are included, particularly concrete casting and casing withdrawal; (ii) installation-induced effects on pile response, such as residual loads or friction fatigue, are inherently incorporated; (iii) scaling effects relating to both geometry and time are removed; and (iv) the natural variability of soil and installation conditions is directly incorporated into the analysis.

Two field test campaigns were conducted: one at Amaliahaven in the port of Rotterdam and another at the Flood Proof Holland test site in Delft. All piles were installed using methods and installation parameters resemblant of industry practice. By using DFOS to measure the deformation of the piles under axial compressive loads, it was possible to accurately determine the base and shaft resistances, which were then correlated with CPT measurements performed at the location of each pile.

To complement these field tests and provide more statistical certainty in the findings, a database of load tests on screw displacement piles was compiled (Appendix A). The findings from the instrumented field tests were incorporated into the database assessment, revealing the accuracy of current design methods and giving a best-fit to the instrumented results.

1.5. Thesis outline

This dissertation is formatted as a collection of journal papers, arranged in chronological order.

- Chapter 2 (Duffy, Gavin, Korff, et al., 2024) compares three different piles installed at the same test site: driven closed-ended, driven cast-in-situ and screw injection piles. The site at Amaliahaven—like much of the port of Rotterdam—is underlain by very dense sand, a challenging soil in which to install piles. Comparing these piles at the same site gave unique insights into the performance of each pile

under axial loading, particularly at base and shaft resistances far beyond limiting resistances in design standards.

- Chapter 3 (Duffy, Gavin, de Lange, and Korff, 2024) follows on from the results of Amaliahaven by focussing on the base response of screw injection piles at Delft. Two pile types were installed, a screw injection pile with a permanent casing (Tubex) and a screw injection pile with a reusable casing (Fundex), with all piles instrumented with DFOS. To supplement the load test results, a database was compiled of all screw displacement pile types, giving clear insights into the base response of screw displacement piles.
- Chapter 4 (paper under review) synthesises the findings of the two test campaigns into a meta-analysis of screw displacement pile tests and design methods. A best-fit to measured base and shaft capacities from a load test database was derived and compared to design methods from Belgium, France, the Netherlands and the USA, using a larger database of both uninstrumented and instrumented test records.

The screw displacement pile database is presented in its entirety in Appendix A, as well as another database on driven cast-in-situ piles in Appendix B.

The installation and test procedure of all load tests has been developed in coordination with the Dutch national pile testing committee and the Dutch standard for pile testing NPR 7201 (2017). Factual reports have been published as part of this process, each thoroughly documenting the methodology and execution of each pile test. For brevity, this dissertation includes a reduced version of the methodology and the factual reports can be found through the following references:

- Duffy, K. J. (2020). *Report on pile test results at Maasvlakte II: Driven Precast Piles.* TU Delft. Delft, The Netherlands. https://research.tudelft.nl/en/publications/report-on-pile-test-results-at-maasvlakte-ii-driven-precast-piles
- Duffy, K. J. (2021a). *Report on pile test results at Maasvlakte II: Screw injection piles.* TU Delft. Delft, The Netherlands. https://research.tudelft.nl/en/publications/report-on-pile-test-results-at-maasvlakte-ii-screw-injection-pile
- Duffy, K. J. (2021b). *Report on pile test results at Maasvlakte II: Vibro piles.* TU Delft. Delft, The Netherlands. https://research.tudelft.nl/en/publications/report-on-pile-test-results-at-maasvlakte-ii-vibro-piles
- Duffy, K. J. (2024). *Delft screw injection pile tests: Factual report.* TU Delft. Delft, The Netherlands. https://research.tudelft.nl/en/publications/delft-screw-injection-pile-tests-factual-report

A third set of field tests were also performed during the PhD research, investigating the behaviour of partially embedded driven precast piles at Delft using DFOS. These tests are reported separately to this dissertation and partially published in Duffy et al. (2022).

1.6. The InPAD project

This research was part of the InPAD project (*Investigation of the Axial Capacity of Piles in Sand*). The TU Delft-led project ran from 2019 to 2023 and was supported by TKI Deltatechnologie along with six industry partners: Deltares, the Dutch Association for Foundation Contractors (NVAF), Fugro, the Ministry of Infrastructure and Water Management (*Rijkswaterstaat*), Port of Rotterdam Authority and Rotterdam City Council (*Gemeente Rotterdam*).

The InPAD project focussed on hidden safety factors in design methods, with three PhD projects examining different aspects through different investigation techniques. The PhD project associated with this dissertation analysed field tests of full-scale piles, redolent of pile types used in practice. The second PhD project (Dirk de Lange, Deltares/TU Delft) also analysed full-scale tests on open-ended piles, in addition to centrifuge and calibration chamber tests that focussed on limiting resistances and the influence of thin weak zones on pile penetration (dissertation to be published). The third PhD project (Fei Chai, University of New South Wales, Australia) used finite element modelling and discrete element modelling, also investigating how thin weak zones influence pile penetration (Chai, 2024).

2

Influence of installation method in very dense sand

Three driven precast, four driven cast-in-situ and four screw injection piles were installed in dense to very dense sand at Amaliahaven in the port of Rotterdam. Each pile was instrumented with two types of fibre optic sensors and loaded under axial compression. Through these tests, a comparison could be made of how different installation methods influence the pile base and shaft response. For example, large residual base stresses were measured in the driven precast piles after installation. These piles also reached the highest base stresses of the three pile types, mobilising their full base resistance at comparatively low displacements. The base response of the driven cast-in-situ piles was also like that of a driven precast pile with residual stresses excluded. In contrast, the screw injection piles mobilised much lower base capacities and at a much lower rate. In terms of shaft resistance, the precast piles showed friction fatigue effects, but this effect was not evident for the driven cast-in-situ or screw injection piles. Finally, shaft and base resistances measured in the dense to very dense sand layers were greater than limiting resistances prescribed in several design standards.

This chapter is based on the following publication: Duffy, K.J., Gavin K.G., Korff, M., de Lange, D.A., Roubos, A.A. (2024). Influence of installation method on the axial capacity of piles in very dense sand. *Journal of Geotechnical and Geoenvironmental Engineering*, 150(6), 04024043.

2.1. Introduction

Much of the industry focus has been brought to the design of piles in dense to very dense sand, particularly because of growing wind energy development in the North Sea, an increased need to upgrade or renew port infrastructure (Roubos, 2019) or intensifying urban development. However, there are several installation risks associated with dense sand. For instance, driven concrete and steel piles become prone to damage and risk not reaching their design depth (Randolph, 2003; de Gijt and Broeken, 2013; Jardine, 2020; Prendergast et al., 2020). For cast-in-situ piles, reusable steel casings can become stuck and irretrievable. Alternatively, the high radial stresses imposed by the soil can affect the pile shape and concrete quality, reducing the structural integrity of the pile (O'Neill, 1991; Fleming et al., 2008). In the end, all these risks can lead to large financial and environmental costs and create severe project delays.

Different installation methods can mitigate these risks (Figure 2.1). Water jetting during the installation of a driven precast (DP) pile can reduce the number of hammer blows needed and decrease the likelihood of pile damage. Screw injection (SI) piles inject grout from the pile tip during installation, reducing the shaft resistance on the casing as it screws itself into the ground. Driven cast-in-situ (DCIS) piles combine a reusable steel casing with an oversized base plate, reducing the shaft resistance on the pile during installation.

A reliable design method should account for these installation effects. Methods that link the pile base resistance q_b and pile shaft resistance q_s to the cone penetration test tip resistance q_c have provided reliable estimates of the pile axial capacity (Jardine et al., 2005; Lehane et al., 2005; Lacasse et al., 2013). In the Netherlands for example, the capacities are calculated using:

$$q_b = \alpha_p q_{c,avg} \leq q_{b,lim} \tag{2.1}$$

$$q_s = \alpha_s q_c \leq q_{s,lim} \tag{2.2}$$

where α_p and α_s are correlation factors that depend on the pile type and installation method, $q_{b,lim}$ and $q_{s,lim}$ are limiting resistances to the pile base and shaft capacities and $q_{c,avg}$ is a weighted average of cone resistances around the pile base. Several methods are available to determine $q_{c,avg}$, including the '4D/8D Dutch method' $q_{c,4D/8D}$ (van Mierlo and Koppejan, 1952; Reinders et al., 2016) and the adapted filter method $q_{c,filter}$ (Boulanger and DeJong, 2018; de Boorder, 2019). More discussion on these methods is provided in Chapter 3.5.1.

Adjustments to these two equations can account for different soil-structure interaction effects. For example, the new 'Unified' design method for offshore driven piles (Lehane, Liu, et al., 2020) includes a factor describing the cyclic degradation of shear stress during pile driving, known as friction fatigue (Vesic, 1965; Lehane et al., 1993; White and Lehane, 2004; Gavin and O'Kelly, 2007). This reduction is modelled as a function of the distance h from the pile base normalised by the pile (equivalent) diameter D_{eq}:

$$\alpha_s \propto \frac{h}{D_{eq}}^{-c} \tag{2.3}$$

where c is a constant (= 0.4 in the Unified method) that depends on the number of load cycles experienced during installation and the pile-end condition, to name but a few (Jardine

et al., 2013; Anusic et al., 2019; Lehane, Liu, et al., 2020). For cast-in-situ or bored piles, in contrast, this effect is shown not to be present (Gavin et al., 2009). Yet for DCIS piles, the complex combination of load cycling during installation, concrete casting and casing withdrawal means it is not clear if their ultimate capacity is affected by friction fatigue (Flynn and McCabe, 2016, 2021).

Furthermore, some design methods limit the shaft or base capacity in high strength soils. These can be simple limiting thresholds, such as in the Netherlands (NEN, 2017b) and Belgium (NBN, 2022), or they can also depend on the soil strength or relative density, such as in China (JGJ, 2008), France (AFNOR, 2018) and the offshore design code (American Petroleum Institute, 2011). Limitations are also introduced implicitly, for example, within the averaging methods used to determine $q_{c,avg}$ or through lower correlation factors. These limitations primarily came from the lack of reliable load tests performed in very dense sand (te Kamp, 1977; Poulos et al., 2001), creating an uncertainty which also propagated towards coarser gravelly sand (Ganju et al., 2020). While limiting resistances offer an apparent degree of safety, they can also lead to larger piles and create difficult and costly installation procedures.

In 2019, a test site was established at Amaliahaven in the port of Rotterdam. The site is redolent of North Sea geological conditions, underlain by dense to very dense sands with q_c values of up to 80 MPa. Three different pile types were tested (Figure 2.1): three driven precast piles, four driven cast-in-situ piles and four screw injection piles. Each pile was instrumented along its full length with two types of fibre optic sensors and loaded in axial compression. As a result, the site gives a unique insight into the base and shaft response of full-scale piles in dense to very dense sand, allowing for a direct comparison of different pile types installed at the same test site.

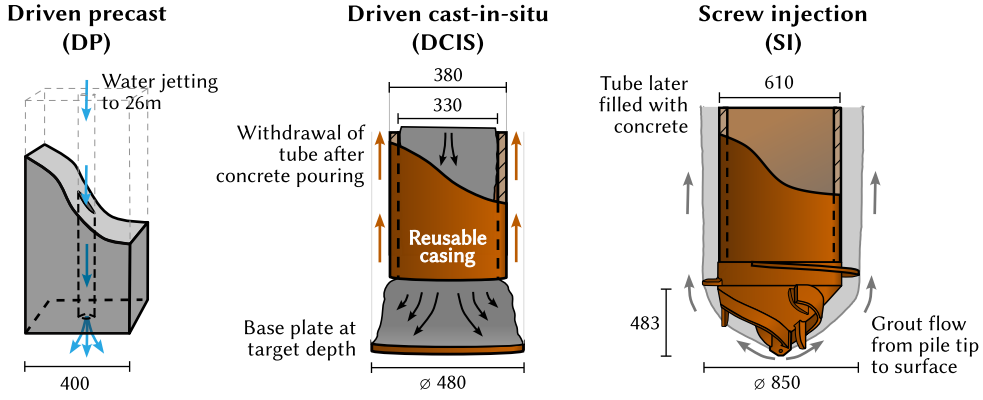

Figure 2.1: Notable installation features of the three pile types and their geometries. All dimensions are in millimetres unless otherwise stated.

2.2. Experimental programme

2.2.1. Ground conditions

The test site was located at the southern end of the harbour of Amaliahaven in the port of Rotterdam (Figure 2.2). The harbour was formed in 2013 from reclaimed land, created as part of an extension of the port into the North Sea known as the Second Maasvlakte. The local geology has been well researched (Hijma, 2019; Vos et al., 2015) and a large amount of subsurface data from the site and the surrounding area is publicly available in electronic format (www.dinoloket.nl). The test piles were arranged in two rows, with at least sixteen metres between each pile (Figure 2.2). Prior to installation, one CPT was performed at the centre of each location and at least three more CPTs were made around two metres away from each location. A selection of these CPT profiles is shown in Figure 2.3.

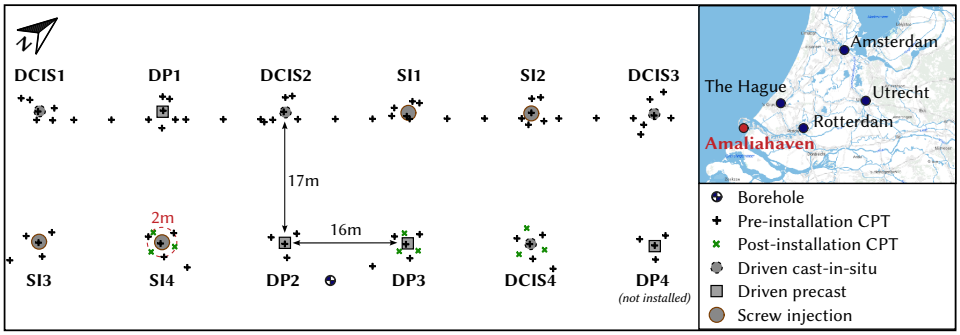

Figure 2.2: Layout and location of the Amaliahaven test site (inset map courtesy of www.pdok.nl).

For interpreting the pile tests, the soil profile has been divided into the Ground Units (GU) outlined in Table 2.1. The uppermost unit GU1 consists of around 10 m of fine to coarse reclaimed sand, followed by eight metres of very fine to fine sand from the marine-deposited Southern Bight Formation. Across GU1, the cone resistances vary from 5 to 20 MPa, with peaks of up to 50 MPa. Underlying this unit are marine and fluvially deposited soils, referred to as GU2. These are very closely spaced to closely spaced thin laminations of very fine sand and clay from the Holocene epoch Naaldwijk and Echteld Formations. A geological deposit known as the Wijchen Member defines the lower boundary of GU2: a one metre bed of stiff clay with cone resistances between 1.5 and 2.0 MPa. This deposit has been amalgamated into GU2.

The defining feature of the site is GU3, a dense to very dense sand around 27 m below the surface. GU3 is a fluvial middle to late-Pleistocene sand called the Kreftenheye Formation, a formation widespread across the Netherlands and the Dutch North Sea Sector (Rijsdijk et al., 2005; Hijma et al., 2012). At the test site, the formation is a poorly sorted slightly to moderately gravelly, coarse silica sand. Its q_c values increase rapidly within the first two metres of the unit to an average of 40 MPa. Peaks of up to 80 MPa are evident, although pockets of loose sand and clay also appear occasionally, for example at 34.5 m depth in Figure 2.3.

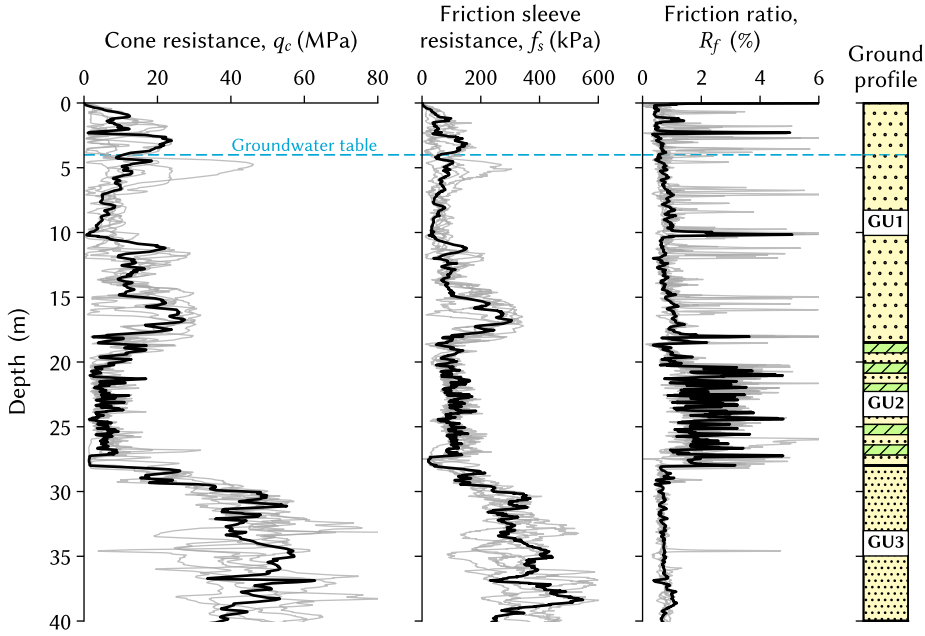

Figure 2.3: Selected CPT results from the Amaliahaven test site and the interpreted ground units. All CPT records are available in electronic format on www.dinoloket.nl.

Table 2.1: Ground units used for the interpretation of the Amaliahaven pile tests.

Unit	Soil type	Geological formation	Depth (m)	Mean q_c (MPa)
GU1	Loose to dense very fine to coarse SAND	Anthropogenic & Southern Bight Formation	0.0–18.5	14.5
GU2	Interlaminated CLAY and SAND	Naaldwijk & Echteld Formations	18.5–27.0	6.4
GU2	Stiff CLAY	Wijchen Member	27.0–28.0	1.7
GU3	Dense to very dense coarse gravelly SAND	Kreftenheye Formation	25.0–45.0	43.9

2.2.2. Pile descriptions

Three driven precast, four driven cast-in-situ and four screw injection piles (Table 2.2) were installed and tested between October 2019 and January 2020. Each pile type has its own unique installation features which make installation easier in dense sand (Figure 2.1). The piles were installed to a pre-defined depth at least $6.8D_{eq}$ into layer GU3.

Table 2.2: Overview of the test piles at Amaliahaven.

Pile	D_{eq} (mm)[a]	L (m)	$q_{c,filter}$ (MPa)	$q_{c,4D/8D}$ (MPa)	Pile age (days)
DP1	450	31.7	45.5	38.0	28
DP2	450	31.3	44.1	33.5	30
DP3	450	31.8	45.3	34.0	78
DCIS1	480	32.5	40.9	16.7	59
DCIS2	480	32.5	52.4	41.1	34
DCIS3	480	32.5	51.0	30.3	50
DCIS4	480	32.5	50.5	39.8	52
SI1	850	37.0	43.4	35.6	43
SI2	850	37.1	45.5	31.8	49[b]
SI3	850	35.0	31.5	22.1	78
SI4	850	34.1	35.0	17.3	50

[a] Defined as the outermost diameter at the pile base for the DCIS and SI piles, equivalent diameter for the DP piles.
[b] Retested after 95 days following attempted fluidisation in GU1 and GU2 around the pile.

Driven precast (DP) piles

The three 400 mm square pre-stressed DP piles (C90/105 concrete) were installed with a Junttan HHK12A hydraulic hammer. Simultaneously with hammering, water was jetted from the pile base until the piles reached two metres above GU3. As a result, less than 50 blows per 25 cm was needed to penetrate GU1 and GU2 (Figure 2.4), although the hammer energy (derived from the block weight and falling height) varied across the three piles in GU2. The blow count increased significantly as the pile penetrated through GU3 at 27 m, reaching up to 250 blows per 25 cm with comparable hammer energies across the three piles. In the end, each pile received around 2300 blows in total.

Driven cast-in-situ (DCIS) piles

The DCIS piles used a reusable steel casing with an outer diameter of 380 mm and a wall thickness of 25 mm. A sacrificial steel base plate was fitted at the bottom to prevent soil from entering the casing. This base plate had an outer diameter of 480 mm, creating an offset of 50 mm with respect to the reusable steel casing. The casing and the base plate were then driven to the target depth using an IHC S-120 hydraulic hammer.

The piles experienced relatively easy driving in the upper layers, with blow counts of around 10 blows per 25 cm (Figure 2.4a). In GU3, the blow counts started to increase gradually with depth (Figure 2.4b). However over last few metres, the blow count began to

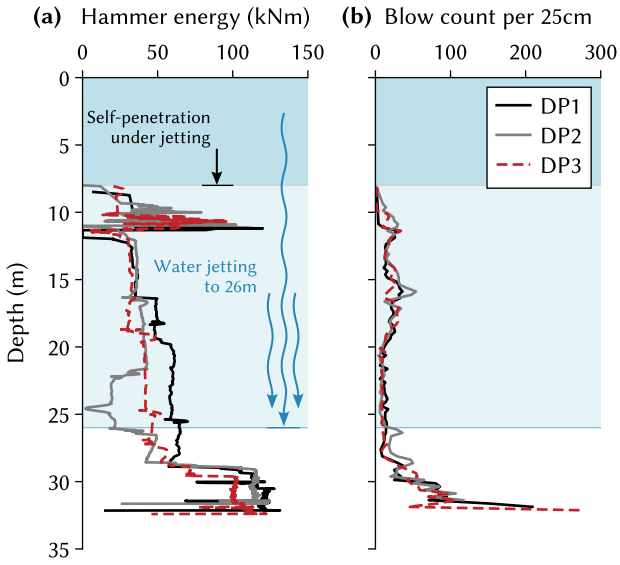

Figure 2.4: Installation data from the driven precast piles.

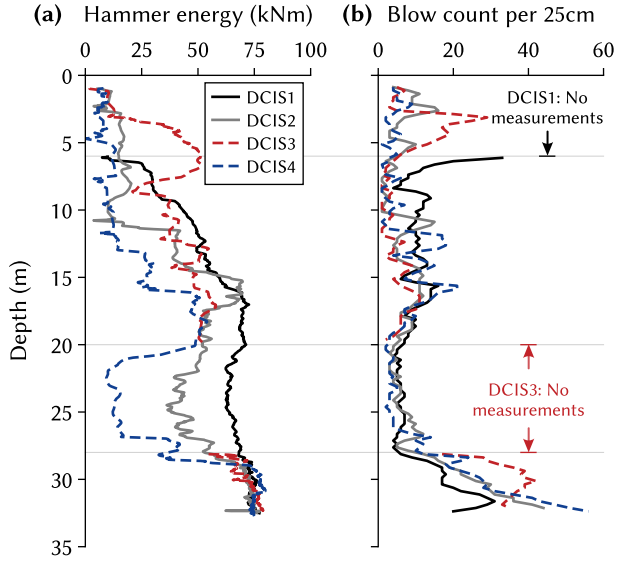

Figure 2.5: Installation data from the driven cast-in-situ piles.

reduce for piles DCIS1 and DCIS3, even though all DCIS piles were subjected to similar hammer energies.

Once the DCIS piles reached the target depth, it was checked that no water intruded between the casing and the base plate. The reinforcement cage (4 × 50 mm diameter bars) was then placed inside the empty casing, followed by free-fall pouring of concrete from the top of the casing (C35/45 XC2 S3, maximum aggregate size 8 mm). Finally, the casing was withdrawn using a reverse hammering action, leaving the base plate at the target depth.

Screw injection (SI) piles

The SI piles consisted of a sacrificial steel tube (S355, 610 mm outer diameter, wall thickness of 24 mm) welded to a larger, 850 mm diameter screw tip—a pile colloquially known as a *Tubex* pile (described in more detail in Chapter (3.2). Screw injection piles are installed using a combination of torque and a crowd force on the pile head, a force created by the pullup and pulldown winches in the drilling rig. During penetration, grout is injected horizontally from the pile tip, fluidising the soil and flowing up the annulus created by the enlarged screw tip. To prevent fluidising the soil underneath the pile base, the injection is then turned off across the final part of installation—in the case of the Amaliahaven test site: a couple of centimetres above the final pile tip depth. The steel tubes of the SI piles remained in-situ after installation, and were later filled with concrete (C35/45 XC2 F4 concrete with maximum particle size of 16 mm).

Piles SI1 and SI2 were longer than SI3 and SI4 to investigate regions of higher and lower q_c around the pile base (Table 2.2). All piles used grout with a water-cement ratio of 2:1 and injected at a constant rate of 180 L/min across most of the installation depth, increasing to 215 L/min and 200 L/min in the final five metres of installation for piles SI3 and SI4 respectively (Figure 2.6d). Each pile used a total of 13 to 20 m^3 of grout, although the grout flowing out at the ground surface could not be accurately quantified.

Pile SI2 penetrated at a higher velocity through the first 20 m compared with the other three SI piles (Figure 2.6b). The penetration velocity reduced in all piles to around 0.8 cm/sec through GU3, with SI2 penetrating slightly faster despite the higher grout injection rates of SI3 and SI4. Both this penetration velocity and rotational velocity were then incorporated into a term known as the advancement ratio (the inverse of which is sometimes referred to as the *scrape factor*):

$$AR = \frac{\Delta z_h}{p_h} \tag{2.4}$$

where Δz_h is the pile's vertical displacement for one full rotation and p_h is the helical pitch at the screw tip (= 35 mm). Similar to its penetration rate, SI2 recorded different advancement ratios to the other SI piles during installation (Figure 2.6c), particularly towards the end of installation as the pile approached the target depth, where $AR \approx 2$. For all other piles, AR ranged from 0.5 to 1.0

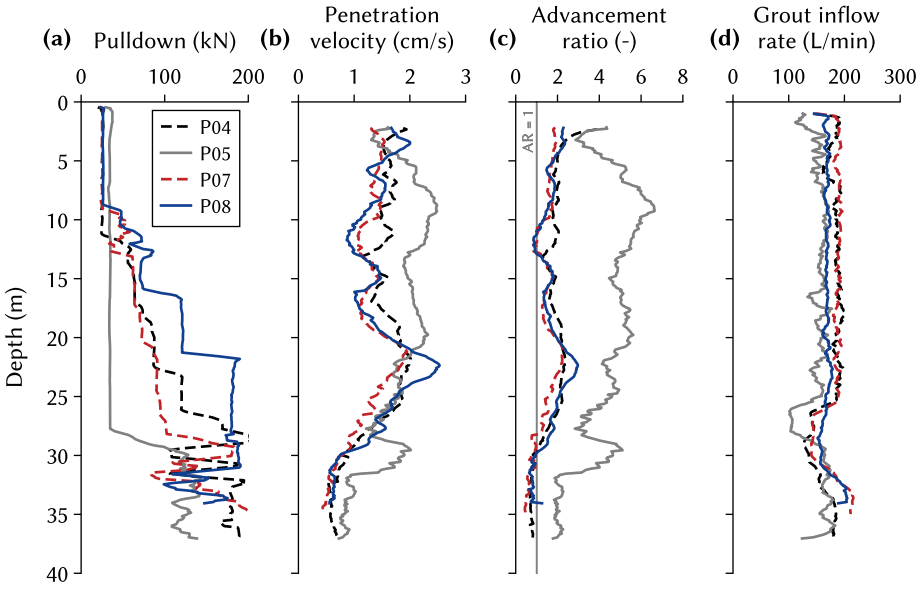

Figure 2.6: Installation data from the screw injection piles.

2.2.3. Instrumentation

Test frame

During testing, loads of up to 25 MN were generated by a test frame tied-in by up to twelve anchors (Figure 2.7). Each anchor was grouted in GU3 and inclined away from the pile to prevent any interaction between the pile and the anchors. The load tests then began at least two weeks after anchor installation to allow for grout curing. Six hydraulic jacks applied the load on the pile, distributed evenly across the pile head using a steel cap. A load cell on top of each jack measured the applied load Q_0 while four linear variable displacement transducers recorded the pile head displacement s_0. The displacement was measured relative to a reference frame with supports 3.7 m away from the test pile. Inclination of the test frame was also monitored and controlled for during each test.

Strain measurements

Two different types of fibre optic measurements recorded the change in strain along the pile: Fibre Bragg Gratings (FBG) and Brillouin Optical Frequency Domain Analysis (BOFDA). At nineteen different levels on each pile, a 1 cm long FBG was etched onto a glass fibre reinforced polymer fibre optic cable. At each FBG, a Micron Optics sm125 interrogator provided a discrete strain measurement every ten seconds. Conversely, the BOFDA system gave a continuous strain distribution along the full length of the pile with a spatial resolution of 20 cm. The BOFDA measurement was performed using the fibrisTerre fTB 2505 interrogator and the BRUsens V9 fibre optic cable. Compared to the FBG system, the BOFDA system measured at a slower frequency of every four minutes. To assess residual loads in the driven precast piles, temperature compensation was applied to the

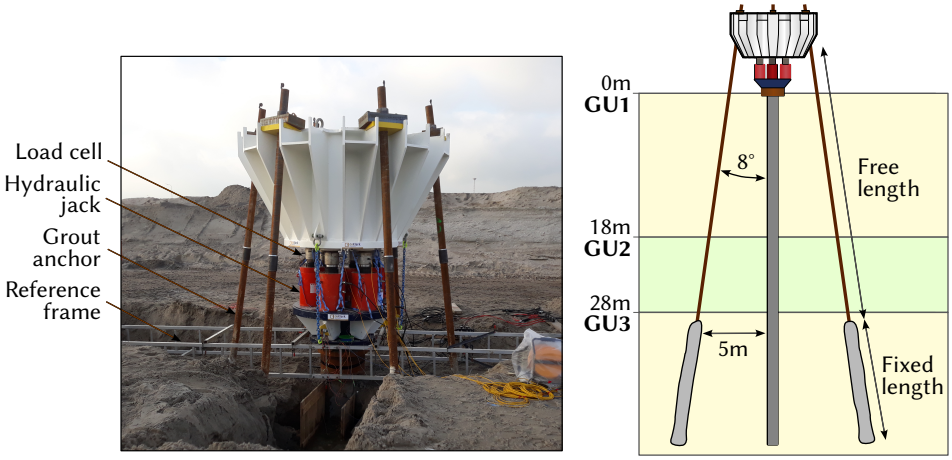

Figure 2.7: Test frame used to load the piles at Amaliahaven in axial compression.

strain measurements using distributed fibre optic temperature sensing (Raman scattering). The temperature compensation process is outlined in Duffy et al. (2022).

The DP piles were the only piles to be instrumented prior to concrete casting in the manufacturing plant, with the fibre optic cables placed along the central axis of each DP pile. The DCIS piles were instrumented on-site by attaching the fibre optic cables to opposite sides of the reinforcement cage. The instrumented cage was then placed in the empty reusable casing just before concrete pouring. The SI piles were instrumented after installation using two axially opposing reservation tubes on the inside of the primary steel tube. After placing the fibre optic cables in the reservation tubes, grout was then used to fix the cables in place.

Strain readings were converted to normal force using the tangent stiffness method by Fellenius (2001). For each pile, the derived stiffness agreed well with the theoretical stiffness and the converted forces in the upper part of the piles were compatible with the forces measured by the load cells.

2.2.4. Pile test procedure

All piles were loaded in static compression, in general compliance with the Dutch guidance document for pile load tests NPR 7201 (2017). Each pile was loaded in a minimum of eight steps, with each step being held for a minimum of 30 minutes and a maximum of 120 minutes. During each step, the creep rate at the pile head was assessed by:

$$k = \frac{s_2 - s_1}{\log t_2 - \log t_1} \tag{2.5}$$

where s_1 and s_2 is the displacement (in millimetres) of the pile head at a time of t_1 and t_2 respectively (in minutes). Depending on the magnitude of this creep rate, the step was either prolonged or progressed to the next load step. The test ended when the pile base displaced by at least 10 % of the pile's (equivalent) diameter, referred to as geotechnical failure.

The first load test was performed on pile DP1 and included an unload/reload cycle after

each load step, as stipulated in NPR 7201. Subsequent tests excluded load cycles unless they were required for operational reasons, for instance, if excessive inclination of the test frame created a safety risk.

2.3. Experimental results

2.3.1. Load-displacement response

The following observations can be made from the load-displacement response of all piles (Figure 2.8):

1. The DP piles behaved very similarly and failed at loads between 8.0 and 8.6 MN (Figure 2.8a). The lowest capacity was reached by DP1 where load cycles were performed after each step. To investigate the effect of pile aging, pile DP3 was tested seven weeks after DP1 and DP2. However, pile DP3 did not reach a higher failure load than the two other DP piles.
2. The DCIS piles reached similar loads to the DP piles but showed more variability in the failure loads, ranging from 7.4 to 9.0 MN (Figure 2.8b; Table 2.3). Pile DCIS2 was the only DCIS pile not subjected to a load cycle and reached the highest capacity of 9 MN. However at this load, the concrete cracked just underneath the pile cap and so the pile could not be safely loaded to geotechnical failure.
3. The SI piles mobilised the largest loads, reaching up to 24 MN. The longer piles, SI1 and SI2, reached higher capacities than the shorter piles SI3 and SI4 (Figure 2.8c). While testing SI2, the reaction anchors began to deform as the load approached 24 MN and the test had to stop before reaching geotechnical failure. Before the retest six weeks later, fluidisation of soil in GU1 and GU2 was attempted by flushing bentonite around the pile. This was done to reduce the shaft resistance in the two ground units so that the base and shaft resistance in GU3 could be fully mobilised within the capacity of the test frame. The retest reached a load of 21.5 MN, less than the maximum load in the initial test.
4. At high test loads, each SI pile displaced very suddenly and the previous peak load could not be reached again. The result is the softening response shown in the load-displacement curves, where the load reduces by up to 5 MN with increasing displacement. This response was also shown in the test on SI4 and the retest on SI2, both of which did not have any load cycles during the test. Under this reduced load, all piles reached the target base displacement.

2.3.2. Load distribution

The BOFDA and FBG systems gave independent measurements of force with depth in the test piles (Figure 2.9). These readings were collected for all piles except for pile SI3 because of a breakage in the optical fibres. For the DCIS and SI piles, a zero-load condition was assumed at the start of testing because the curing grout or concrete could not lock in any of the residual stresses that may have developed during installation. In contrast, residual stresses were measured in the three DP piles at the start of each load test (Figure 2.9a). These residual stresses show a similar trend with depth: at the surface, the load begins with the weight of the test frame resting on the piles at the time of measuring. The load increases

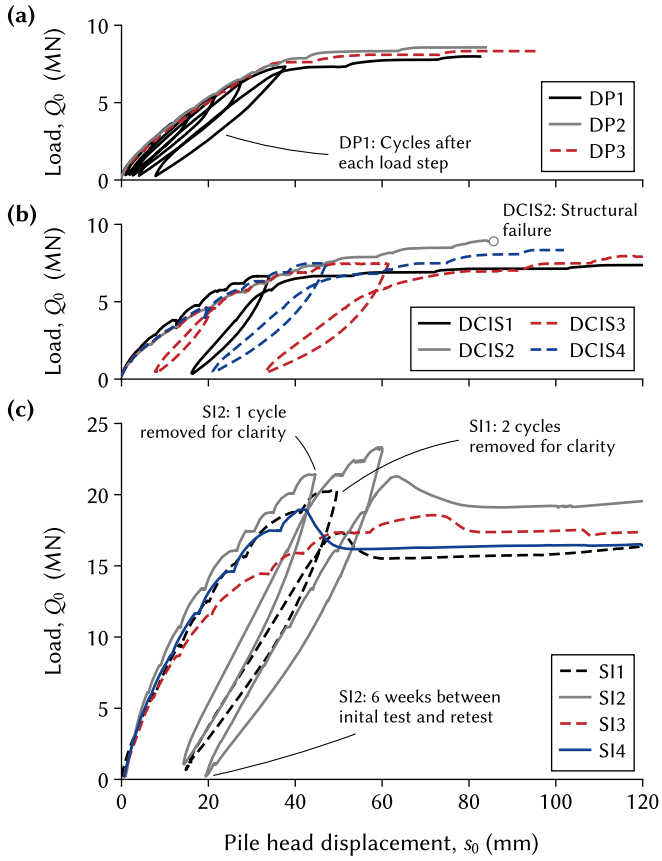

Figure 2.8: Measurements at the pile head from (a) the driven precast piles (b) the driven cast-in-situ piles and (c) the screw injection piles.

gradually with depth, most substantially in GU3, reaching a maximum load of 1.8 MN near the pile base. This base load corresponds to a stress of approximately 10 MPa, or 20 % of $q_{c,filter}$ (Table 2.2). To balance this residual base stress, Figure 2.9a suggests that each pile mobilised negative shear stresses along the entire pile length, acting in equilibrium with the load underneath the pile base. No time dependent effects are evident in the residual stress measurements, as pile DP3 exhibits a similar trend to DP1 and DP2 even though the residual stress measurement was performed seven weeks later.

Figure 2.9 presents the load distributions at the highest applied load on the pile, with residual loads included in the distributions of the DP piles. For all three pile types, the reduction of force with depth is relatively constant in GU1 and GU2. In GU3, the slope of the distribution changes suddenly. For the DP and SI piles, this sharp reduction in force shows that the two pile types mobilised much more shaft resistance in GU3 than in GU1 or GU2. Surprisingly, the DCIS piles show a very different pattern in GU3, with both the BOFDA and FBG readings showing a lot of noise and an increase in force with depth.

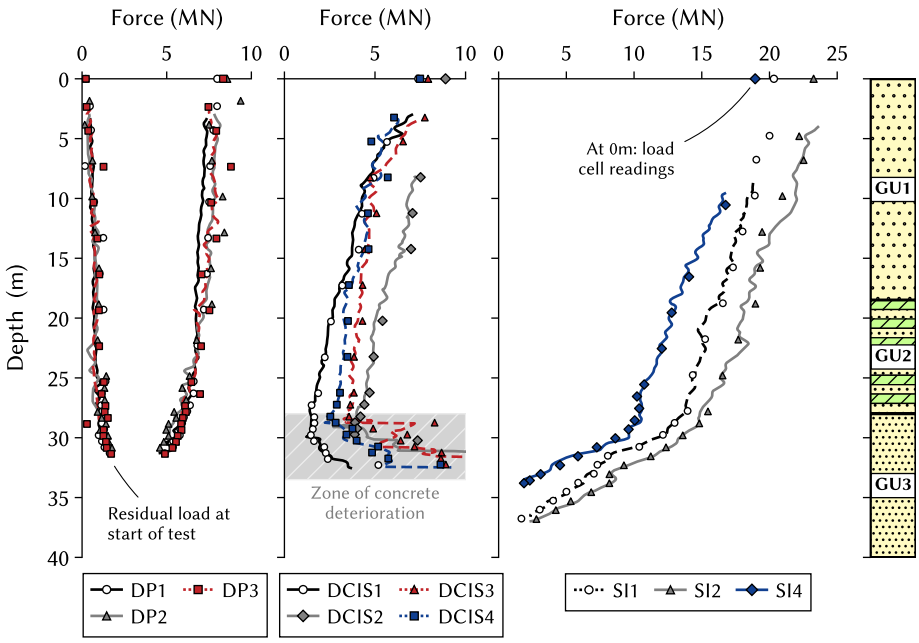

Figure 2.9: Axial force distribution at peak applied load $Q_{0,max}$ of all piles as well as the residual load in the DP piles at the start of testing. BOFDA readings are represented by continuous lines, FBG readings by discrete points.

Table 2.3: Peak resistances mobilised by each pile at Amaliahaven.

		$q_{s,avg}$ (kPa)			
Pile	$Q_{0,max}$ (MN)	GU1	GU2	GU3	q_b (MPa)
DP1	8	27	56	201	31
DP2	8.6	40	125	224	29
DP3	8.3	26	85	253	31
DCIS1	7.4	156	98	—	9
DCIS2	9	114	112	—	23
DCIS3	8	131	87	—	20
DCIS4	8.4	139	78	—	25
SI1	20.3	100	110	480	10
SI2	23.3	116	180	539	12
SI3	18.6	—	—	—	—
SI4	19	136	149	524	11

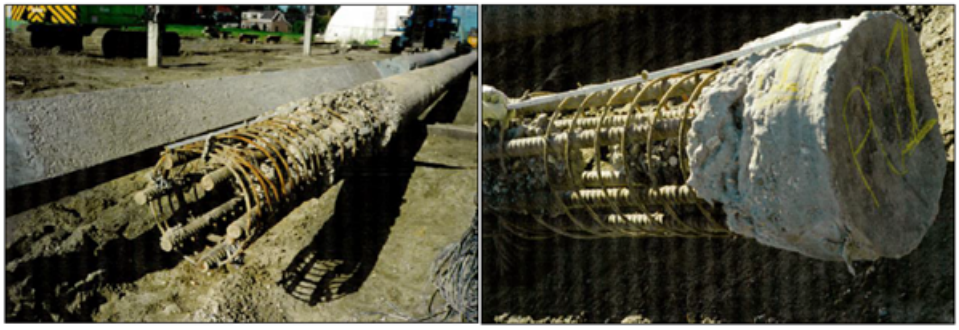

Figure 2.10: The base of two DCIS piles extracted from De Gaag near Delft (Geerling and Janse, 1997). The DCIS piles at Amaliahaven were assumed to have a similar shape.

It is not certain how the DCIS piles actually responded in GU3 because the piles were not extracted after testing. The magnitude and scatter of the measured forces suggests that there was little to no concrete present in the piles across GU3. This problem has been observed before with driven cast-in-situ piles embedded in dense to very dense sand (van Weele and Lencioni, 1999) and several explanations were given for this, including low workability of the concrete mix, congestion created by the reinforcement cage, or the influence of surrounding soil and groundwater on the curing concrete.

Crucially, the DCIS piles at Amaliahaven used a larger-than-normal reinforcing cage to reduce the likelihood of structural failure during load testing. The size of the cage left little room for concrete pouring and both the cage and the casing may have trapped coarse aggregates or cement particles during pouring—abetted by the large falling height of the concrete mix. The fact that scattering in the strain readings was coincident with the layer boundary between GU2 and GU3 may also suggest an influence of the local ground conditions. For instance, the hydrostatic pressure created by the wet concrete column may not have been enough to resist the high radial stresses imposed by GU3 after casing removal. Both scenarios would have led to poor concrete quality at the bottom of the pile and it is expected that little to no concrete was present across GU3 (like in Figure 2.10), causing much higher and more variable strain measurements in this ground unit. Consequently, this analysis assumes that no shaft friction could develop over GU3. Instead, the load at the GU2-GU3 interface was transferred directly through the reinforcement and onto the base plate.

2.3.3. Shaft resistance

To calculate the average shaft resistance $q_{s,avg}$, the change in normal force across a ground unit was taken. To convert this force to shaft resistance, the outermost diameter of the DCIS (= 480 mm) and SI piles (= 850 mm) was used. Table 2.3 summarises the results for all test piles and a selection of mobilisation curves are presented in Figure 2.11. Since good agreement was shown in all piles between the BOFDA and FBG readings, only the FBG readings are considered from hereon because of their higher measurement frequency compared to the BOFDA readings.

Installation-induced negative shear stresses were measured in all three ground units at

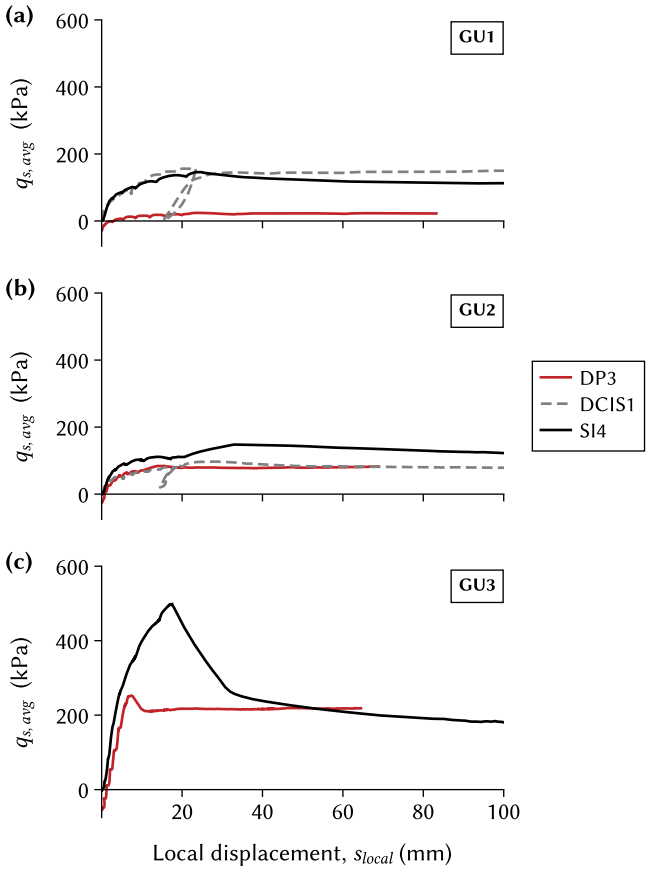

Figure 2.11: Mobilised shaft resistance of selected piles. No shaft resistance could be measured in the DCIS piles in GU3 because of structural deterioration.

the beginning of the driven precast pile tests. These stresses were greatest in GU3, where around −80 kPa of shear stress was acting on the piles at the start of testing compared to only −20 kPa of shear stress in GU1. During the load tests, the DP piles mobilised low shaft resistances in GU1, with peak resistances of around 30 kPa (Figure 2.11a). On the other hand, the DCIS and SI piles reached much higher shaft resistances in GU1, ranging from 100 to 156 kPa. The two pile types mobilised this peak resistance at a slower rate than the DP piles, at displacements of around 4 % (DCIS piles: 19 mm; SI piles: 34 mm) of the pile diameter, compared to 1.5 % (7 mm) for the DP piles where the stresses reversed from being in tension at the start of testing, to under compression at the maximum applied test load.

A similar response was shown by all three pile types in the interlaminated ground unit GU2 (Figure 2.11b). The highest peak resistances were recorded by the SI piles with an average of around 145 kPa, whereas the DP piles recorded the lowest peak resistances of around 90 kPa. However, the rate at which these peak values were mobilised was similar

across the three pile types.

Very high shaft resistances were measured in the dense to very dense sand layer, GU3. The DP piles recorded peak resistances of 201 to 253 kPa, occurring within a displacement of 7 mm or 1.5 % of the equivalent diameter (Figure 2.11c). Interestingly, pile DP3 showed softening behaviour in its response, with the shaft resistance reducing from a peak of 253 kPa to 215 kPa. This softening response was not exhibited by the two other DP piles, tested seven weeks earlier. The SI piles mobilised high shaft resistances in GU3, ranging from 480 to 539 kPa and mobilising at displacements of 15 – 20 mm, 2 % of the pile diameter. Notably, a sharp reduction in shaft resistance occurred with increasing displacement, corresponding with the post-peak reduction observed in the total load-displacement curves (Figure 2.8c).

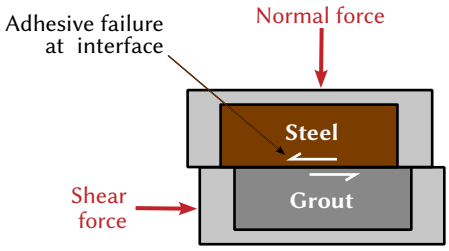

Figure 2.12: Direct simple shear test on the steel-grout interface of the screw injection piles.

To investigate the cause of this sharp reduction, direct simple shear tests were performed (ter Steege, 2022) to investigate the adhesive strength of the steel-grout interface and to see if debonding could have occurred between to the two materials (Figure 2.12). Seven samples were prepared to capture potential changes in steel roughness and grout water-cement ratios due to installation. Three samples were tested on smooth steel (roughness $\approx 4\,\mu m$) and four samples on rough steel (roughness $\approx 156\,\mu m$), with the water-cement ratio ranging from 1:1 to 2:1 within both groupings.

Each sample was first sheared at a low normal stress and if adhesive failure did not occur at the interface, the normal stress was then increased incrementally towards magnitudes expected for the test site. Six of the seven samples failed at a normal stress of 1459 kPa. At this normal stress, the four rough steel samples failed at shear stresses ranging from 927 to 1222 kPa and two smooth samples failed at shear stresses of 379 kPa and 500 kPa. The last remaining smooth sample failed at a normal stress of 912 kPa and a shear stress of 312 kPa.

The laboratory results indicate that the shear stresses reached in GU3 during pile testing were close to the ultimate bond strength of the steel-grout interface. As a result, it is likely that adhesive failure occurred in GU3 at the steel-grout interface, causing a sharp reduction in the shaft resistance in the soil unit. No adhesive failure occurred in GU1 and GU2 due to the low shear stresses mobilised in the two soil units (no more than 160 kPa), less than the lowest shear stress at failure during the laboratory tests.

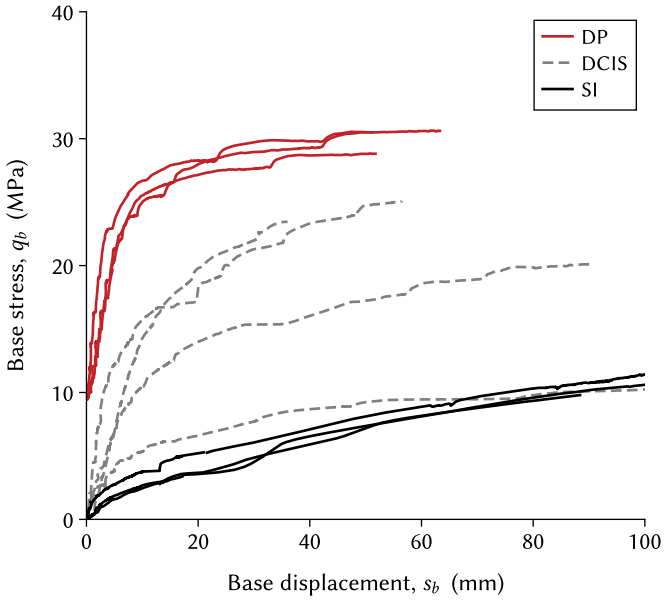

Figure 2.13: Mobilised base resistance across all piles, including the residual stress contribution of the DP piles. For clarity, loading cycles have been removed.

2.3.4. Base resistance

The base resistance of the piles was extrapolated from the lowest FBG measurement, generally within one pile diameter from the pile base. This resistance was then converted to a stress using the outermost diameter of the DCIS (= 480 mm) and SI piles (= 850 mm). A wide spectrum of responses was recorded across the three pile types (Figure 2.13; Table 2.3). The DP piles mobilised the highest base resistances, building up from a residual stress of 10 MPa at the start of testing, to peak capacities of around 30 MPa. This peak resistance develops quickly, within a base displacement of just 30 mm.

Some variability in the assumed base resistances of the DCIS piles was exhibited, ranging from 10 – 25 MPa. Two DCIS piles behaved very similarly upon loading, reaching peak capacities of up to 25 MPa. In contrast, DCIS1 only mobilised a base stress of 10 MPa and the other pile, DCIS3, exhibited a response in between the two extremes. Given the likely absence of concrete in the lower section of the pile and the resulting transfer of load through the reinforcing cage, such variability is likely due to installation problems rather than a real pile response.

The SI piles mobilised the lowest base resistances of the three pile types, reaching peak resistances of 10 – 12 MPa—just one-third of the base resistance recorded by the DP piles. All three of the SI piles mobilised their resistance at a very similar rate, a rate much slower than the DP and DCIS piles. Figure 2.13 also suggests that some additional capacity could have been mobilised if the SI piles were displaced further.

2.4. Discussion

2.4.1. Limiting resistances

By instrumenting and load testing piles in the dense to very dense sands of the test site, some unique data points have been collected to understand pile behaviour at high cone resistances. Of the three pile types tested, the DP piles recorded the largest base resistances of around 30 MPa (Figure 2.13). For example, this is twice as much as the 15 MPa limitation in the Dutch design standard (NEN, 2017b) and the 12 MPa limitation in the offshore design code (American Petroleum Institute, 2011).

The residual base stresses (=10 MPa) were a substantial component of the base response of each DP pile, measuring one third of their peak base capacity. These residual stresses alone bring the base resistance close to existing limitations and had they not been measured before load testing, the ultimate pile base capacity would have been misinterpreted. Three of the four DCIS piles also reach base resistances greater than 15 MPa, not including residual stresses (if present).

Similar inferences can be made in terms of limiting shaft resistances. The DP piles mobilised resistances of around 200 kPa in GU3, greater than the 150 MPa limitation in the Dutch design standard or the 115 kPa limitation in the offshore design code. The DCIS piles also mobilised resistances just under their prescribed limiting resistances (=210 MPa in the Dutch design code), even though the shaft resistance of the DCIS piles was only assessed in the looser GU1 and GU2 ground units.

The largest and longest piles tested, the SI piles, reached shaft resistances of more than 500 kPa across GU3 and greatly exceeded prescribed limiting resistances. However at these stresses, structural failure occurred at the grout-steel interface and greatly reduced the available shaft resistance. This suggests that the geotechnical capacity is not limited within the range of shear stresses measured in the presented pile tests, although allowances for the structural capacity of the pile should still be made, particularly for piles with complex structural interfaces.

2.4.2. Normalised base resistance

Figure 2.14 compares the base response of the three pile types by normalising with D_{eq} and $q_{c,filter}$ (Table 2.2). The DP piles developed the highest normalised base resistance α_p of between 0.65 and 0.75, with residual stresses included. In comparison, the DCIS piles showed a much more diverging behaviour, with α_p ranging from 0.20 to 0.45.

Part of this diverging behaviour may reflect the variation in soil strength around the pile base. It could also suggest some sensitivity of the DCIS base response to the surrounding soil and installation conditions. For instance, the pile base of DCIS2 and DCIS4 responded quite similarly during testing and both piles also experienced a high number of hammer blows towards the end of installation (Figure 2.5). On the contrary, the blow count reduces over the final couple of metres for DCIS1 and DCIS3, with both piles also recording much lower α_p values.

Just like the DP piles, it would be expected that the DCIS piles would also develop some residual base stress after installation given the similarity in installation processes. However, the removal of the reusable casing and placement of wet concrete would result in the upward movement of the base plate until the residual base stress and the self-weight

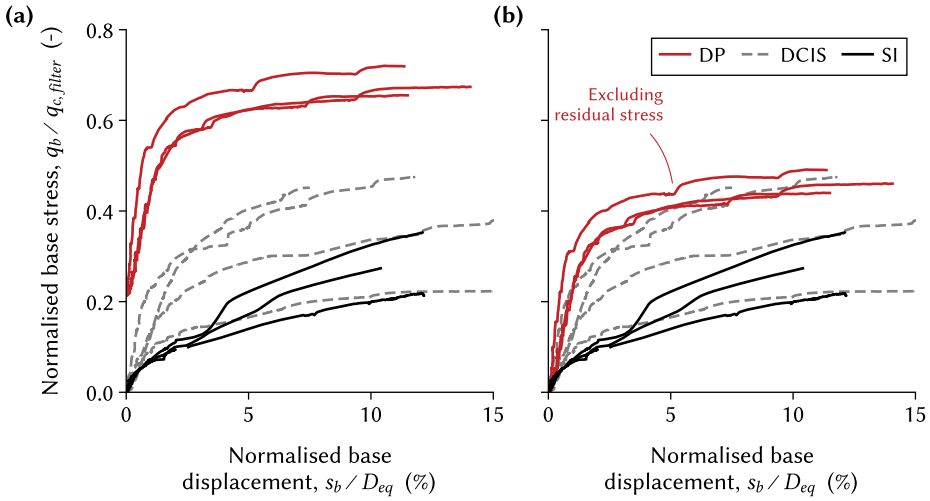

Figure 2.14: Comparison of the normalised base resistance across all piles (a) with residual loads included in the DP piles (b) with residual loads excluded in the DP piles.

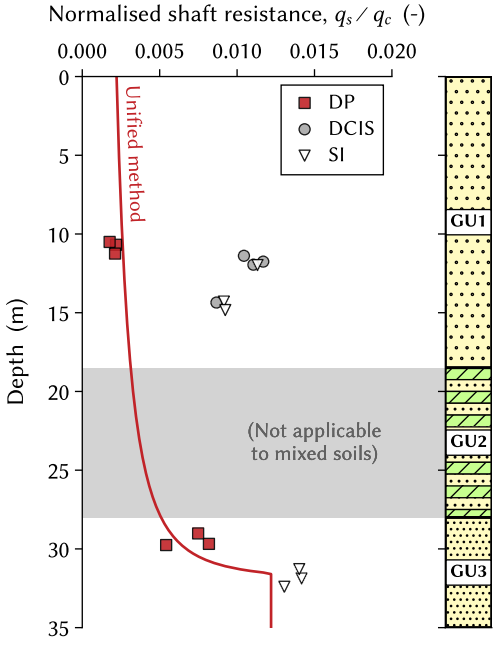

Figure 2.15: Normalised peak shear stress of all piles in GU1 and GU3, including residual stress in the DP piles.

of the concrete column reached an equilibrium. Consequently, piles DCIS2 and DCIS4 responded quite similarly to the DP piles with residual loads excluded (Figure 2.14b), with very similar α_p values at a normalised displacement of 10 %.

The SI piles mobilised the lowest α_p values of between 0.20 and 0.35. The rates at which the SI piles reached these peak values were also much slower than the DCIS and DP piles. For instance, the DP piles mobilised almost all their base capacity within 3 % D_{eq} but at the same displacement, the SI piles mobilised only 30 % of their base capacity. This slow response of the SI piles resembles more of a bored pile than a displacement pile. The α_p values reached are also lower than the typical range of 0.50–0.63 listed in design standards (NEN, 2017b; NBN, 2022) when using the standard-specific averaging methods and this is later expanded on in Chapter 3.5.1.

2.4.3. Normalised shaft resistance

Figure 2.15 compares the normalised peak shear stresses α_s of the three pile types in the two clean sand layers, GU1 and GU3. Towards the bottom of the pile, the DP piles recorded α_s values 50 % lower than those mobilised by the SI piles. This difference is even more pronounced towards the top of the pile, with the same DP piles mobilising resistances three to four times lower than the SI and DCIS piles. This variation with depth in normalised shaft resistance is modelled well by the Unified design method (Lehane, Liu, et al., 2020), which includes a friction fatigue term (Equation 2.3) to describe the cyclical degradation of shaft friction caused by pile installation. In contrast, less variation in the SI piles was exhibited across their length with slightly higher α_s mobilised in GU3 compared with GU1 at h/D_{eq} of 20 to 30. In GU1, the DCIS piles mobilised significantly greater α_s values than the DP piles, reaching values similar to the SI piles.

Further insight into the shaft resistance distributions given in Figure 2.16. The figure compares the measured load distribution at the peak mobilised pile capacity $Q_{0,max}$ to that predicted using either a constant α_s of 0.011 (the average measured value across the DCIS and SI piles, Figure 2.15) or an α_s that varies with h/D as per the Unified design method (Equation 2.3). The predicted load at a given depth is calculated by subtracting the cumulative predicted shaft resistance to that depth from the maximum measured load resistance at the pile head. The conclusions for each pile type are as follows:

1. For the DP piles, a constant α_s of 0.011 overestimates the shaft resistance by 2 MN in GU1, shown by the deviation between the measured and predicted readings at the interface between GU1 and GU2. In GU3 on the other hand, the observed reduction in force matches that predicted by a constant α_s. By contrast, the Unified method gives a good fit to the measurements—even in GU1 where water jetting was performed. While the influence of jetting and friction fatigue cannot be separated from one another based on these field tests alone, the strong agreement with the Unified method suggests that water jetting had little influence on reducing the already low residual shear stresses that were incurred by friction fatigue.

2. For the DCIS piles, the Unified method underestimates the shaft resistance of DCIS2 by 2 MN in GU1. In contrast, adoption of a constant α_s agrees well with the measured data. Even though the DCIS piles were also installed by driving,

these results suggest that the piles' shaft capacities were not affected by friction fatigue, despite their high slenderness ratio (h/D). This is likely because the geometry of the DCIS piles creates an annular space between the base plate and the reusable casing (Figure 2.5) during installation. This means that any friction fatigue effects that could have occurred during pile driving will occur at the interface between the reusable casing and the soil. Following installation, the casing is withdrawn and the remaining void is filled with concrete, meaning that the shear interface during pile load testing is not the same as the interface that may have been affected by friction fatigue during installation.

3. For the SI piles, a constant α_s predicts the load distribution well (Figure 2.16). However the Unified method underestimates the shaft resistance, particularly towards the top of the pile in GU1. This is unsurprising, since the friction fatigue mechanisms that affect driven precast piles do not occur in SI piles.

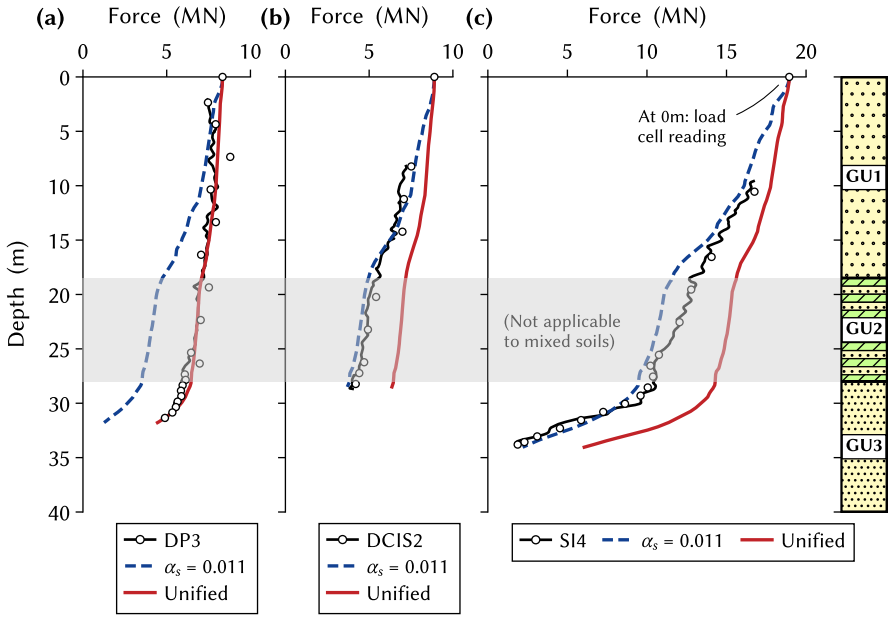

Figure 2.16: Measured load distribution of three different pile types compared to the predictions of a constant α_s with depth alongside the depth-dependent Unified method. The load cell reading is taken as a fixed point from which the predicted shaft resistance is subtracted.

2.5. Conclusion

Driven precast, driven cast-in-situ and screw injection piles were installed at a test site at Amaliahaven in the port of Rotterdam. The site was underlain by dense to very dense sands with CPT cone resistances of up to 80 MPa. Each pile was instrumented with two types of fibre optic systems and loaded under axial compression to failure, meaning that the base and shaft response of each pile could be clearly distinguished. As a result, the tests provide a unique dataset where the influence of different installation methods on the pile response can be compared in similar ground conditions.
The main findings from the tests are as follows:

- The installation of the driven precast piles created large residual base stresses, mobilising all the upper soil layers in negative shaft friction. Upon loading, the driven precast piles mobilised the highest base resistances out of the three pile types and at comparatively low displacements. In contrast, the screw injection piles mobilised the lowest base capacity and exhibited a much softer response—with much higher displacements needed to mobilise the maximum base resistance.
- The normalised shaft resistance of the driven precast piles showed variation with depth. This was in line with design methods describing friction fatigue, even though water jetting was performed in the upper soil layers. Conversely, no friction fatigue effect was shown by the shaft response of the driven cast-in-situ and screw injection piles, which both mobilised comparable normalised shaft resistances.
- Very high base and shaft capacities were recorded during testing, greater than limiting resistances prescribed in design standards. This suggests that these limits introduce excessive conservatism into pile design when applied in dense to very dense silica sands. Nevertheless, interface debonding in the screw injection piles suggests that the structural performance of the pile under high loads should be carefully considered, particularly for composite, cast-in-situ piles.

Using these findings, pile design was optimised for quay wall development across the port of Rotterdam (Roubos et al., 2024), leading to both environmental and financial savings whilst minimising installation risks in the dense to very dense sand layers. Crucially, these tests also fill a gap in pile test databases in very dense sand, providing more certainty into the application of design methods in such conditions.

3

Base resistance of screw displacement piles

The base capacity of the screw injection piles at Amaliahaven was surprising, particularly when compared to the driven precast piles. Therefore, this chapter goes into more detail on the base response of screw injection piles, first looking at a series of full-scale load tests performed at Flood Proof Holland in Delft, then broadening out to screw displacement pile systems as a whole. Each of the five screw injection piles at Delft were founded in medium dense to dense sand and instrumented with distributed fibre optic sensors along its full length, giving insights into the shaft and base response under compressive loads. The test results are then combined with a database of instrumented load tests on screw displacement piles in sand. In this way, the influence of different screw displacement methods and geometries on the base resistance can be assessed. In summary, the analysis showed that all screw displacement pile types tended to mobilise base capacities similar to bored or non-displacement piles. Despite high variability in the database, no significant trend with pile geometry, such as length or diameter, was evident.

This chapter is based on the following publication: Duffy, K.J., Gavin K.G., Korff, M., de Lange, D.A. (2024) Base resistance of screw displacement piles in sand. *Journal of Geotechnical and Geoenvironmental Engineering.* 150(6), 04024043.

3.1. Introduction

Screw injection piles are part of a group of piles known as screw displacement piles, otherwise known as drilled displacement or auger displacement piles in North America (Figure 3.1). Screw displacement piles are installed using both torque and a push-in force. Unlike bored piles, continuous flight auger (CFA) piles or screw anchors, screw displacement piles displace the soil radially away from the pile shaft and underneath the pile base, minimising the degree of soil transportation. Generally, this is assumed to be favourable for the pile capacity, implying that screw displacement piles provide comparatively high capacities whilst producing low noise and vibration during installation. Therefore, screw displacement piles are an attractive alternative to bored or driven pile types, particularly in dense, urban areas with variable soil conditions. They constitute roughly 9 % of the worldwide piling market (Bottiau, 2015) and are also used as rigid inclusions for ground improvement (Varaskin et al., 2016; Suleiman et al., 2016).

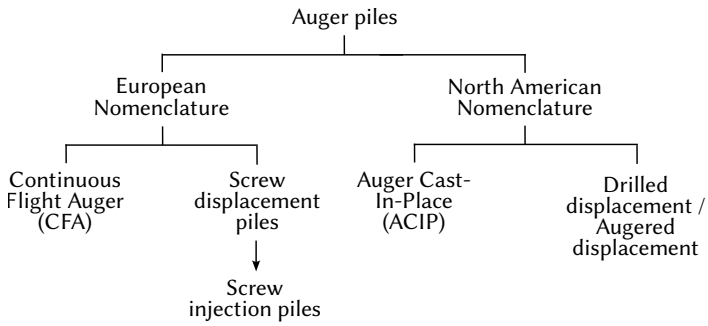

Figure 3.1: Nomenclature for piles in Europe and USA (modified after Basu et al., 2010). More details on the different installation methods for screw displacement piles are given in Chapter 4.2.

Design methods for screw displacement piles often use the cone penetration test to predict their base capacity (Kempfert and Becker, 2010; Huybrechts et al., 2016; van Seters, 2016; Moshfeghi and Eslami, 2019; Gavin et al., 2021), defining the base capacity $q_{b,0.1D}$ at a base displacement of 10 % of the pile diameter D. The empirical correlation factor α_p (Equation 2.1) is also relatively high for a screw displacement pile. For example, the Dutch design code (NEN, 2017b) prescribes an α_p of 0.63 when $q_{c,avg}$ is determined by the 4D/8D averaging method. In this case, the α_p is much closer to that of a driven closed-ended pile ($\alpha_p = 0.70$) compared to that of a bored pile ($\alpha_p = 0.35$). Essentially, the high α_p implies that the installation process of a screw displacement pile improves the stress state around the pile base and so the pile performs more like a fully displacing pile than a non-displacing pile.

Yet exactly how the installation of a screw displacement pile affects its base capacity is difficult to quantify. Laboratory tests (Slatter, 2000) have shown how soil is displaced downwards and radially away from the drilling tool of a screw displacement pile—a phenomenon controlled by both the drilling tool geometry and installation parameters, such as the rotational speed and crowd force. Numerical analyses (Pucker and Grabe, 2012;

Basu et al., 2014; Knappett et al., 2016) have also supported these findings, showing that the soil densified in a zone one to three pile diameters away from the pile. However, the mechanisms occurring around the pile base are also affected by direct transport of soil up the screw flights, particularly when the displacement body of the pile is offset away from the pile base, like in the case of Omega piles (Slatter, 2000). Translating these models to full-scale piles brings another layer of complexity: when the hollow drilling tool is filled with wet concrete and subsequently withdrawn, another series of stress changes and re-equalisation are initiated (Bustamente and Gianeselli, 1998; W. F. van Impe, 2001), potentially leading to a non-uniform pile base in terms of both geometry and stiffness.

To investigate the base resistance of screw displacement piles in sand, this chapter first presents the results of static load tests on five instrumented screw injection piles. Each pile was instrumented with distributed fibre optic sensors, giving detailed insights into the geotechnical and structural response of the piles. The test results are then combined with a newly compiled database of instrumented load tests on screw displacement piles founded in sand. Using the database, the chapter shows the importance of averaging methods in CPT-based design formulations for the pile base resistance and compares the base response of different screw displacement pile types to investigate if different installation methods have an influence on the pile base capacity.

3.2. Background of screw injection piles

Screw injection piles are a type of screw displacement pile which are installed using an injection fluid simultaneously with a push-in force and torque. The fluid is injected from the pile tip, passing along the pile shaft and out through an annular space around the pile at the ground surface, reducing the resistance acting on the pile shaft and on the pile tip. If grout is used as the injection fluid, an outer shell is created around the pile upon grout hardening, filling the annular space and increasing the pile's cross-sectional area. Overall, this means the pile type is quite adept at installing in dense sand and variable deposits, whilst still generating low noise and vibrations. These reasons, for instance, are why screw injection piles are steadily becoming more and more common in the Netherlands and Belgium (Bottiau and Huybrechts, 2019).

Precisely how screw injection piles are installed varies from contractor to contractor. Variations can include screw tip shape, grout properties, the location of the injection outlet or with how the casing is extracted. Two common screw injection pile types include the *Fundex* and *Tubex* systems, which are often used as colloquial names for all screw injection piles. A key installation characteristic of Fundex piles (Figure 3.2) is the thick-walled reusable steel casing with a sacrificial screw tip. Tubex piles, on the other hand, use a thin-walled sacrificial steel tube with a screw tip permanently welded to the bottom. Because the tube remains in-situ, a reinforcement cage is often not needed and so only concrete is placed in the tube after installation.

The combined screwing and injection makes it challenging to understand how different pile sizes, screw tip shapes and installation parameters (e.g. penetration rate, crowd force, revolutions per minute, grout flow rate, grout pressure, grout water-cement ratio) affect the base and shaft response under axial loading, particularly given the interdependencies between the parameters. An increased crowd force, for instance, increases the penetration rate and subsequently requires an increased grout flow rate to maintain the grout body

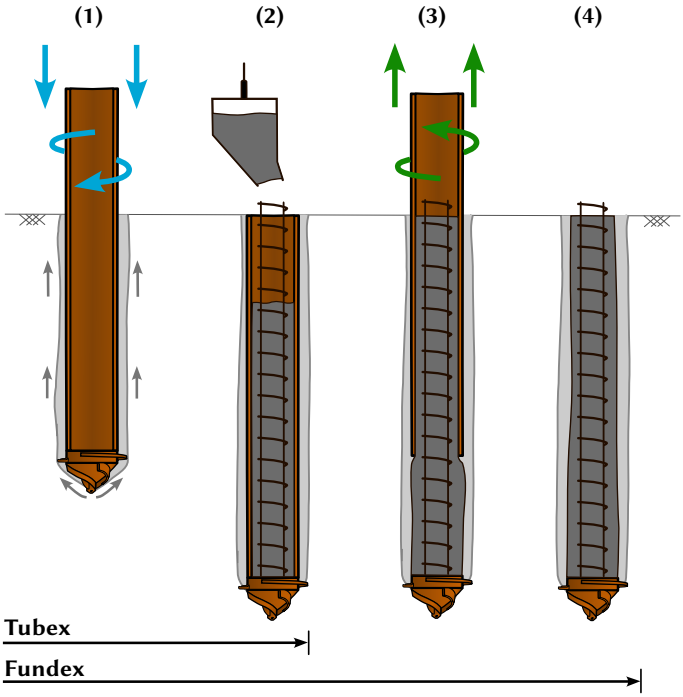

(1) The casing is installed using a torque and crowd force, whilst grout is injected from the pile tip and passing up to the surface.

(2) At the target depth, reinforcement is placed in the empty casing and concrete is poured. For Tubex piles, the strength provided by the casing is often sufficient.

(3) Fundex piles only: the casing is extracted using a pull-up force and alternating clockwise and anti-clockwise rotations.

(4) A completed Fundex pile, consisting of a concrete core, grout shell, reinforcement and sacrificial screw tip.

Figure 3.2: Installation procedure of two types of screw injection piles: Fundex and Tubex.

around the pile. For example, research from screw anchors (Sharif et al., 2021; Bittar et al., 2023; Cerfontaine et al., 2023) has demonstrated how the installation resistance and pile capacity is highly dependent on the advancement ratio (Equation 2.4). However, extrapolation of these results to screw injection pile—and screw displacement piles in general—should be done with caution because of the distinct differences in pile geometries and installation procedures.

Some tests have been specifically performed on screw injection piles. Admiraal et al. (2022) performed tension load tests in the field on fifteen scaled screw injection piles, investigating how grout injection parameters such as flow rate and water-cement ratio affected the pile shaft resistance. The results indicated that different water-cement ratios in the grout mixes did not create any observable changes in the piles' tensile capacities, although higher grout flow rates may lead to lower ultimate shear stresses. Other research (van Baars et al., 2018; van der Geest et al., 2020) investigated the axial compressive response of screw injection piles with different tip geometries and installation procedures. However, difficulties with interpreting the instrumentation meant clear conclusions on the base capacity of full-scale screw injection piles could not be made. In summary, the static load tests from Amaliahaven (Chapter 2), remain one of the few well-instrumented tests on screw injection piles, particularly where the pile base resistance has been properly interpreted.

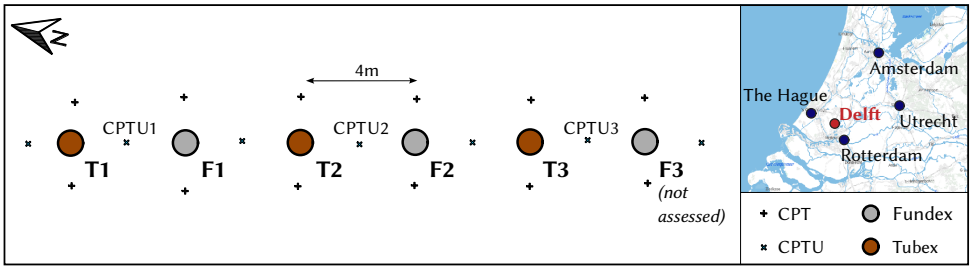

Figure 3.3: Layout of the Delft test site at Flood Proof Holland (inset map courtesy of www.pdok.nl).

3.3. Experimental programme

3.3.1. Ground conditions

Pile installation and testing was performed in early 2022 at the Flood Proof Holland test site on the campus of TU Delft. Six screw injection piles were installed, spaced at least four metres apart (Figure 3.3). Prior to installation, four CPTs were performed within two metres of each pile location. The upper two metres of the site was a made ground fill composed of coarse sand, gravel and cobbles. Underneath this were six metres of soft Holocene clay and clayey peat with CPT cone resistances of around 0.2 MPa (Figure 3.4), underlain by a two-metre-thick medium-dense sand layer and a three-metre-thick firm clay layer. The test piles extended through these layers and down to a medium dense to dense sand layer located 16 m below ground level. This founding layer had cone tip resistances between 10 to 25 MPa, with an average value of around 15 MPa. This sand layer is the same geological formation as that of GU3 at Amaliahaven, that is, the late-Pleistocene fluvial sand known as the Kreftenheye Formation. For the purpose of pile test interpretation, the ground profile has been stratified into the Ground Units outlined in Table 3.1.

Table 3.1: Ground units used for the interpretation of the Delft pile tests.

Unit	Soil type	Geological formation	Depth (m)	Mean q_c (MPa)
GU1	Very soft to soft CLAY and clayey PEAT	Nieuwkoop & Naaldwijk Formations	0.0–8.0	0.3
GU2	Loose SAND and firm sandy CLAY, with medium bed of peat	Nieuwkoop & Echteld Formations	8.0–16	1.0
GU3	Medium dense to dense coarse gravelly SAND	Kreftenheye Formation	16.0–30.0	14.9

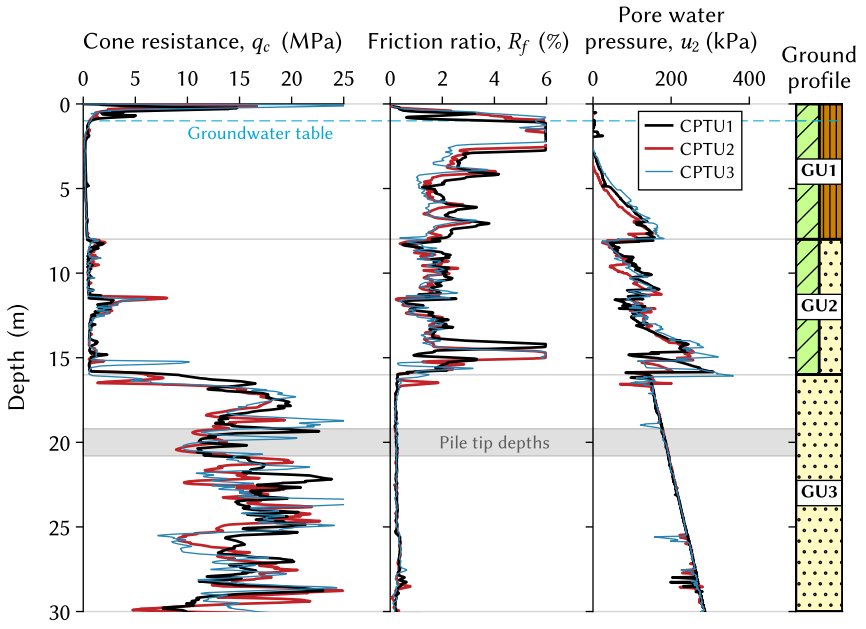

Figure 3.4: Selected CPTs from the Delft test site. The location of each CPT is given in Figure 3.3.

3.3.2. Pile geometry and installation

Three screw injection piles with a reusable casing (F1, F2 and F3, Fundex piles) and three with a permanent casing (T1, T2 and T3, Tubex piles) were installed by the contractor Fundex Piling Group to compare the base and shaft response of two different types of screw injection piles under similar site conditions. Both pile types had identical screw tips (Figure 3.5), with a single helical screw flange measuring 470 mm at its outermost diameter. Two injection outlets were located in these tips, facing in opposite directions. These outlets injected grout with a water-cement ratio of 1.5 until just above the target depth, from which point the piles were screwed in an additional 25 cm without any grout injection.

The Fundex piles were installed by a reusable casing with an outer diameter of 380 mm and a wall thickness of 32 mm. The soft upper clay layer increased the risk of pile bending and structural failure, particularly in the event of eccentric loading. To mitigate this risk, a single H-beam profile (HEB 160) was used as reinforcement in the Fundex piles and was placed in the reusable casing before concrete pouring, resting directly on the screw tip. For the Tubex piles, each screw tip was welded to a sacrificial tube with an outer diameter of 382 mm and a wall thickness of 13 mm. Because the steel tube remained in-situ after installation, no additional steel reinforcement was used. All piles were filled with C45/55 concrete.

A key consideration in the installation of screw injection piles is balancing the incoming and outcoming grout flow rate, helping to reduce the installation resistance and to create a continuous grout shell around the pile. During installation of the first pile, pile T1, no grout

Table 3.2: Overview of the screw injection piles tested at Delft.

Pile	Diameter D (mm)	Length L [a] (m)	$q_{c,filter}$ (MPa)	$q_{c,4D/8D}$ (MPa)	Pile age (days)
Installed with a reusable casing (*Fundex*)					
F1	470	20.0	11.9	10.0	65
F2	470	19.2	13.3	8.9	70
F3[b]	470	20.0	12.4	9.4	—
Installed with a permanent casing (*Tubex*)					
T1	470	19.9	11.3	9.6	64
T2	470	20.3	11.3	9.2	68
T3	470	20.8	14.8	12.1	73

[a] The pile base elevation was defined as the shoulder of the conical tip (35 cm in height).
[b] Test results of pile F3 not assessed because of problems with casing extraction.

outflow was observed at the ground surface despite the constant rate of incoming grout at 120 L/min (Figure 3.6d). This suggests that some of the grout may have percolated through permeable soil layers or created enlarged areas of the pile shaft in the softer layers. For the remaining Tubex piles, the penetration velocity was reduced through the upper layers and the grout flow rate was increased to 180 L/min to encourage more grout outflow, but no grout outflow was subsequently observed. The Fundex piles used the same incoming grout flow rate as piles T2 and T3, albeit with a higher penetration velocity to reduce the risk of the screw tip dislodging from the casing during penetration. Grout outflow was observed for piles F1 and F2 as the pile penetrated through the lower sand layer GU3 but no outflow was observed across this layer for pile F3. In spite of the issues with grout outflow, the advancement ratio (Equation 2.4) in GU3 was kept at pitch-matched ($AR = 1$) for all five piles.

Subsequent problems with extracting the reusable casing of pile F3 meant that the pile was of insufficient quality to be considered a suitable test pile. As a result, pile F3 has not been considered further.

3.3.3. STRAIN INSTRUMENTATION

All piles were instrumented along their full length with steel-reinforced fibre optic cables. For the Fundex piles, the fibre optic cables were glued to the H-beam reinforcement at its two flanges and in the centre of the web. For the Tubex piles, two 5 mm deep grooves were formed in the outside of the casing (Figure 3.5) into which a fibre optic cable was glued. Both pile types were instrumented in an indoor, temperature-controlled environment and the steel was scoured and degreased before gluing with two-part epoxy.

During load testing, the cables were interrogated using Brillouin Optical Frequency Domain Analysis (BOFDA) through a fibrisTerre fTB 5020 interrogator. This process gave a continuous profile of strain along the length of the pile at a spatial resolution of 20 cm and at a frequency of 90 seconds. Strain readings were then converted to a normal force based on the stress–strain response of the upper part of the pile and using the tangent and secant stiffness method described by Fellenius (2001). The measured stiffness response agreed well

Figure 3.5: The base of a Tubex screw injection pile. The Fundex pile also uses an identical screw tip.

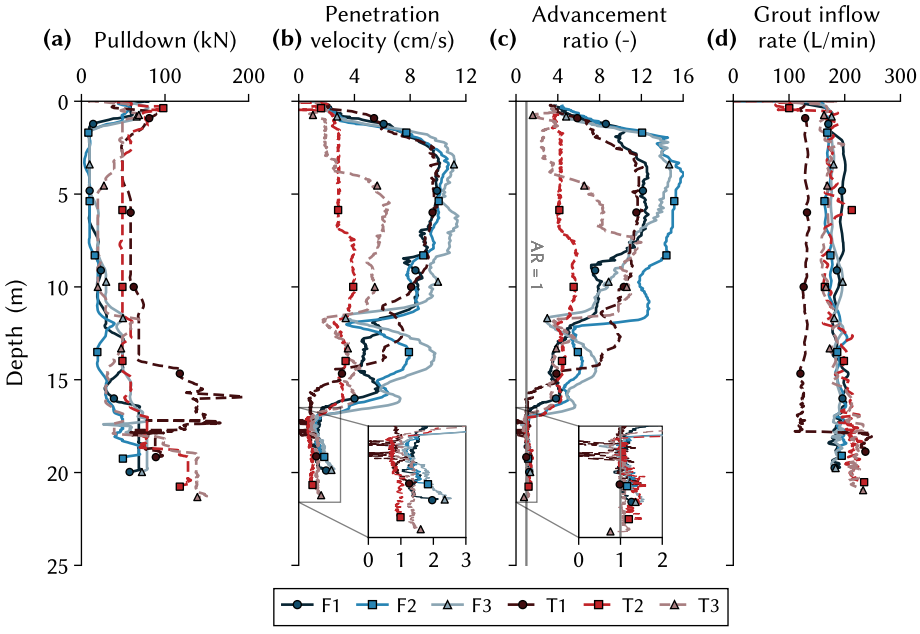

Figure 3.6: Installation results of the six piles at Delft. The pullup force was not recorded and so the pulldown force is considered as the maximum applied crowd force.

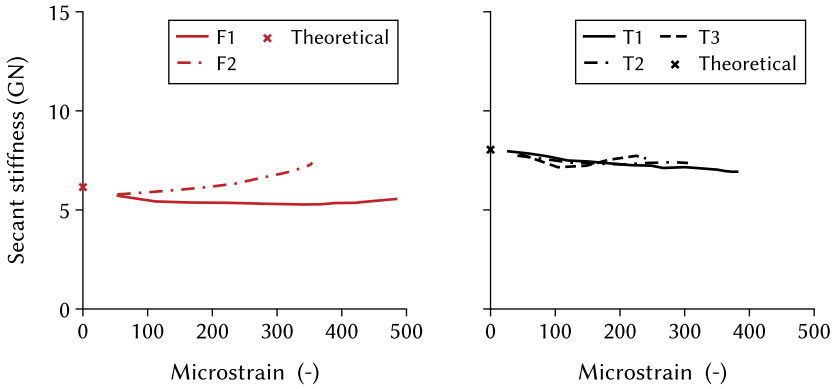

Figure 3.7: Secant stiffness measured by the uppermost strain readings in each pile. The theoretical initial stiffness was derived using the composite steel-concrete-grout stiffness.

Table 3.3: Decision tree for the termination or extension of each load step, based on the creep parameter k (Equation 2.5)

$k < 0.75$ mm	Increase load by full step
0.75 mm $< k <$ 2.00 mm	Increase load by half step
$k > 2.00$ mm (and decreasing or stable)	Increase load by a quarter step
$k > 2.00$ mm (and decreasing or stable)	Continue load-holding period. If an additional 60 mins have elapsed, increase by a quarter step

(Figure 3.7) with the theoretical initial stiffness—derived using the composite steel-concrete-grout stiffness, and assuming a grout stiffness of 10 MPa and a shaft diameter of 470 mm. As expected, a slight degradation in stiffness with increasing strain is visible across most of the piles. The only outlier is pile F2, which shows an apparent strain-hardening response with increasing strain.

Variations in stiffness are inevitably expected along the length of the pile because of potential changes in material strength and pile diameter. However, since the piles were not extracted following testing, a constant stiffness has been assumed for the entire length of the pile.

3.3.4. Load test procedure

All piles were subjected to incremental, axial compression loads using a single hydraulic jack and a reaction provided by kentledge (Figure 3.8). To reduce the risk of prohibitively long test times and to accurately capture the failure point of the test pile, the creep criteria in Chapter 3 (i.e. from NPR 7201) was adjusted. Until a load of 50 % of the predicted pile capacity, the minimum duration of each load step was thirty minutes; beyond this load, the load was held for at least sixty minutes. At the end of each step, the creep criteria in Table 3.3 determined if the load step was to be held for longer, and if not, the load was increased by the specified amount.

To measure the pile head displacement, four potentiometers were installed around the

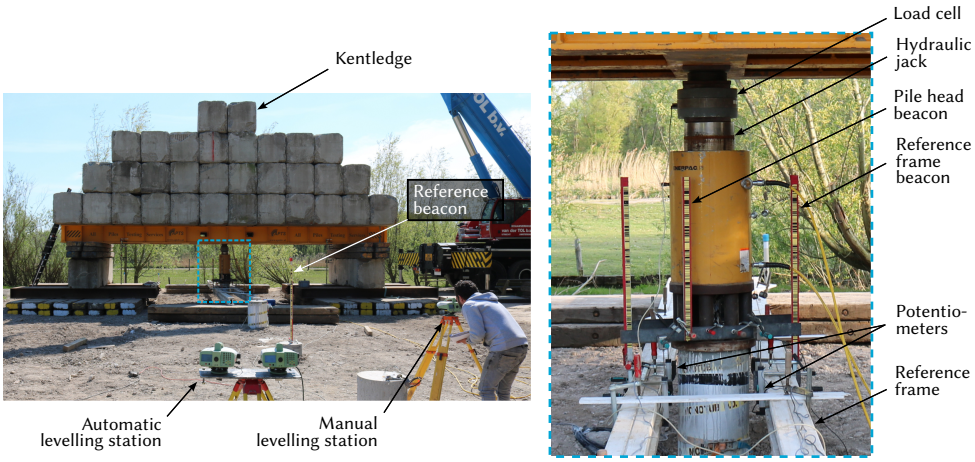

Figure 3.8: Test set-up at Delft, with a kentledge frame used to load the piles in axial compression.

pile head and measured with respect to two wooden reference beams either side of the pile (Figure 3.8). These displacement measurements were also cross-checked by two different levelling stations, located around 10 – 20 m away from the pile. A steel rod known as a telltale was left free-standing in a tube within each pile, resting directly on the pile tip. By measuring the change in elevation of the top of the telltale with respect to the pile head, the elastic compression of the pile body could be deduced and so the telltale acted as a verification of the pile base settlement derived from the BOFDA strain measurements.

The piles were unloaded once the pile base displacement reached at least 0.1D. Thereafter, an attempt was made to reload the pile to this failure load.

3.4. Experimental results

3.4.1. Load-displacement response

All piles showed very similar load-displacement responses up to a load of around 1.2 MN (Figure 3.9). From this point, piles F1, F2 and T1 reached maximum loads of approximately 2.6 MN, each exhibiting rapid plunging failure and bringing the piles to the 0.1D failure criterion. Load cycles at the end of the the initial tests failed to return to these maximum loads. Up until a load of 2.3 MN, pile T2 responded similarly to these three piles. However, one hour into this load step, the pile displaced suddenly and the hydraulic pump could not pump quickly enough to sustain the 2.3 MN load. Subsequent load cycles could not reach loads greater than 1.5 MN because of the high displacement rate of the pile.

On the other hand, the behaviour of pile T3 was notably different to the other piles: the pile exhibited high creep rates during maintained load steps from 1.0 MN onwards. The pile reached the 0.1D failure criterion at a maximum load of 1.7 MN, with very large pile head displacements occurring at this load. In the subsequent reload cycle, the pile reached peak loads similar to the load at failure.

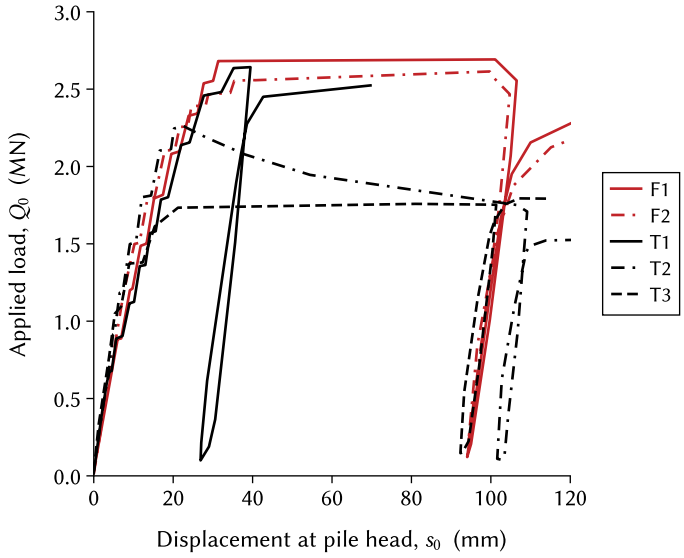

Figure 3.9: Load-displacement response of the screw injection piles under axial compressive loading.

3.4.2. Load distribution

The measured axial force distribution with depth shows several distinct features (Figure 3.10). All five piles transferred little of the applied load to GU1 in the first 8 m below the surface. From 8 m to 16 m, the higher shaft resistance of the loose sand and firm clay led to a greater reduction in the axial force compared to the soft clay. Piles F1 and F2 showed localised deviations in the measured load across this ground unit, particularly when compared to the Tubex piles. These deviations can potentially be explained by the removal of the steel tube of the Fundex piles, increasing the chance of localised changes in pile stiffness or cross-sectional area.

The load distribution distinctly changes at the boundary between GU2 and GU3 at 16 m depth. At this boundary, the apparent axial force in piles F1, F2 and T1 reduces rapidly with depth to the pile base. Contrastingly, piles T2 and T3 show a different pattern. Taking pile T2 for instance, the load distribution is similar to that of pile T1 up until a load of 2 MN. However, one hour into the 2 MN load step, sudden displacement of the pile led to a corresponding reduction in its total capacity. When the pile reached an equilibrium at 1.5 MN, the slope of the load distribution changed in GU3 (Figure 3.10). Little to no reduction in load was exhibited across this ground unit, implying that little shear resistance could be mobilised. This same effect is also shown in pile T3 for applied loads greater than 1 MN. Beyond this load, high creep rates were observed at the pile head during load-holding periods.

It is likely that structural failure occurred in Tubex piles T2 and T3: that is, either a shear failure in the grout body itself or else adhesive failure at the grout–steel interface, similar to that described in Chapter 2. Because of the structural failure, piles T2 and T3

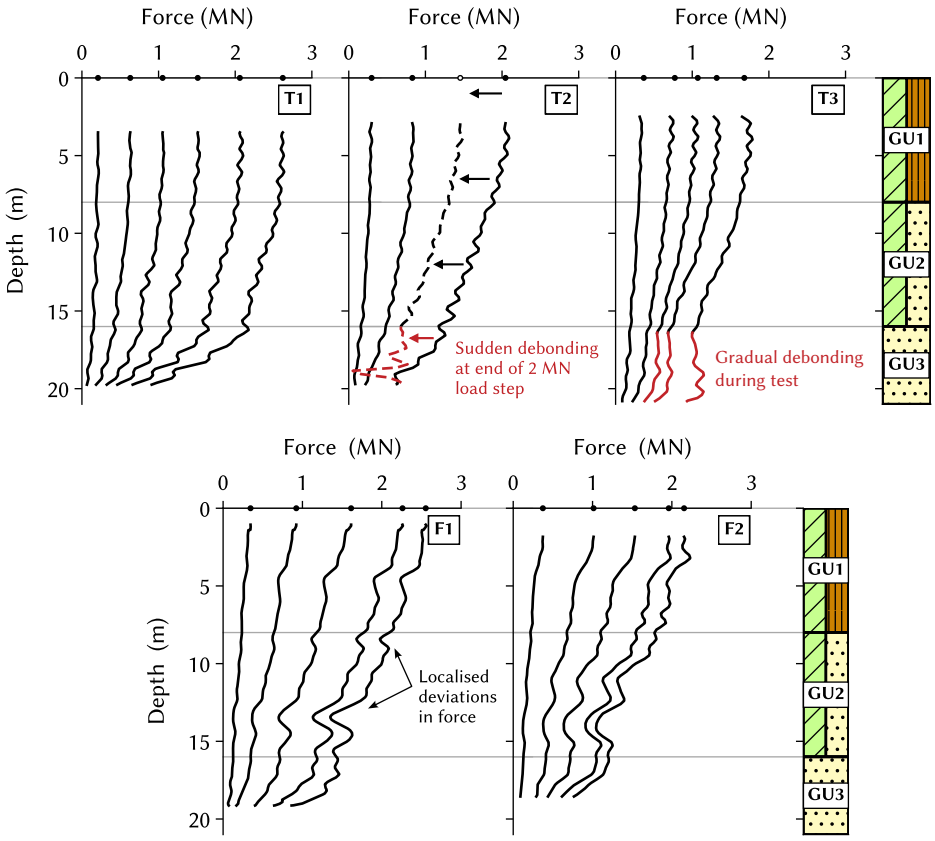

Figure 3.10: Axial force distribution measured by the BOFDA system during each test. The load cell readings on top of the pile are given by discrete points.

mobilised little to no shaft resistance in the primary load-bearing unit GU3. The reduction in available shaft capacity also corresponds to a lower total load at failure (Figure 3.9). At plunging failure, piles T2 and T3 could only mobilise a load around 1.0 MN less than the other test piles—piles which showed no evidence of structural failure in their measured load distributions.

The installation conditions likely affected the structural integrity of the piles. During installation, no return grout flow was observed in all three Tubex piles, suggesting that some grout may have either percolated in between permeable and impermeable layer or caused localised bulges in the soft, impermeable clay and peat. Screw injection piles, both in industry practice and during these tests, typically use a relatively high water-cement ratio of 1.5. For future test sites or projects, a reduced water–cement ratio may improve the shear resistance and adhesive resistance of the grout, although dummy piles should be used to verify that the mix provides sufficient fluidisation.

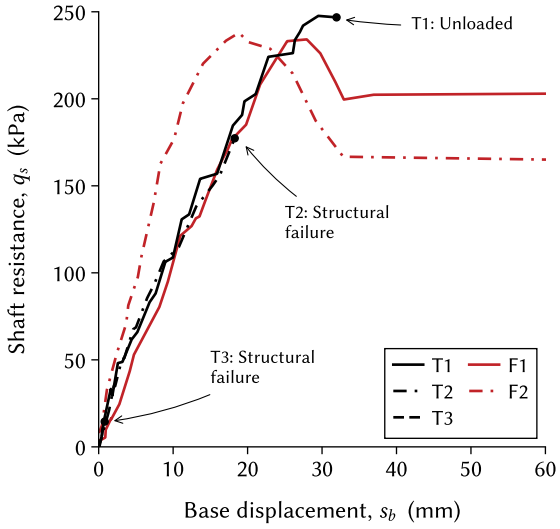

Figure 3.11: Shaft response of the screw injection piles in the lower sand layer GU3.

3.4.3. Shaft resistance

While this chapter primarily focusses on the base resistance of the test piles, the peak shaft resistances mobilised in each layer is presented in Table 3.4. To understand the response of each pile in the primary load-bearing layer, the full shaft response in the lower sand layer GU3 is also presented in Figure 3.11. The two Fundex piles, F1 and F2, mobilised maximum shaft resistances of 225 kPa at displacements between 15 and 25 mm. Both piles show post-peak softening with increasing displacement, reducing the shaft resistance to between 150 and 200 kPa. Tubex pile T1 also mobilised its resistance at a similar rate to the Fundex piles, reaching a maximum value of 240 kPa. However at this resistance, the pile was unloaded and so no clear softening could develop in the shaft response. Lastly, piles T2 and T3 reached maximum shaft resistances in GU3 of only 175 kPa and 15 kPa respectively before debonding occurred at the grout-steel interface.

3.4.4. Base resistance

To determine the base resistance, the load distribution was extrapolated to the pile base from the lowermost strain reading, a reading always within one pile diameter from the pile base. To convert from a resistance to a stress, the maximum diameter of the helical screw was used (=470 mm). Grout injection stopped 25 cm prior to the pile reaching its final depth, so it is assumed that no grout is present underneath the screw tip.

The base resistances mobilised by piles T1, T2, F1 and F2 were very similar until a pile base displacement of 15 mm (Figure 3.12). After this point, the responses diverged: pile T1 reached the highest resistance of 5 MPa, pile T2 the lowest of 2.5 MPa and the two Fundex piles reached resistances in between these two extremes. The third Tubex pile, pile T3, appeared to behave much stiffer than the four other piles, although its response may have been affected by the structural failure of the grout body early on in the test. Ultimately,

Table 3.4: Peak shaft resistances mobilised by each pile at Delft. Piles T2 and T3 failed structurally in GU3 and so the full shaft capacity was likely not reached.

	$q_{s,avg}$ (kPa)			α_s (-)		
Pile	GU1	GU2	GU3	GU1	GU2	GU3
F1	33	64	233	0.127	0.062	0.017
F2	49	50	235	0.213	0.057	0.018
T1	9	34	247	0.031	0.034	0.017
T2	19	49	176	0.070	0.051	0.012
T3	19	50	33	0.076	0.070	0.002
Mean	26	49	185	0.103	0.055	0.013
COV (%)	60	21	48	68	25	51

Table 3.5: Base resistances mobilised by each pile at Delft, including α_p derived by each averaging method. An explanation of each averaging method is given in Chapter 3.5.1.

		α_p (-)			
Pile	$q_{b,0.1}$ (MPa)	Filter	4D/8D	De Beer	LCPC
F1	3.0	0.25	0.28	0.29	0.25
F2	3.5	0.27	0.39	0.37	0.28
T1	4.8	0.39	0.49	0.48	0.35
T2	2.4	0.24	0.29	0.29	0.23
T3	4.7	0.34	0.38	0.38	0.34
Mean	3.6	0.30	0.36	0.36	0.29
COV (%)	29	21	23	22	19

pile T3 yielded a maximum base resistance of 5 MPa, similar to pile T1.

To account for variations in soil conditions around the pile base, the base resistances have been normalised by the adapted filter method $q_{c,filter}$ (de Boorder et al., 2022), shown in Figure 3.13. At a pile base displacement of 10 % of the pile diameter, the normalised resistances α_p ranges from 0.20 to 0.30 for four of the five piles. Additional gains in capacity are marginal at displacements beyond $0.1D$. The only exception is pile T1, which reached an α_p of around 0.40.

Considering standard specific averaging methods (Table 3.5), the α_p factors range from 0.25 to 0.45 when using the 4D/8D averaging method prescribed by the Dutch standard (van Mierlo and Koppejan, 1952; NEN, 2017b) and from 0.30 to 0.45 when using the de Beer method (de Beer, 1971) in the Belgian standard (NBN, 2022). These mobilised values are much closer to the α_p values of a non-displacement pile where α_p ranges from 0.25 to 0.50 in both standards. This suggests that pile installation at the Delft test site created little to no improvement in the pile base resistance, performing like a low displacement pile or a bored pile.

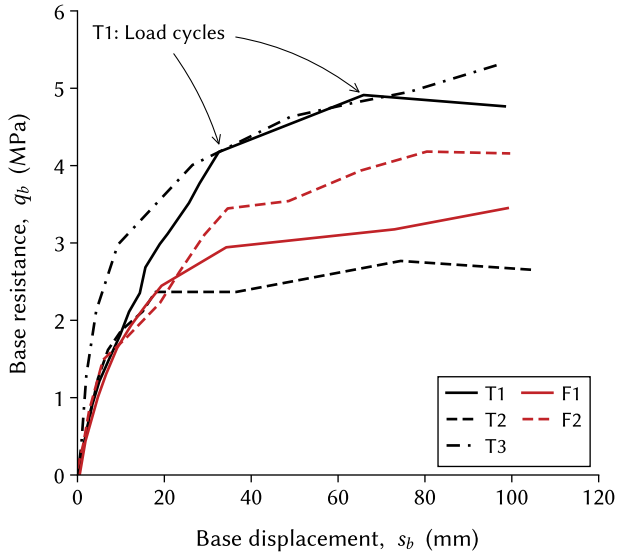

Figure 3.12: Measured base response of the screw injection piles.

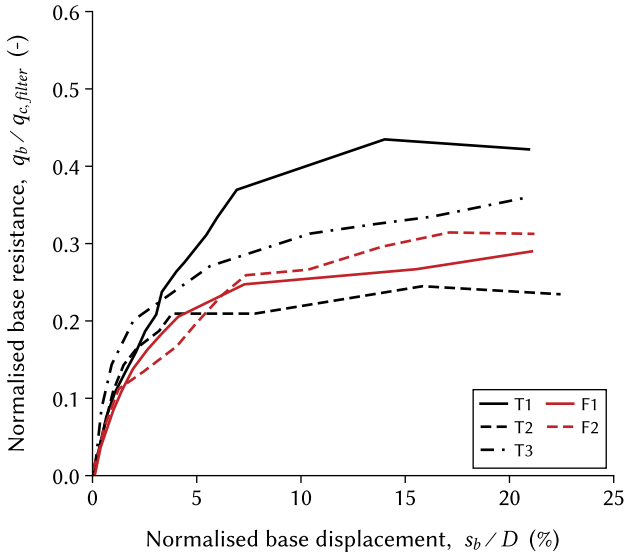

Figure 3.13: Normalised base response using the adapted filter method.

3.4.5. Comparison with the Amaliahaven pile tests

When comparing the Delft results in medium dense sand with the screw injection piles at Amaliahaven in very dense sand (Figure 3.14), the piles are mainly differentiated by the rate at which they mobilised their base capacity. At a normalised base displacement of $0.1D$, all piles mobilised α_p values of roughly 0.30. However, the piles at Delft responded much stiffer compared to the Amaliahaven test piles, mobilising most of their resistance within a displacement of 5 % and showing a clear plunging failure beyond this point. In contrast, the Amaliahaven piles mobilise their base resistance much more gradually, with the base stress continuing to rise as the normalised displacement approached 10 %.

The installation procedure was relatively comparable for all sets of piles, which were all installed "in-the-dry" towards the end of installation—a typical industry practice where the grout injection is turned off to prevent loosening the soil around the pile base. At Amaliahaven, the very dense sand meant that the piles could only penetrate a couple more centimetres without grout injection, whereas at Delft, the piles penetrated 25 cm without grout injection.

Mechanistically-speaking, some insights during this phase can be gained from research on screw anchors (Sharif et al., 2021; Bittar et al., 2023; Cerfontaine et al., 2023), albeit where the relative proportion of the stem-to-helix diameter in a screw anchor is much smaller than the casing-to-helix diameter of a screw injection pile. The research showed that the advancement ratio (Equation 2.4) has a large effect on a screw anchor's installation resistance and its ultimate capacity. At Amaliahaven and Delft, the advancement ratio ranged from 0.6 to 1.3 (Figure 3.15), with pile SI2 being the one notable exception—installed at $AR = 1.8$. Nevertheless, the mobilised α_p values show no clear trend across the range of advancement ratios.

Similarly, installation-induced changes in the stresses underneath the pile base can influence the rate at which the piles mobilise their base resistance, analogous to differences observed between full-displacement driven precast piles and non-displacement bored piles (e.g. Gavin and Lehane, 2007). While the base stresses were not measured during installation, the crowd force applied on the pile head (taken as the pulldown force $Q_{pulldown}$ because of the lack of pullup measurements at Delft) can be seen as the maximum stress at the pile base. Similar to the advancement ratio, no clear trend can be seen between the normalised pulldown force and α_p (Figure 3.15).

In summary, no clear correlation between the installation parameters and the mobilised α_p can be observed from the results at Delft and Amaliahaven. Nevertheless, the screw injection piles at the two sites differ by the rate they mobilise their base resistance. This mobilisation rate is likely correlated to the relative density (and soil stiffness) at the two sites, in line with findings from previous studies (e.g. Fleming, 1992; Atkinson, 2000; Gavin and Lehane, 2007).

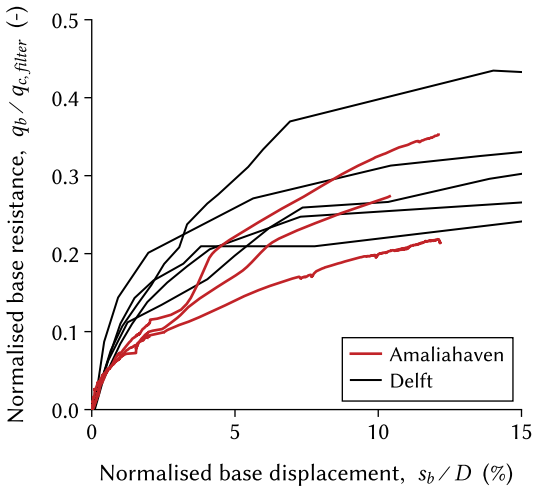

Figure 3.14: Comparison of base mobilisation rates the Amaliahaven and Delft test piles.

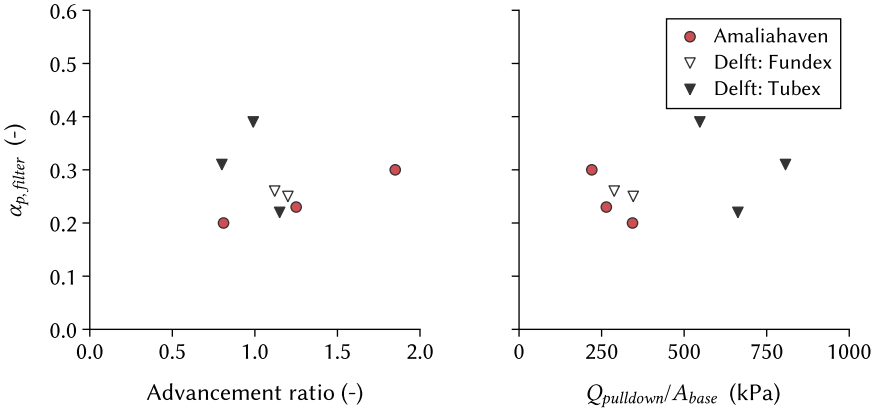

Figure 3.15: Comparison of installation parameters over the final part of installation to $\alpha_{p,filter}$ at a displacement of $0.1D$, where the pulldown force is normalised by the area of the pile base

3.5. Database assessment

To investigate if the base response was affected by ground and installation conditions specific to screw injection piles, the analysis was expanded to a broader assessment of screw displacement piles. Twenty-four tests were selected (Table 3.6) from the larger database presented in Appendix A. Each one of the selected tests directly measured the pile base resistance and loaded the pile to displacements of at least 5 % of the pile diameter. At least one CPT was performed near each pile, giving a clear profile of the soil stratigraphy around the pile base. The outermost diameter D was used to determine the pile base resistance—generally the width of the helical flange at the screw tip.

For simplicity, these piles have been categorised into four types: Type 1, Type 2, Type 3 and Type 4 piles, described in detail in Chapter 4.2.

3.5.1. Influence of partial embedment

It is well-documented (Ahmadi and Robertson, 2005; White and Bolton, 2005; Xu et al., 2008; de Lange, 2018; van der Linden et al., 2018; Tehrani et al., 2018; Chai et al., 2025) that the tip resistance of a pile and a CPT cone depends on the soil conditions within a zone above and below the tip. These soil conditions can be accounted for in design using so-called averaging methods. With this in mind, four averaging methods are considered:

- The **4D/8D method** (van Mierlo and Koppejan, 1952; Reinders et al., 2016), also known as the Dutch method or the Koppejan method, assumes a Prandtl-wedge failure mechanism in sand, propagating into a logarithmic spiral shaped failure mechanism up to four pile diameters below the pile tip and eight pile diameters above the pile tip. To derive $q_{c,avg}$, the method combines the weighted average of q_c values in this zone with a minimum path rule—a rule which essentially prioritises the effect of weak layers on $q_{c,avg}$. The method is proposed in the Unified design method for driven piles in sand (Lehane, Liu, et al., 2020) as well as in the Netherlands (NEN, 2017b) where α_p for screw displacement piles is 0.63.
- The **De Beer method** is based on the averaging method developed by Meyerhof (1959) which assumes a logarithmic spiral failure plane like the 4D/8D method. De Beer (1971) updated the method with an analytical approach that takes the scaling effect into account between a CPT and a pile. The De Beer method is popular in Belgium where screw displacements piles are widely used and researched, most notably the test campaigns on screw displacement piles at Limelette (Huybrechts and Whenham, 2003) and Sint-Katelijne-Waver (Huybrechts, 2001). Using the De Beer method, the Belgian standard (NBN, 2022) prescribes an α_p of 0.50
- The **LCPC 1.5D method** (Bustamente and Gianeselli, 1982) arithmetically averages the q_c values in a zone 1.5 pile diameters above and below the pile tip, limiting the q_c values to ± 30 % of the arithmetic average. The LCPC method is generally considered the most common averaging method (Bittar et al., 2022). The French design method (AFNOR, 2018; Verheyde and Baguelin, 2019) prescribes an α_p of 0.50 for screw displacement piles using a variant of the original LCPC method, later described in Chapter 4.
- The **adapted filter method** (de Boorder et al., 2022) is a simplification of the filter

Table 3.6: Database of static load tests on screw displacement piles in sand, where the base resistance was directly measured.

Site & Pile	Pile Type	D [a] (mm)	L (m)	$s_{b,max}/D$ (%)	$q_{b,0.1D}$ [b] (MPa)	$q_{c,filter}$ (MPa)	$q_b/q_{c,filter}$
Type 1: Smooth shaft							
Beemster P2	Fundex[c]	150	2.9	28	7.0	15.0	0.47
Beemster P3	HEK pile[c]	150	2.9	27	7.0	31.3	0.22
Beemster P6	Fundex[c]	150	2.9	25	8.4	20.3	0.41
Beemster P7	HEK pile[c]	150	2.9	29	7.0	31.6	0.22
Type 2: Helical shaft							
Zeeland O1	Olivier	460	9.1	14	3.4	14.6	0.23
Zeeland O2	Olivier	460	8.0	11	5.9	22.0	0.27
Zeeland O3	Olivier	460	9.5	14	6.5	17.0	0.38
Type 3: Displacement body							
Elblag P9	DPDT	400	7.5	6	3.7	9.7	0.38
Grottgera P600	SDP	400	11.0	10	3.0	9.7	0.31
Loenhout S2	Omega	410	9.5	14	2.8	9.4	0.30
Lomme P1	De Waal	360	8.5	9	5.2	26.2	0.20
Oostende P1	Omega	460	21.6	10	4.2	30.1	0.14
Pruszcz b1	SDC	356	7.5	5	4.0	9.8	0.41
Żuławy P6293	CMC	400	12.6	11	2.6	7.0	0.37
Type 4: Screw injection							
Amaliahaven SI1	Tubex	850	37	11	9.6	35.8	0.27
Amaliahaven SI2	Tubex	850	37.1	12	10.5	52.7	0.20
Amaliahaven SI4	Tubex	850	34.1	12	9.9	29.9	0.33
Delft F1	Fundex	470	20.0	23	3.0	11.9	0.25
Delft F2	Fundex	470	19.2	23	3.5	13.0	0.27
Delft T1	Tubex	470	19.9	23	4.8	12.3	0.39
Delft T2	Tubex	470	20.3	26	2.4	9.9	0.24
Delft T3	Tubex	470	20.9	22	4.7	13.9	0.34
Haren P1	Fundex	660	16.4	8	8.2	13.7	0.60
Rosmalen P3	Tubex	400	7.4	22	1.4	12.0	0.12

[a] The outer diameter of the pile at the pile tip was used.
[b] If $5\% \leq s_b/D \leq 10\%$, extrapolation to 10 % was performed using the method by Chin 1970.
[c] The tests at Beemster were scaled versions of existing pile types.

method by Boulanger and DeJong (2018) and is calibrated against penetrometer tests in interlayered soils (de Lange, 2018). In general, the filter method aims to correct for the influence of surrounding layers on the base resistance by using two weighting factors: one factor accounting for the distance from the pile base and the second factor accounting for differences in soil strength. The filter method itself has been shown to improve on existing averaging methods when analysed in laboratory and field tests (Bittar et al., 2022) and is recommended for use in the recently developed Unified design method for driven piles in sand (Lehane, Liu, et al., 2020).

Figure 3.16 compares the α_p from these four different averaging methods to the normalised distance L_p/D between the pile base and an overlying clay layer, referred to as the pile embedment into sand. Across the dataset, the mean α_p using the 4D/8D and De Beer methods is 0.48 and 0.60 respectively. Crucially, the mean value is affected by high variation in α_p at low embedment depths, in other words, when the pile base is located close to the boundary between a weak upper layer and the founding sand layer. In contrast, the LCPC and adapted filter methods give mean α_p values of around 0.30 Across these two averaging methods, the variation is much smaller and consistent across all embedment depths compared to the 4D/8D and De Beer methods.

The variation suggests that particular care should be taken when using the 4D/8D and De Beer averaging methods for shallow penetration of piles in the founding sand layer. This is in line with reviews (Randolph, 2003; White and Bolton, 2005) of a driven precast pile database where partial embedment was found to introduce variation and geometrical trends in α_p across the database. The LCPC and adapted filter methods give very similar results for the piles in the database. In general, this similarity can be expected for homogeneous sands, as was the case for the piles in the database. For more variable or interlaminated sand layers, the adapted filter method should be considered (Lehane, Liu, et al., 2020).

3.5.2. Influence of pile geometry

When α_p is determined using the LCPC or the adapted filter methods, the database has a coefficient of variation (COV) in α_p of around 35 % across all piles. Comparing piles within individual test sites, the within-site variation ranges from 16 % (Amaliahaven) to 36 % (Zeeland)—for sites where at least three piles were tested. To put these values into context, the COV from other pile databases is 23 % for closed-ended driven piles (Xu and Lehane, 2008), 30 % for driven cast-in-situ piles (Flynn and McCabe, 2021) and 17 % for non-displacement piles (Gavin et al., 2013) when using the LCPC averaging method. Patently, the presented screw displacement pile database shows higher variability in α_p when compared to other load test databases.

To investigate the variation further, α_p is compared to the pile length, pile diameter, pile slenderness and $q_{c,LCPC}$ (Figure 3.17). Despite the variation in α_p, no clear trend is evident with pile length, pile diameter or pile slenderness. In terms of the design cone resistance $q_{c,LCPC}$, no clear trend is shown between resistances of 10 to 40 MPa, although more data is needed beyond 40 MPa to confirm the existence or non-existence of any trend.

The database includes a range of pile tip shapes. Not only do these vary across different types of screw displacement piles, but variations also occur within each pile type because of different construction procedures, soil conditions or hydrological conditions. These

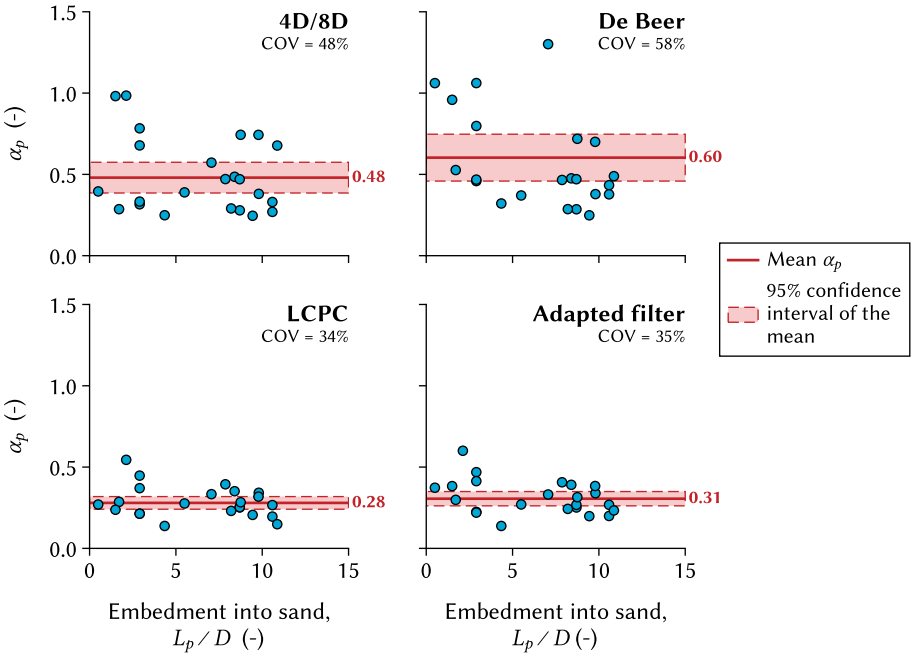

Figure 3.16: Variation in α_p using four different averaging methods to determine $q_{c,avg}$ (and correspondingly, α_p).

variations can influence the mobilisation rate and the ultimate value of the pile base resistance (Sharif et al., 2021; Tovar-Valencia et al., 2021) . However almost all the piles in the database were not extracted after testing and so the true realised shape of each pile is unknown. Consequently, it is likely that some of the variability in the ultimate base resistances can be attributed to differences in realised pile base geometries, incurred by both installation-related effects on the surrounding soil, concrete pouring and casing extraction.

3.5.3. Influence of pile installation

As well as differences in pile tip geometries, some variation in the base resistances may have been caused by changes in installation procedures. This includes variations not just between different screw displacement pile types, but also within each pile type. Some influencing parameters include the installation energy, rate of penetration, concreting pressure or the rate of extraction of augers or reusable casings (Bustamente and Gianeselli, 1998; Slatter, 2000; W. F. van Impe, 2001).

Assessing the influence of installation on the pile base capacity was not possible because of the lack of complete installation data reported by the database records. Comparing the different screw displacement pile types to one another, no distinct differences in the mean α_p can be observed. For instance, screw displacement piles installed with grout injection (Type 4 piles) and those without grout injection (Types 1, 2 and 3), yielded mean α_p values

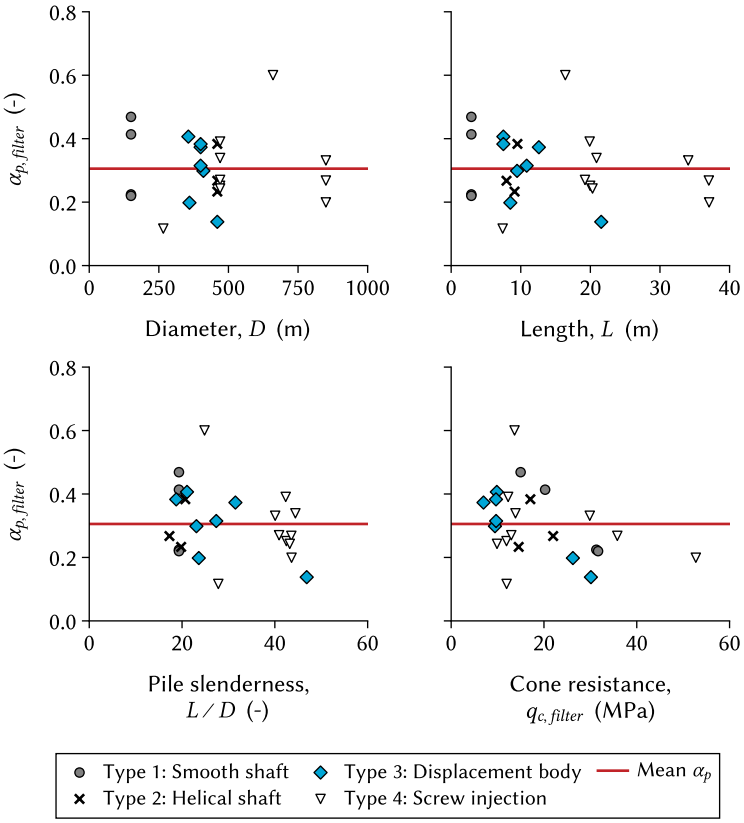

Figure 3.17: Variation in α_p with pile geometry and soil conditions.

of 0.28 and 0.27 respectively. Alternatively, screw displacements piles with a helical shaft (Type 2 piles) and those with a smooth shaft (Types 1, 3 and 4) yielded mean α_p values of 0.28 and 0.24 respectively.

A component also not considered in the database is the influence of residual loads. For cast-in-situ piles, residual loads can develop from volumetric changes in curing concrete and also from the dissipation of excess pore pressures in cohesive soils, inducing a downdrag on the pile (Fellenius, 2002; Siegel and McGillivray, 2009; Flynn et al., 2012; Krasiński and Wiszniewski, 2021). Directly measuring these residual loads is difficult for cast-in-situ piles: firstly, because of the complexity in separating curing-induced strains from mechanically induced strains, and secondly, the constantly changing stiffness of the pile during concrete curing means converting strains to a normal force is not trivial. Nevertheless, no clear trends were observed in α_p when considering the screw injection pile tests at Delft or similar sites (Loenhout, Oostende, Pruszcz and Żuławy) where the pile penetrated through a large amount of soft clay and where downdrag may incur a response at the pile base.

3.5.4. Comparison with other pile types

Figure 3.18 compares screw displacement piles to a database of bored and CFA piles (Gavin et al., 2013) and also to a database of driven closed-ended piles with residual loads excluded (Xu and Lehane, 2008; Bittar et al., 2020). To compare the three databases, $q_{c,LCPC}$ is used because $q_{c,filter}$ values could not be derived from the Gavin and Lehane (2007) dataset—although Figure 3.16 suggests that both averaging methods give similar α_p values for most cases.

The general trend in Figure 3.18 shows that screw displacement piles behave more like a non-displacement pile than a full displacement pile type. Notwithstanding, the high variation in the screw displacement pile database is evident. Part of this variation may be attributed to interpretation uncertainty, for example, when estimating the pile tip geometry and the pile base resistance. However, the variation may also suggest the sensitivity of screw displacement piles to installation, both in terms of the influence of installation on the influence zone around the pile tip as well as the soil-structure interaction mechanisms occurring at the screw tip under loading.

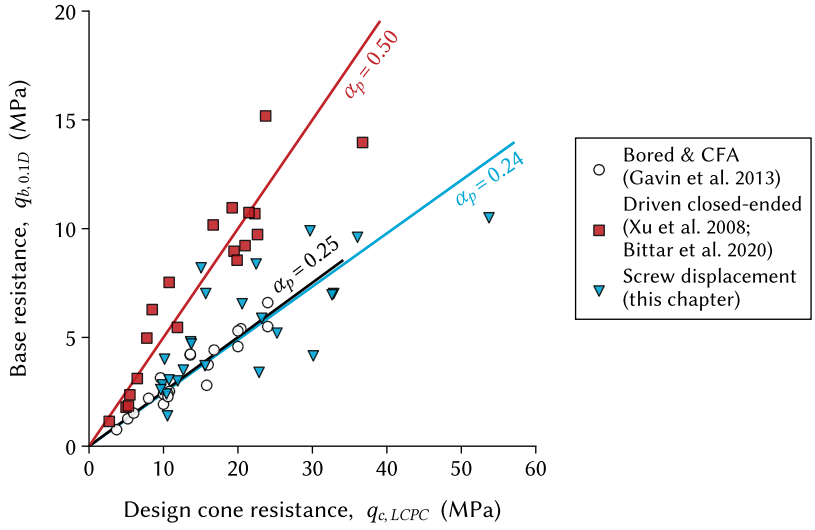

Figure 3.18: Screw displacement pile database compared to databases of non-displacement and full-displacement pile tests. Residual loads have not been included.

3.6. Conclusion

Five compression load tests were performed in Delft, the Netherlands, on full-scale screw injection piles (two Fundex and three Tubex piles), installed in soft clay and founded in medium dense to dense sand. Each pile was fully instrumented with distributed fibre optic sensors, showing clearly the base and shaft response of each pile. These measurements showed that the total capacity of two of the three Tubex piles was affected by structural failure of the grout body, resulting in the transfer of load directly to the pile base. All five piles could only mobilise a base capacity roughly 50 % than that predicted by the Dutch design standard.

To investigate this further, the study was extended to a database analysis of all types of screw displacement piles. The analysis demonstrated the importance of CPT q_c averaging methods in the derivation of the ultimate base capacity, showing that some averaging methods can be affected by weak soils overlying the pile base. Using the LCPC 1.5D averaging method, the analysis showed that all the screw displacement pile types mobilised base resistances comparable to a soil-replacing pile instead of a fully displacing pile, suggesting that the installation of screw displacement piles leads to little improvement in its base resistance. Nevertheless, large variability in the normalised base resistances suggests that pile tip shape, concreting procedures and other installation-related effects can have an impact on the pile base response and the interpretation of the test results.

4

CPT-BASED DESIGN OF SCREW DISPLACEMENT PILES IN GRANULAR SOILS

Divergences in design standards means there is no definitive consensus on the axial response of screw displacement piles. To address this, a high-quality database of load tests on screw displacement piles is presented in this chapter—the largest of its kind in published literature. The subsequent analysis uses both instrumented and uninstrumented records to compare different CPT-based design methods for screw displacement piles in granular soils. The instrumented data showed that existing design methods tend to overestimate the base capacity of screw displacement piles, yet underestimate their shaft capacity. Consequently, a new design method was developed based on a best-fit to the instrumented data, showing improved predictions of the total pile capacity when compared to both instrumented and uninstrumented records. However, the variability in predictive performance suggests that installation-related mechanisms may influence the overall capacity of these piles, particularly piles with an oversized displacement body.

This chapter is based on the following publication: Duffy, K.J., Gavin K.G. (2025) CPT-based prediction of screw displacement pile capacity in granular soils. *Proceedings of the Institution of Civil Engineers - Geotechnical Engineering*. (under review).

4.1. Introduction

The first research and development of screw displacement piles occurred primarily in the Netherlands and Belgium during the 1990s and early 2000s (Basu et al., 2010; Bottiau and Huybrechts, 2019). Pile design methods were developed in parallel, particularly methods which correlated the base and shaft capacities to CPT parameters such as the cone tip resistance, like those introduced in Chapter 2. These correlations were often calibrated using both public and private pile test records (e.g. de Cock, 2001; Frank, 2017; Huybrechts et al., 2016; NeSmith, 2002), forming the basis for many design methods internationally. Several examples of CPT-based design standards include that used in France (AFNOR, 2018), Belgium (NBN, 2022), the Netherlands (NEN, 2017b) and the USA (NeSmith, 2002; Brown et al., 2007).

Yet unlike the recent advancements in CPT-based design of driven piles (Lehane, Liu, et al., 2020) and bored piles (Niazi and Mayne, 2016; Doan and Lehane, 2021), recent advancements in screw displacement pile design is relatively limited. Indeed, several database approaches have given some indications regarding the accuracy of different design methods (de Cock, 2008; Basu et al., 2010; Jeffrey, 2012; Park et al., 2012; Larisch, 2014; Moshfeghi and Eslami, 2019; Figueroa et al., 2022). However, these analyses rarely consider the individual pile base and shaft capacities, partly because of the lack of publicly available records of instrumented static load tests, but especially tests paired with a neighbouring CPT that would allow α_p and α_s values to be derived. Synthesising new findings with respect to q_c averaging methods and limiting resistances has also not been assessed for screw displacement piles. Moreover, the conclusions from Chapter 3, as well as recent tests in soft clay (Siegel et al., 2019), have suggested an α_p factor much lower than currently prescribed in design standards, which has not been accounted for in any analyses to date.

To address this research gap, this chapter focusses on design methods for screw displacement piles in mainly coarse-grained, granular soil. First, a new categorisation of these piles is given to identify potential differences in installation methods that may affect their capacity. Pile test data from public literature and archived records have been compiled, all satisfying the requirements of a high-quality pile test database. Four CPT-based design methods are considered, first in the context of the measured base and shaft resistances, and later in terms of the total measured capacity of each test pile. A best-fit method to the instrumented data has also been included for comparison.

4.2. Categorising screw displacement piles

In the Netherlands alone, there are at least twenty different names for the different screw displacement piles on the market. These names are often registered trademarks, sometimes with just minor variations in the installation procedure or drilling tool geometry. For simplification, screw displacement piles have been categorised into four types: Type 1, Type 2, Type 3 and Type 4 (Figure 4.1). A detailed summary of the different installation procedures can be found in Basu and Prezzi (2010).

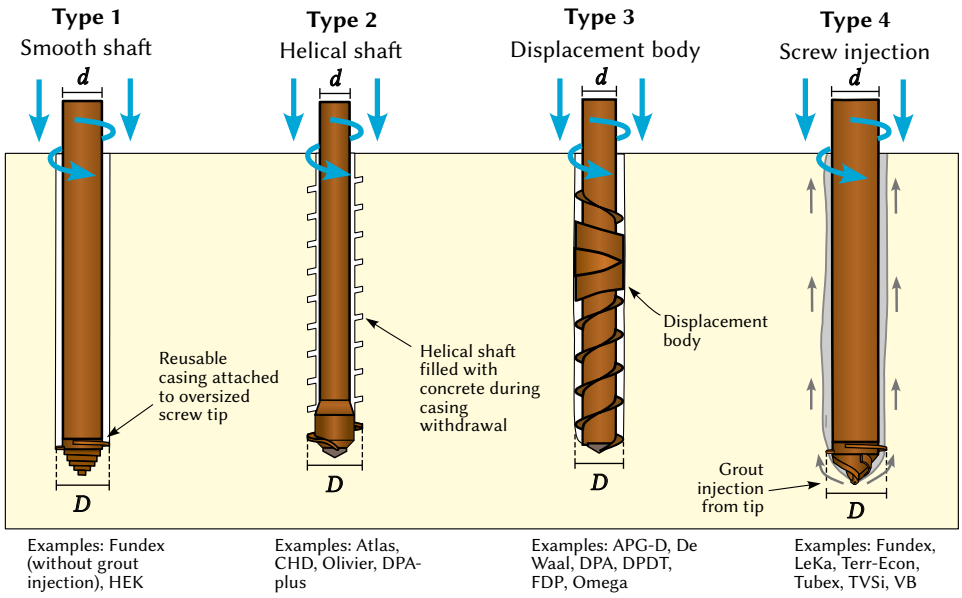

Figure 4.1: Four different types of screw displacement piles, indicating the casing diameter d and the outermost diameter D.

Type 1: Smooth shaft

Type 1 piles are installed with a sacrificial screw tip with a diameter larger than the diameter of the steel casing. Once the screw tip reaches the target depth, concrete is poured into the casing and the casing is extracted, filling the annular space around the pile with concrete and leaving the screw tip behind. The resulting pile therefore has a relatively smooth concrete shaft with a screw tip at the base. Alternatively, some Type 1 piles use a thin-walled casing that is welded to the screw tip, both of which remain in-situ after installation. Common Type 1 piles include the first generation of Fundex piles (without grout injection) or the HEK pile.

Type 2: Helical shaft

For Type 2 piles, a helical screw is integrated into a hollow drilling tool. A sacrificial base plate or pointed tip is then fitted to the base of the drilling tool, sealing the tool during installation and providing a base resistance. Once the target depth is reached, the drilling tool is filled with concrete and extracted at a rate matching the pitch of the helical screw, creating a helical concrete shaft. The Atlas pile is one of the pioneering pile types in this regard (Imbo, 1984; de Cock and Imbo, 1994), installed using a purpose-built rig. Olivier piles are another common Type 2 pile, particularly for fixed leader piling rigs.

Type 3: Displacement body

Type 3 piles use a drilling tool with several screw flights above and below an oversized displacement body, located several diameters away from the pile base. A sacrificial base plate is fitted to the bottom of the drilling tool, which is filled with concrete and extracted

once the target depth is reached, creating a relatively smooth-shafted pile. Initial development of Type 3 piles began with the De Waal pile in the late 1980s, later evolving into more geometrically complex drilling tools like the Omega pile (Bottiau and Cortvrindt, 1994; W. F. van Impe, 1996). This evolution led to the proliferation of other similar drilling tools and have been further categorised (Larisch, 2014) into rapid-displacing and progressive displacing piles depending on the shape of the drilling tool and the mechanisms of soil transport around the screw and displacement body.

Type 4: Screw injection

Screw injection piles use an injection fluid, such as grout, along with a push-in force and torque during pile installation. These piles closely resemble Type 1 piles, albeit modified to facilitate fluid injection from the pile base, like the Fundex or Tubex piles presented in Chapter 3. Once the fluid is injected from the pile tip, it flows up the annular space around the pile shaft and out at the ground surface, reducing the soil resistance on the pile shaft and on the pile base. When grout is used as the injection fluid, the cross-sectional stiffness of the pile increases upon curing and hardening of the grout shell.

4.3. Design methods for screw displacement piles

Both Equation 2.1 and Equation 2.2 are commonly used for screw displacement piles to determine their resistance at failure, where failure is considered as the period where most, if not all, of the base and shaft capacity has been fully mobilised. However, precisely defining the moment of failure during a static load test is a point of contention (NeSmith and NeSmith, 2006; Stuedlein et al., 2014), particularly since the mobilisation rate of the base resistance is governed by the relative stiffness of the surrounding soil and the pile diameter (White and Bolton, 2005; Gavin and O'Kelly, 2007). For design, the pile capacity is often defined at a certain displacement, generally a pile base displacement s_b of 10 % of the pile diameter.

Four design methods for screw displacement piles were analysed further, chosen based on the popularity of screw displacement piles in their respective countries:

- **AFNOR (France):** Also referred to as the LPC or LCPC method, this approach was developed using a database of 174 static load tests on different pile types. The design method for screw displacement piles mainly draws on research by Bustamente and Gianeselli (1998). In this chapter, the description of the AFNOR method in Frank (2017) and Verheyde and Baguelin (2019) has been used.
- **NBN (Belgium):** Developed based on mainly unpublished static load tests and includes the extensive research campaigns on screw displacement piles at Sint-Katelijne-Waver (Huybrechts, 2001) and Limelette (Huybrechts and Whenham, 2003). The 2022 update of the NBN method reduced α_p of screw displacement piles by around 40 % (WTCB, 2020). Additional information prior to the 2022 update can be found in Huybrechts et al. (2016).
- **NEN (The Netherlands):** Design method created in parallel with initial development of the CPT cone and CPT-based design methods, primarily using unpublished test data (Stoevelaar et al., 2014). A 2017 update to the design code

led to a 30 % reduction in α_p across all pile types, including screw displacement piles. Further details on the design method can be found in Gavin et al. (2021))

- **FHWA (USA):** Recommended design method by the Federal Highway Administration (FHWA) in the USA (Brown et al., 2007). Developed based on a database of forty tests on pressure-grouted Type 3 piles, presented in NeSmith (2002). The three European design methods, AFNOR, NBN and NEN, are all country-specific complements to Eurocode 7, first published in 2007.

Granular soils

Using Equation 2.1 and Equation 2.2, a simplified overview of the design methods is presented in Table 4.1. Some method-specific variations include:

- The FHWA method specifies the failure load $Q_{0,1inch}$ as the load on the pile when the head displacement s_0 reaches 25.4 mm (1 inch). This is in contrast to the three other design methods where failure is specified as the load $Q_{0,0.1D}$ at a base displacement of 10 % of the pile diameter.
- Each method uses its own q_c averaging method for which their respective α_p factors are calibrated. The Belgian and Dutch methods use the De Beer (de Beer, 1971) and 4D/8D (van Mierlo and Koppejan, 1952) averaging methods respectively, as described in Chapter 3.5.1. The averaging method in AFNOR follows a process similar to the LCPC averaging method, although the influence zone extends just $0.5D$ above the pile tip and also includes a reduction factor for piles with a short embedment depth. Lastly, the FHWA method follows the method by Fleming and Thorburn (1983), with a zone of influence $4D$ above and $4D$ below the pile base.
- The NBN and NEN methods include a shape factor (λ and β respectively) to account for the influence of an oversized pile base on the pile response, depending on the relative base-shaft diameters. These factors may reduce q_b by up to 30 %.
- The AFNOR and NBN methods use a non-linear relationship between q_s and q_c depending on the soil type, named f_{sol} and η_p^* respectively. This non-linear dependence implicitly limits the maximum shaft resistance to 200 kPa and 90 kPa for the AFNOR and NBN methods respectively.
- The FHWA method adds an additional factor w_t to Equation 2.1 and w_s to Equation 2.2 that depends on soil gradation and angularity. For example, for uniform, rounded sand with a fines content of up to 40 %, w_t is taken as 0 MPa and a limiting base resistance of 7.2 MPa is applied. For well-graded angular sand with less than 10 % fines, w_t is taken as 1.35 MPa with a limiting base resistance of 8.62 MPa. Interpolation is used for sand with a fines content or angularity between these bounds.
- Recent updates to the NBN and NEN standards allows for the use of contractor-specific α_p and α_s factors upon approval by an independent committee—generally on the condition that several static load tests are performed on the piles.

Table 4.1: Summary of design methods for screw displacement piles in granular soils.

Country	Method	α_s (-)	$q_{s,lim}$ (kPa)	α_p (-)	$q_{b,lim}$ (MPa)	Averaging method	Failure criterion
Belgium	NBN	0.0060[a]	90	0.50	—	De Beer	$s_b = 0.1D$
France	AFNOR	0.0145[b]	200[c]	0.50	—	LPC 2012	$s_b = 0.1D$
Netherlands	NEN	0.0090	135	0.63	15	Dutch 4D/8D	$s_b = 0.1D$
USA	FHWA	0.0100	160–210	0.40	7.2–8.62	Fleming and Thorburn, 1983	$s_0 = 25.4\,\text{mm}$

[a] Includes a non-linear dependency between q_s and q_c depending on the soil type (Figure 4.2).
[b] Reduced to 0.0040 for Type 1 piles with a permanent casing.
[c] Reduced to 90 kPa for Type 1 piles with a permanent casing.

Fine-grained soils

For fine-grained soils (clay, silt or intermediate soil), only one design method was used for all calculations to keep the prediction error constant in fine-grained soils and to give a better comparison of design method performance in granular soils. The method by Bustamente and Gianeselli (1998) was used, a method which also forms the basis of the AFNOR design method and recommended in a study of Type 3 piles by Larisch (2014). The method is a graphical approach (Figure 4.2), where the curve is chosen based on the soil type and whether or not the screw displacement pile uses a permanent or temporary casing. For example, a screw displacement pile with a temporary casing—so most piles in the database—uses curve Q1 for clay ($q_c < 1\,\text{MPa}$), Q3 for silty clay ($q_c > 1.5\,\text{MPa}$) and Q4 for sandy clay ($q_c > 3\,\text{MPa}$). A screw displacement pile with a permanent casing uses curve Q1 for clay and Q2 for both silty clay and sandy clay.

4.4. Screw displacement pile test database

To assess the design method performance, sixty tests were taken from the larger database (Appendix B), all meeting the following criteria:

- At least one CPT was performed next to each test pile and to a penetration depth at least four pile diameters below the pile base.
- The tests were first-time static compression load tests, reaching a pile head displacement of at least 25 mm, that is, the failure criterion of the FHWA design method.
- The base of all piles was located in a sand layer and all piles derived at least 50 % of their total capacity from granular soils.

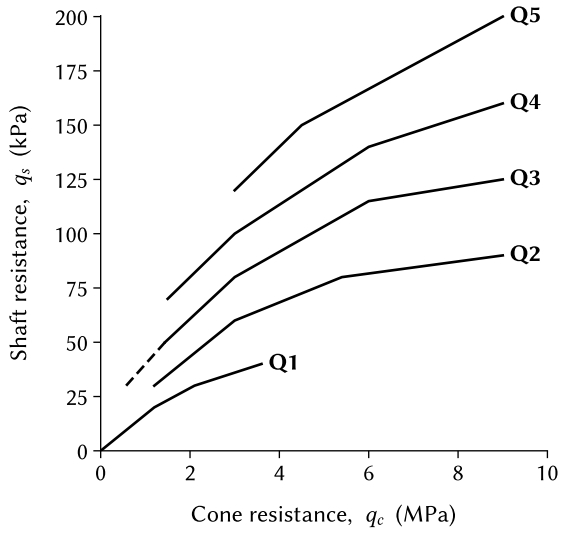

Figure 4.2: Design chart for fine-grained soils, adapted from Bustamente and Gianeselli (1998). The curve is chosen based on the soil type and pile type.

Table 4.2: Pile tests used for assessing screw displacement pile capacity in granular soils.

Site & Pile	d (mm)	D (mm)	L (m)	$q_{c,tip}$ (MPa)	$Q_{0,max}$ (MN)	$s_{0,max}/D$ (%)
Type 1: Smooth shaft						
Almere SBP4	360	430	13.1	12.4	1.8	8
Almere SBP5	360	430	10.2	4.4	1.0	8
Almere SBP6	360	430	10.2	2.9	1.0	6
Limelette A1	380	450	9.6	20.5	3.1	17
Limelette C1	380	450	9.6	21.7	1.6	7
Seildeich P1	440	560	14.8	15.8	2.6	5
Seildeich P2	440	560	13.8	18.3	3.0	5
Terneuzen P02	460	560	21.4	12.7	6.0	10
Terneuzen P04	460	560	20.0	16.2	5.3	13
Terneuzen P06	460	560	19.9	14.8	4.4	14
Zimmerplatz P1	420	560	14.0	17.0	3.0	6
Type 2: Helical shaft						
Berlin P2	460	560	14.2	12.4	3.5	5
Gent P1	460	510	13.0	8.1	2.8	9
Gent P2	460	510	13.5	9.7	3.3	15
Limelette A2	360	510	9.2	21.0	3.1	5
Limelette B3	360	510	9.4	22.8	3.6	13
Limelette B4	360	510	9.4	23.1	3.4	11
Limelette C2	360	510	9.1	22.0	2.7	5

Continued on next page …

Table 4.2 (continued)

Site & Pile	d	D	L	$q_{c,tip}$	$Q_{0,max}$	$s_{0,max}/D$
Oldenburg P1	510	560	9.5	21.2	2.3	5
Oldenburg P2	510	560	7.0	7.5	1.8	6
Oostwoud P27	340	410	14.2	14.0	1.3	14
Oostwoud P28	340	410	13.8	15.9	1.5	12
Zeeland O1	310	460	9.1	31.5	1.4	16
Zeeland O2	310	460	8.0	23.6	1.6	12
Zeeland O3	310	460	9.5	20.0	1.8	16
Werkendam P5	273	410	16.6	11.9	1.7	8
Werkendam P6	273	410	16.6	12.1	1.8	6
Werkendam P8	273	410	16.1	12.1	1.7	7
Type 3: Displacement body						
Elblag P9	300	400	7.5	16.6	1.1	7
Gdansk P809	300	400	12.9	9.7	1.7	11
Grottgera P600	300	400	11.0	12.6	1.2	11
Grottgera P602	300	400	10.8	15.0	1.5	10
Hamburg PA	310	510	10.4	11.9	3.2	8
Hamburg PB	n/a	440	8.4	12.5	2.2	13
Limelette A3	n/a	410	9.4	22.0	2.9	12
Limelette A4	n/a	410	9.5	22.6	2.6	16
Limelette C3	n/a	410	9.4	20.7	2.9	14
Limelette C4	n/a	410	9.5	19.4	2.5	20
Loenhout S2	n/a	410	9.5	13.2	1.2	14
Lomme P1	273	360	8.5	23.8	1.6	14
Oostende P1	n/a	460	21.6	29.5	3.6	16
Oostwoud P1	273	360	16.0	16.8	1.6	17
Oostwoud P22	273	360	18.0	12.0	1.8	15
Oostwoud P6	273	360	16.5	14.0	1.1	19
Santa Cruz C2	350	450	9.5	9.0	2.4	28
Vilvoorde P5	410	410	8.2	13.7	1.9	14
Werkendam P1	273	410	17.4	9.6	2.4	11
Werkendam P2	273	410	17.8	5.4	2.4	8
Werkendam P3	273	410	17.4	10.9	2.3	9
Werkendam P4	273	410	17.8	8.7	2.2	10
Zulawy P6293	n/a	400	12.6	14.1	0.9	11
Type 4: Screw injection						
Amaliahaven SI1	610	850	37.0	36.5	20.3	14
Amaliahaven SI2	610	850	37.1	49.4	23.3	7
Amaliahaven SI3	610	850	35.0	22.5	18.6	18
Amaliahaven SI4	610	850	34.1	54.7	19.0	15
Delft F1	315	470	19.8	12.7	2.7	42
Delft F2	315	470	19.0	13.6	2.6	41
Delft T1	382	470	19.9	11.3	2.6	46
Terneuzen P03	460	560	20.2	13.5	6.1	13
Terneuzen P05	460	560	20.2	15.3	6.4	15

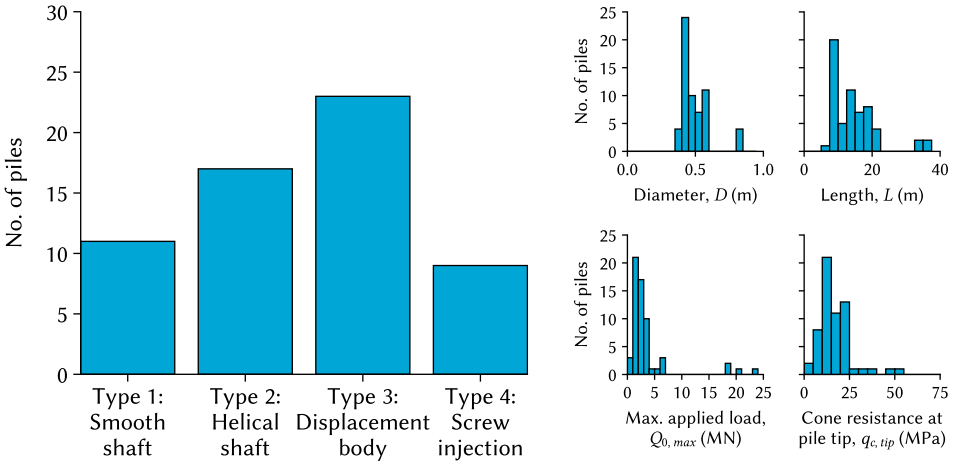

Figure 4.3: Visual summary of the pile tests used to predict the total pile capacities.

Type 3 piles are the most common pile type in the database (Table 4.2; Figure 4.3), representing 38 % of all piles. Type 4 piles are the least common, although the increasing use of these piles (Bottiau and Huybrechts, 2019) means that most of the tests have been performed more recently—such as the tests presented in Chapter 2 and Chapter 3.

Regarding pile geometry, almost all piles have an outermost diameter D ranging from 360 mm to 500 mm. The casing diameter d ranges from 57 % to 91 % of the outermost diameter, with an average of around 80 %. These diameters are typical of industry practice, with designers balancing the need to have a large enough pile whilst keeping the installation torque to a minimum. The only exceptions are the 850 mm diameter screw injection piles at Amaliahaven. These piles were founded 35 – 40 m deep in a very dense sand layer, where cone resistances at the pile tip were around 50 MPa. These piles also have the highest capacity of the database piles, ranging from 18 MN to 24 MN in total. The rest of the database piles have capacities of 2 – 3 MN, with the pile base founded in medium dense to dense sand where $q_{c,tip}$ ranges from 10 – 25 MPa.

4.4.1. Pile shape and diameter

For design and load test evaluation of cast-in-situ piles, assumptions are often needed regarding the realised diameter. However, pile extraction is often costly and complex, meaning only a limited amount of records are available from extracted screw displacement piles. Records from the broader database (Figure 4.4) show that the measured diameter D_{meas} tends to be equal to the nominal, outermost diameter of the drilling tool D. Nevertheless, some piles exhibit substantial differences between the minimum and maximum recorded diameters, varying by up to ±20 % of the mean pile diameter. Based on these observations, the external pile diameter D was used to derive the shaft resistance of each pile. The only exception were the test piles at Limelette, which were the only piles that met the analysis criteria and were also extracted following testing—for these piles the average measured diameter was used.

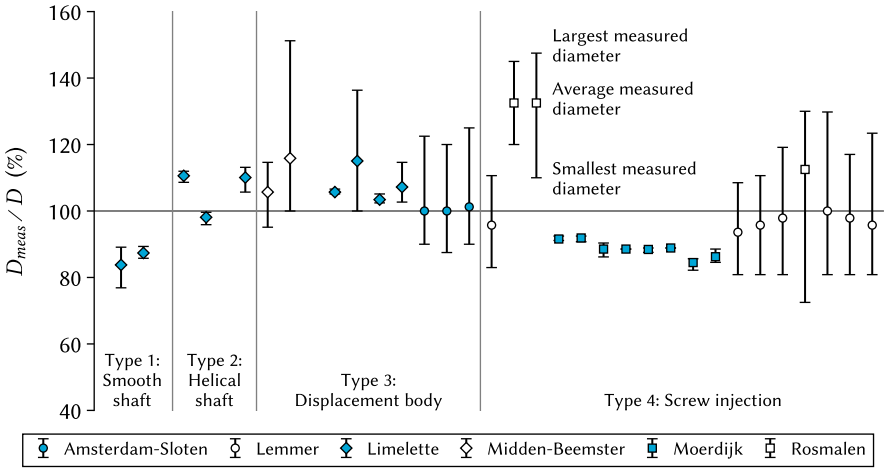

Figure 4.4: Measured shaft diameters of extracted piles across the full database in Appendix A. The nominal diameter D ranges from 400 mm to 550 mm.

Similar uncertainties exist with the shape of the pile base. Records of extracted piles show a range of pile tip shapes: from relatively cylindrical pile tips to tapered pile tips to slightly bulbous pile tips. Variation in shape may also occur within pile types at the same site, for example, across two Type 2 piles and two Type 3 piles (Figure 4.5) founded in a dense sand layer, overlain by soft to firm clay. Inevitably, many different variables can create this variation in pile tip shape, including the soil conditions, concrete specification, installation procedure and extraction procedure. In most cases, a sacrificial screw tip is present at the bottom of the piles, somewhat reducing the uncertainty in the pile tip geometry. Consistent with the assumption for the shaft resistance, the external diameter D has also been used to derive the pile base resistance.

4.5. Instrumented screw displacement pile behaviour

In total, 25 % of the tests were instrumented, allowing for a clear distinction between the base and shaft components of the total pile capacity. Most of these tests used long-gauge (0.5 – 2 m) retrievable extensometers, placed within a central reservation tube after pile installation. At Amaliahaven and Delft, fibre optic sensors were installed on opposite sides of each test pile, including discrete FBG measurements and distributed BOFDA measurements. None of the Type 1 piles were instrumented and so no measured shaft and base resistance data is available from these piles.

4.5.1. Shaft resistance

For each instrumented pile, the average shear stress at failure q_s was determined from measurements made entirely in sand and using the external nominal diameter D. The AFNOR, NBN and NEN methods, which all use the same $s_b = 0.1D$ failure criterion, differ

Figure 4.5: Base of four extracted screw displacement piles, all installed at the site.

substantially in their predictions at cone resistances of less than 10 MPa (Figure 4.6). At q_c values less than 10 MPa for instance, the AFNOR method predicts the highest shaft resistances whereas NBN predicts shaft resistances approximately half that of AFNOR. Across this same range, Type 3 piles tended to mobilise higher resistances compared to the Type 2 and Type 4 piles.

Beyond cone resistances of 15 MPa, the limiting resistances of the AFNOR, NBN and NEN methods begin to take effect and the measured shaft resistances become substantially underestimated. This underprediction is particularly pronounced for the 850 mm Type 4 piles tested at Amaliahaven, where the three piles mobilised shaft resistances of around 500 kPa before structural failure occurred. Clearly, existing design methods significantly underestimate the shaft response of screw displacement piles in dense to very dense sand.

A best-fit α_s of 0.012 was derived from the measured shaft resistances. Nevertheless, there is still some variability in the predictions with this method, with a coefficient of variation of 37 %. This variability may arise from subjectivities in the strain interpretation process and the influence of localised deviations in pile diameter and stiffness around each gauge level. Drilling tool geometry during penetration and subsequent withdrawal and equalisation between the concreting pressures and radial stresses may also contribute to this variability.

To investigate whether the mobilised shaft resistance was affected by the depth considered, the normalised shaft resistances at failure is plotted with the distance from the pile base (Figure 4.7). While the data is scattered, no depth-dependent effects are immediately apparent. Nevertheless, more datapoints would be needed to confirm the presence or absence of depth-dependent effects across all four pile types.

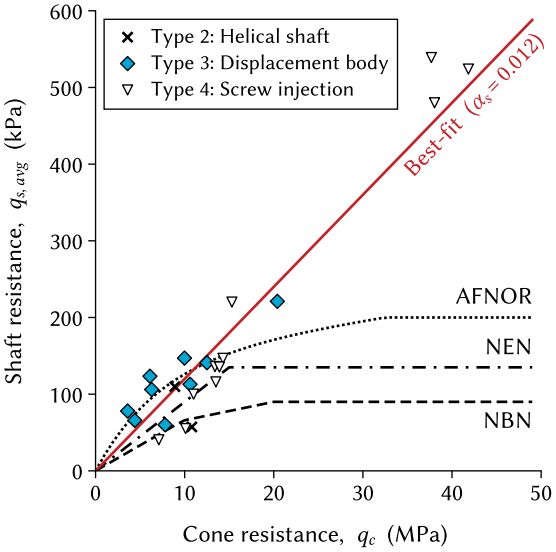

Figure 4.6: Variation in q_s with q_c in granular soils, including the best-fit. Predictions were made for a screwed cast-in-situ pile with casing removed. No instrumented test results on Type 1 piles were in the database.

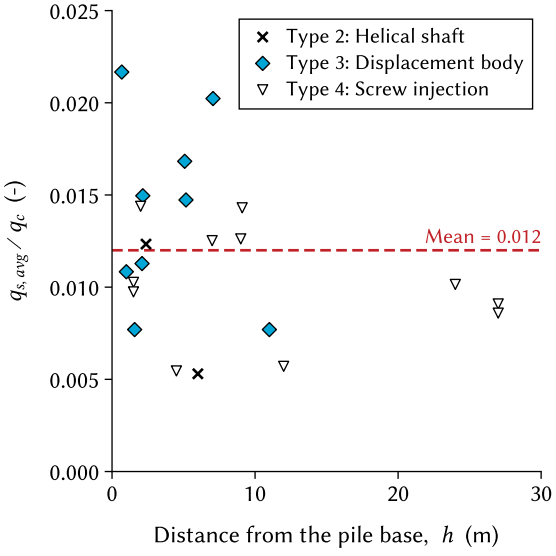

Figure 4.7: Variation in normalised shaft resistance with distance from the pile base. No instrumented test results on Type 1 piles were in the database.

4.5.2. BASE RESISTANCE

The base resistances were derived from the lowermost gauge measurement, extrapolated to the pile base. The measurements in Figure 4.8 show that AFNOR, NBN and NEN overestimate the base resistance, in some cases by a factor of four. NBN performs the best of the existing design methods, albeit with a high COV of 44 %. Part of this variation can be attributed to the q_c averaging method, as shown previously in Figure 3.16. In summary, the De Beer and 4D/8D averaging methods of the NBN and NEN design methods were shown to introduce bias in the derived α_p when the pile base was only embedded at a shallow depth into the load-bearing sand layer. In contrast, the adapted filter method (de Boorder et al., 2022) was shown to have no bias with shallow embedment and Figure 3.18 indicated a best-fit α_p of 0.25 across all screw displacement pile types—a much lower α_p compared to the other design methods.

With these findings in mind, Figure 4.8 presents the results of the adapted filter method and the best-fit α_p to all datapoints. The best-fit results in a mean prediction accuracy $q_{b,pred}/q_{b,meas}$ of 1.02 with a COV of 31 %, substantially lower than the COV from the NBN and NEN design methods and a better predictive accuracy compared to all methods. The resulting α_p values show no distinct trend across the three pile types, with a constant α_p fitting well across the entire range of cone tip resistances.

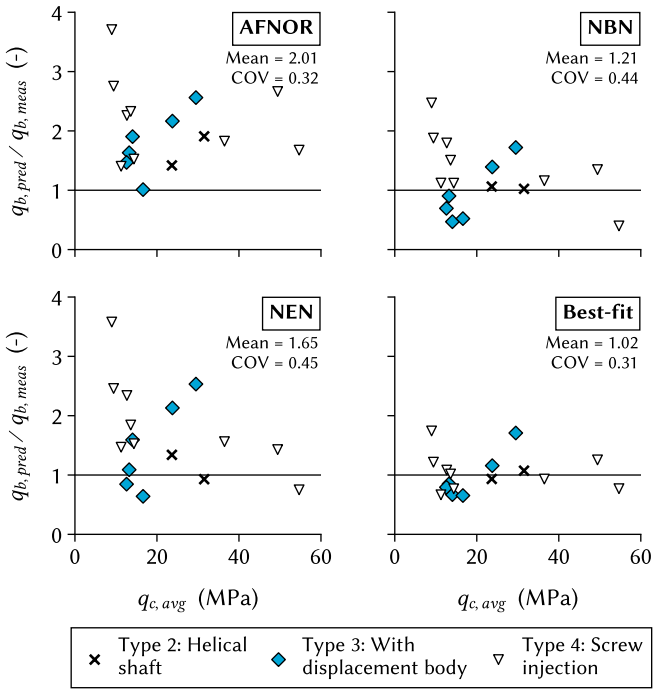

Figure 4.8: Predictions of the pile base resistance by four different design methods. The standard-specific averaging method was used to determine $q_{c,avg}$ and no instrumented test results on Type 1 piles were in the database.

4.6. Total capacity prediction

The performance of the design methods, including the best-fit to the instrumented records (α_p = 0.25, α_s = 0.012), was made for both instrumented and uninstrumented load tests by looking at the total failure load. In doing so, several procedures and assumptions were made:

- No extrapolation of the load-displacement curves was performed, such as the Chin (1970) extrapolation method. Since the FHWA method uses a smaller displacement in its definition of pile failure (Table 4.1), more database entries are available for the FHWA method compared to the other methods.
- Based on the conclusions from Chapter 4.4, the nominal diameter D was used to determine the pile base and shaft resistance. For Type 1, Type 2 and Type 4 piles, this was usually the width of the screw tip, including the helical flanges. For Type 3 piles, this was the maximum diameter of the displacement body. For extracted piles (Limelette), the mean measured diameter was used.
- A mechanical CPT cone was used for nine of the test piles, specifically all the tests reported in de Cock (2001). The q_c profile from the mechanical cone was equated to that of an electrical cone using the correlation by Kulhawy and Mayne (1990):

$$\left(\frac{q_c}{p_a}\right)_E = 0.47\left(\frac{q_c}{p_a}\right)_M^{1.19} \tag{4.1}$$

  where p_a is a reference stress, taken as atmospheric pressure (=101.3 kPa).
- The groundwater level was not reported for twenty-four piles. In these cases, the groundwater level was assumed to be one metre below the surface.
- For tests where the pile base displacement was not measured directly, a load-transfer analysis was used to estimate the elastic displacement of the pile and correspondingly, the pile base displacement.
- CPTs were available in digital format for 43 % of the sites. For the remaining sites, CPT results had to be digitised. This digitisation introduces pseudo-measurement error into the CPT data depending on how clearly the data was originally published. Generally, the effect of digitisation at insignificant for high q_c values (i.e. sandy soils) but is more significant in low q_c regions (i.e. clay soils).
- When determining w_s and w_t in the FHWA method, approximately half of the sites did not indicate the soil angularity and soil gradation. For these sites, w_s and w_t were set to the values for a well-graded, angular material with a fines content less than 10 % (w_s = 160 kPa and w_t = 1.35 MPa).

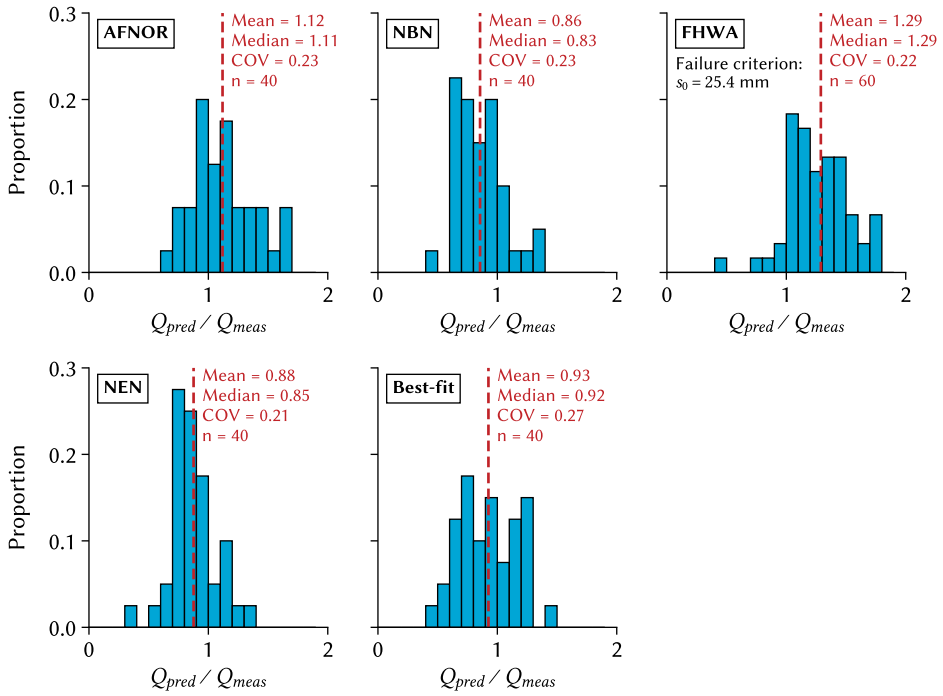

Figure 4.9: Results of the pile capacity prediction. The number of tests n is higher for the FHWA method because of the lower displacement defined as the failure criterion ($s_0 = 1$ inch as opposed to $s_b = 0.1D$).

4.6.1. Overall performance

In total, 40 piles were used to assess the performance of AFNOR, NBN, NEN and the best-fit method, while 60 piles were used to assess the FHWA method because of the difference in failure criteria. These results are shown in Figure 4.9 and Table 4.4, with the ratio of the predicted to measured capacity Q_{pred}/Q_{meas} being used to evaluate the performance of the design methods.

The performance of the five design methods is summarised as follows:

- The best-fit to the instrumented records gave a good agreement on average but with high variability, with a mean Q_{pred}/Q_{meas} of 0.93 suggesting a slight tendency for the method to underestimate the total capacity. The best-fit predicted higher shaft resistances in the sand layers compared to the other design methods (Figure 4.10), conversely predicting lower base resistances in relation to the total predicted capacity Q_{pred}. The areas with the prediction error tended to be in sites dominated by clay and intermediate soils (such as Gent and Limelette)—in other words, where the predicted capacity in sand was relatively low in proportion to the total predicted capacity.
- NBN and NEN both underestimated the total capacity on average, yielding a

mean Q_{pred}/Q_{meas} of 0.86 and 0.88 respectively. AFNOR by contrast, tended to overestimate the total capacity. This is consistent with measured base and shaft resistances (Figure 4.6, Figure 4.8) whereby AFNOR tended to overpredict the pile base and shaft capacity at cone resistances less than 15 MPa.

- The FHWA method gives the lowest prediction accuracy. However, the results were highly dependent on the choice of w_s and w_t, both of which were difficult to interpret from the database cases. Furthermore, the FHWA method specifies the failure point as when the displacement of the pile head reaches 25.4 mm. This is approximately half the median displacement criterion of the other design methods (on average, $0.1D = 40$ mm). At lower displacements, where shaft and base resistances may only be partially mobilised, the other design methods specify characteristic load-transfer curves (Allani and Huybrechts, 2020), curves which are often dependent on the predicted capacity.
- The coefficient of variation across all design methods ranged from 21 % to 27 %. For context, the Unified design method for driven piles (Lehane, Liu, et al., 2020), developed on a high-quality dataset of 71 piles (Lehane et al., 2017), yielded a COV of 24 %. Similar results were also exhibited by a database study on bored and continuous flight auger piles (Doan and Lehane, 2021), where the COV of 30 % was reported for piles in sand, reducing to 20 % in clay.

Table 4.4: Results of the total capacity predictions for each pile and each design method.

	Q_{meas} (MN)		Q_{pred}/Q_{meas} (MN)				
Site & Pile	$Q_{0,1inch}$	$Q_{0,0.1D}$	AFNOR	FHWA	NBN	NEN	Best-fit
Type 1: Smooth shaft							
Almere SBP4	1.7	—	—	0.96	—	—	—
Almere SBP5	1.0	—	—	1.10	—	—	—
Almere SBP6	1.0	—	—	0.75	—	—	—
Limelette A1	2.9	3.0	0.79	0.89	0.66	0.78	0.55
Limelette C1	1.6	—	—	1.42	—	—	—
Seildeich P1	2.6	—	—	1.32	—	—	—
Seildeich P2	3.0	—	—	1.03	—	—	—
Terneuzen P02	5.8	6.0	1.02	1.28	0.88	0.77	1.08
Terneuzen P04	4.8	5.3	1.09	1.46	0.95	0.83	1.11
Terneuzen P06	3.7	4.3	1.26	1.79	1.03	0.95	1.18
Zimmerplatz P1	2.8	—	—	1.02	—	—	—
Type 2: Helical shaft							
Berlin P2	3.3	—	—	1.29	—	—	—
Gent P1	2.6	—	—	1.25	—	—	—
Gent P2	2.6	2.9	0.94	1.08	0.68	0.84	0.60
Limelette A2	2.9	—	—	1.16	—	—	—
Limelette B3	2.9	3.4	0.85	1.11	0.67	0.82	0.71
Limelette B4	2.9	3.3	1.05	1.09	0.76	0.82	0.72
Limelette C2	2.6	—	—	1.19	—	—	—

Continued on next page …

Table 4.4 (continued)

Site & Pile	$Q_{0,1inch}$	$Q_{0,0.1D}$	AFNOR	FHWA	NBN	NEN	Best-fit
Oldenburg P1	2.3	—	—	1.60	—	—	—
Oldenburg P2	1.6	—	—	1.08	—	—	—
Oostwoud P27	1.2	1.2	1.46	1.53	1.12	1.15	1.14
Oostwoud P28	1.3	1.4	1.32	1.37	0.85	1.06	0.94
Werkendam P5	1.6	—	—	1.50	—	—	—
Werkendam P6	1.8	—	—	1.39	—	—	—
Werkendam P8	1.7	—	—	1.35	—	—	—
Zeeland O1	1.2	1.3	1.65	1.78	1.21	0.94	1.29
Zeeland O2	1.5	1.5	1.64	1.74	1.32	1.32	1.29
Zeeland O3	1.5	1.8	1.43	1.67	1.09	0.97	1.11
Type 3: Displacement body							
BEST C2	1.8	2.0	0.62	0.42	0.41	0.37	0.42
Elblag P9	1.1	—	—	1.18	—	—	—
Gdansk P809	1.5	1.6	1.18	1.38	0.92	0.98	0.87
Grottgera P600	1.1	1.2	1.15	1.41	0.72	0.68	0.81
Grottgera P602	1.4	1.5	0.91	1.15	0.62	0.59	0.68
Hamburg PA	2.8	—	—	1.04	—	—	—
Hamburg PB	1.9	2.1	0.86	1.05	0.62	0.68	0.60
Limelette A3	2.5	2.8	0.79	0.95	0.62	0.75	0.62
Limelette A4	2.1	2.4	0.92	1.16	0.73	0.86	0.72
Limelette C3	2.4	2.8	0.79	1.03	0.68	0.74	0.61
Limelette C4	2.0	2.3	1.00	1.11	0.77	0.83	0.73
Loenhout S2	1.0	1.2	1.32	1.44	1.06	1.07	0.88
Lomme P1	1.4	1.5	1.33	1.43	1.06	1.17	0.99
Oostende P1	2.6	3.2	1.20	1.60	0.99	1.00	1.05
Oostwoud P1	1.4	1.5	1.41	1.55	0.98	1.16	1.04
Oostwoud P22	1.7	1.7	1.13	1.19	0.86	0.87	0.92
Oostwoud P6	1.1	1.1	1.66	1.80	1.40	1.25	1.49
Vilvoorde P5	1.4	1.8	1.02	1.27	0.72	0.76	0.80
Werkendam P1	2.1	2.4	0.94	1.25	0.75	0.71	0.88
Werkendam P2	2.3	—	—	1.12	—	—	—
Werkendam P3	2.1	—	—	1.30	—	—	—
Werkendam P4	1.9	2.1	1.16	1.46	0.99	0.89	1.19
Zulawy P6293	0.8	0.9	1.54	2.16	0.80	1.12	0.96
Type 4: Screw injection							
Amaliahaven SI1	15.0	20.4	1.13	1.39	0.93	0.93	1.22
Amaliahaven SI2	16.1	23.4	1.28	1.39	0.92	0.86	1.25
Amaliahaven SI3	13.2	18.6	1.12	1.63	0.91	0.92	1.29
Amaliahaven SI4	14.6	19.0	1.17	1.30	0.76	0.78	1.21
Delft F1	2.5	2.7	0.85	1.03	0.69	0.78	0.72
Delft F2	2.3	2.6	0.92	1.05	0.67	0.73	0.69
Delft T1	2.3	2.5	0.92	1.14	0.76	0.86	0.79
Terneuzen P03	5.0	6.1	0.97	1.43	0.84	0.74	0.95
Terneuzen P05	5.3	6.4	0.94	1.35	0.81	0.72	0.93

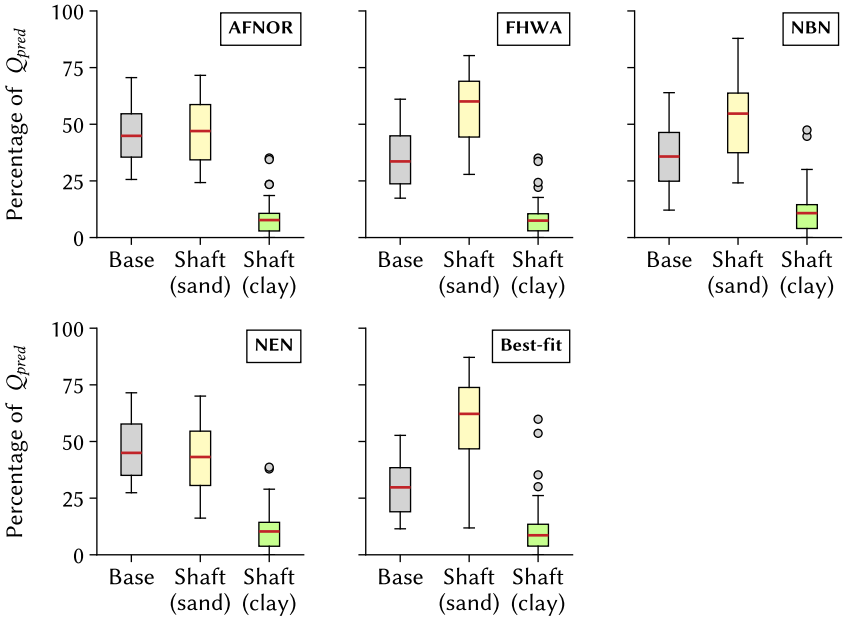

Figure 4.10: Base and shaft capacity components of each prediction in relation to the total predicted capacity Q_{pred}.

Table 4.3: Summary of the total capacity prediction by pile type.

	Mean Q_{pred}/Q_{meas} (-)					COV Q_{pred}/Q_{meas} (%)				
	AFNOR	FHWA	NBN	NEN	Best-fit	AFNOR	FHWA	NBN	NEN	Best-fit
Type 1	1.04	1.18	0.88	0.83	0.98	19	25	18	10	30
Type 2	1.29	1.36	0.96	0.99	0.98	24	17	26	18	28
Type 3	1.10	1.28	0.83	0.87	0.86	25	26	27	26	28
Type 4	1.03	1.30	0.81	0.81	1.01	14	15	12	10	24
All Piles	1.12	1.29	0.86	0.88	0.93	23	22	24	21	27

4.6.2. PERFORMANCE BY PILE TYPE

Table 4.3 shows that the best-fit to the instrumented records performs well for Type 1, Type 2 and Type 4 piles, with Q_{pred}/Q_{meas} close to 1.0 for the three pile types. NBN and NEN also performed well for Type 2 piles, although both methods underestimated the capacity of the other pile types by 10 – 20 % on average. AFNOR returned good predictions for Type 1 and Type 4 piles, but the method overestimated the capacity of Type 2 piles by 29 % and Type 3 piles by 10 %. The FHWA method, calibrated on a dataset of Type 3 piles, tended to overestimate the capacity of all pile types by at least 18 %.

Most of the prediction error occurs with the Type 3 piles. Three design methods, NBN, NEN and the best-fit, tended to underestimate their capacity, while the two other methods, AFNOR and FHWA, tended to overestimate their capacity. The COV of the predictions is also higher for the Type 3 piles compared to other types, with the COV ranging from 25 to 28 % across all design methods.

For Type 3 piles, the design methods also show a bias with pile length (Figure 4.11). The bias may suggest that an increasing contribution of shaft resistance, relative to the base resistance, may lead to changes in the prediction error. This is corroborated by the shaft resistances of the instrumented piles (Figure 4.7), suggesting that Type 3 piles mobilise higher shaft resistances than other screw displacement pile types in granular soils. The bias may also indicate installation-dependent changes in radial stresses or degree of soil displacement. For instance, studies (W. F. van Impe, 2001; Pucker and Grabe, 2012; Shi et al., 2019) of Type 3 piles suggest that penetration and extraction mechanisms, such as drilling tool geometry, penetration rate or concrete pressure, may tend to dominate their axial response. Correspondingly, deeper penetration depths and higher in-situ stresses may affect the radial stress development along the entire length of drilling tool. Some studies have investigated correlations between installation records and the pile capacity (NeSmith and NeSmith, 2006; Krasiński, 2023), although more high-quality data is needed to validate these approaches. Well-instrumented piles installed using different drilling tool geometries at the same test site would help in this regard.

4.7. PRACTICAL IMPLICATIONS

The choice of design method, with the corresponding correlation factors and limiting resistances, invariably affects the interpretation of the total pile capacity. To put this into context, Figure 4.12 shows the required length of a 400 mm diameter pile to support a 4 MN load. The soil in each case is taken as a homogeneous sand with a constant q_c value with depth. When q_c is equal to 10 MPa, a large spread is evident in the required pile lengths, ranging from 17 m to 29 m. The shortest design length is derived by both the FHWA and AFNOR method: the FHWA method in part because of the reduced displacement criterion defining pile failure and the AFNOR method because of the high shaft correlation factor compared to the other methods.

As q_c increases, the design methods' limiting resistances affect the predicted capacity, narrowing the range of design pile lengths. No limiting resistances were applied in using the best-fit to the instrumented records, in line with the findings of Chapter 2. As a result, the best-fit method first transitions from predicting slightly lower capacities at shallow depths, to predicting higher capacities as the pile length increases. In q_c values of 30 MPa, the result is a much shorter design length compared to the other design methods.

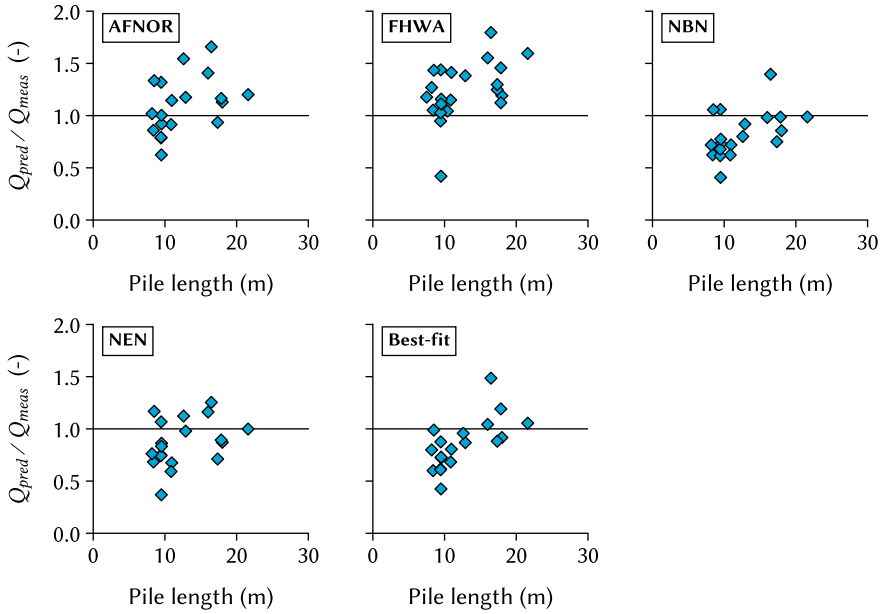

Figure 4.11: Change in prediction performance with pile length for Type 3 piles.

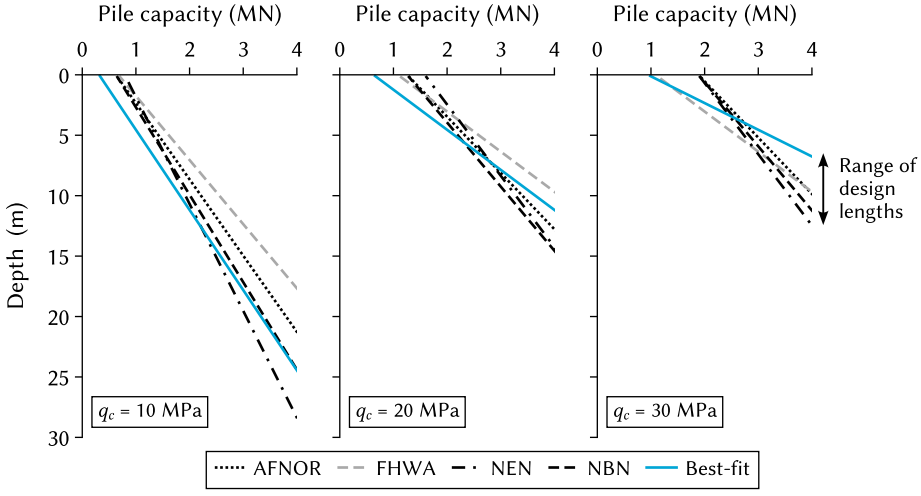

Figure 4.12: Pile length needed to support a 4 MN load in homogeneous sand, where D = 400 mm.

Figure 4.12 is a synthetic example but is intended to reflect the influence each design method has on the derived pile length, in essence, where the shaft contribution is most significant. For conditions where soft soils overly the load-bearing stratum, it is expected that the base resistance of the pile will begin to dictate the overall response and as a result, q_c averaging methods and design factors will begin to have more of an influence.

4.8. Conclusion

This chapter presents a database of static load tests on screw displacement piles that derive most of their capacity from granular soil. The database has been used to assess the performance of CPT-based design methods in predicting both the base and shaft response of instrumented piles, as well as the total pile capacity. The conclusions are as follows:

- Extracted pile records show considerable variability in cross-sectional area, with a tendency for the shaft diameter to be around the maximum drilling tool diameter.
- Current design methods tend to overestimate the pile base contribution, while underestimating the shaft contribution. This underestimation is especially prevalent in very dense sand at Amaliahaven (Chapter 2), where design methods either an implicit or explicit limiting resistances.
- A best-fit to the instrumented data led to the empirical correlation factors $\alpha_s = 0.012$ and $\alpha_p = 0.25$ for the pile shaft and pile base respectively at a pile base displacement of $0.1D$, where the adapted filter method was used for the pile base capacity.
- When compared to the total load from all records (including uninstrumented tests), the predicted capacity based on the best-fit data gave the best agreement on average, but with the highest variability.
- Piles with a displacement body, such as De Waal and Omega piles, consistently exhibited lower capacities than predicted, with a dependency between the prediction error and pile length. Further investigation through pile load tests can help resolve this trend, with a particular focus on the influence of installation procedure and drilling tool geometry on the pile's ultimate capacity..

5

Conclusions and Recommendations

5.1. Conclusions

This dissertation has presented two field test campaigns, comprising of axial load tests on a total of sixteen full-scale piles: driven closed-ended piles, driven cast-in-situ (DCIS) piles and screw injection piles—a type of screw displacement pile. Each pile was instrumented with distributed fibre optic sensors along its full length, showing how each pile transfers its axial load to each soil layer in both shaft and base resistance. These results were then compared to CPT measurements around each test pile and integrated into a broader database analysis. Several conclusions have been made from the results, both in a scientific context and for design methods used in engineering practice.

5.2. Scientific findings

5.2.1. Distributed fibre optic sensing in pile testing

In each test, distributed fibre optic sensors measured the deformation of the pile under axial compressive loading. This measurement was then converted to a force using the cross-sectional stiffness of the pile, from which the pile base and shaft resistance was subsequently derived.

The fibre optic cables had to be instrumented in several different ways because of the different pile types tested. These methods included direct embedment within concrete, mechanical fixation to the reinforcement cage or gluing to steel surfaces. In all cases, the fibre optic cables proved to be remarkably robust: out of the sixteen piles tested, only one pile (SI3 at Amaliahaven) had a breakage in the fibre optic network. The loads measured by the fibre optic cables, along with the derived base and shaft resistances, corresponded directly with the load measured by a load cell at the pile head.

The distributed fibre optic measurements also brought insights that may not have been detected or interpreted with conventional point sensors. At Delft for instance, the screw injection piles with a permanent casing failed at much lower loads than expected (Chapter 3). Interpreting why this occurred could be easily done with the distributed fibre optic sensors: the pile transferred little to no load across almost all of the lower sand layer (Figure 3.10), likely indicating that a form of structural failure occurred. Had just two or three point sensors been used in the lower sand layer, attributing where the pile capacity was lost would have been much more challenging and potentially leading to misinterpretation of the load tests. Similar findings were also made at Amaliahaven, where structural debonding in the screw displacement piles and poor concrete quality in the driven cast-in-situ piles also affected their response in the lower sand layer (Figure 2.9).

5.2.2. Pile response in very dense sand

The lack of publicly available pile tests in very dense sand means that many design methods both explicitly (e.g. through limiting resistances) or implicitly (e.g. within averaging methods or design factors) limit the base and shaft capacity of the pile that can be used for design. While this can be a pragmatic response to the unknown, overly conservative limiting thresholds can lead to excessive material consumption and difficulties in getting the larger piles to the desired depth.

Measurements of installation-induced residual stresses are also seldom reported in literature. The distributed fibre optic results at Amaliahaven showed that the installation of

the driven precast piles mobilised 10 MPa of residual base stress, one-third of the ultimate base capacity. To create an equilibrium with this base stress, all of the upper layers were mobilised in negative shaft resistance (Figure 2.9). Design methods do not deal with residual loads directly. However, identifying the stresses induced by installation is a crucial step in pile test interpretation, ensuring a robust correlation between the CPT measurements and the measured base and shaft capacities.

From the initial residual stress, each driven precast pile mobilised an additional 20 MPa of base stress during testing, corresponding to an α_p of 0.67 and in line with that observed in looser sands in the ISO/API database (Lehane, Liu, et al., 2020). Load tests on two of the DCIS piles also mobilised base stresses of at least 20 MPa, albeit with much more variability across all four piles (Figure 2.14). The results from both sets of tests suggest that, within the observed range of cone resistances, there is no geotechnical mechanism that limits the base capacity in silica sands.

Similar findings were made with the shaft resistance. The driven precast piles mobilised shaft resistances of at least 200 kPa in the very dense sand. Nevertheless, the shaft resistance is limited by friction effects in the upper soil layers, captured well by the Unified pile design method (Figure 2.16). The DCIS did not exhibit friction fatigue, with piles reaching shaft resistances of up to 150 kPa in the upper soil layers.

The screw injection piles mobilised the highest shaft capacities, reaching a peak of 600 kPa in the very dense sand (Figure 2.11). However, the screw injection piles reached their structural limits at this shaft resistance and debonding at the steel-grout interface rapidly decreased the piles' shaft resistances. This suggests that the structural capacity of a pile, as opposed to the geotechnical capacity, is the primary constraint to supporting large loads in very dense sands.

5.2.3. Base response of screw displacement piles

In total, nine screw injection piles were tested: four in the very dense sand of Amaliahaven and five in the medium dense sand of Delft (Chapter 3). At a base displacement of $0.1D$, all screw injection piles mobilised a base capacity around 50 % lower than anticipated by the Dutch code NEN 9997-1. The mobilisation rate of this base capacity was dependent on the soil stiffness: the piles in the denser sands of Amaliahaven showed a ductile response compared to the driven precast piles, with the base resistance continuing to increase beyond displacements of $0.1D$. The Delft test piles, by contrast, mobilised almost all of their base capacity at a displacement of $0.1D$. Installation data from both test sites suggests that the base capacity did not depend on the installation procedure during the final metre of penetration.

To consider a broader range of installation conditions, the analysis was extended to a database review of all screw displacement pile types. The analysis showed that the initial interpretation of α_p may have been affected by the corresponding q_c averaging method, particularly since many of the database piles were only partially embedded into the primary load-bearing layer (Figure 3.16). When the different screw displacement pile types were compared to one another, the mean trend indicated a much lower α_p than anticipated, yielding an α_p redolent of a soil-replacing pile rather than a soil-displacing pile (Figure 3.18).

5.2.4. Shaft response of screw displacement piles

The four piles at Amaliahaven and piles F1, F2 and T1 at Delft mobilised peak α_s values in sand from 0.010 to 0.016. Instrumented results from other test piles also suggests a mean α_s of 0.012 (Figure 4.6). Nevertheless, a best-fit method to the instrumented results and four current design methods had a poor predictive performance of screw displacement piles with an oversized displacement body, referred to as Type 3 piles in this dissertation.

Indeed, instrumented records suggest that Type 3 piles mobilise higher shaft resistances when compared to other screw displacement pile types (Figure 4.7). However, soil removal mechanisms near the pile tip combined with soil displacing mechanisms around the oversized body, may create a depth-dependency in the radial stress development, and consequently, the shaft resistance. Therefore, an α_s of 0.012 is likely to be a conservative approach for these Type 3 piles.

Both the Amaliahaven and Delft tests are an example of how the structural integrity of a pile can greatly affects its capacity. Adhesive debonding at the steel tube–grout interface reduced the total capacity of the Amaliahaven screw injection piles, albeit at a very high shaft resistances. However, in spite of the lower shaft resistances at Delft (Figure 3.10), a sudden and complete loss of shaft resistance was exhibited by the screw injection piles with a permanent casing (*Tubex* piles). The exact mechanisms of this failure are not clear, but observations of the grout outflow during installation indicates that the failure was likely abetted by poor adhesive bonding at the steel–grout interface, or by poor strength of the grout body itself.

5.3. Recommendations for engineering practice

The outcomes of this research are intended to benefit both industry and society as a whole. With this in mind, the results from Amaliahaven are the first set of results to be approved and published on the Dutch national pile test database (NEN, 2017a). The results have also been approved for quay wall design at the port of Rotterdam, already leading to substantial financial and carbon emission savings whilst maintaining a high level of reliability (Roubos et al., 2024). Combined with findings from the wider *InPAD* project, recommendations have been made for the Dutch pile design standard NEN 9997-1 and are published separately to this dissertation.

Specifically in the context of this dissertation and the full-scale field tests, the recommendations for engineering practice are as follows:

5.3.1. Limiting resistances in design

When assessing the geotechnical capacity of a pile, existing limiting resistances should be increased to the highest observed resistances at Amaliahaven, that is, $q_{b,lim}$ = 30 MPa and $q_{s,lim}$ = 600 kPa. The structural assessment needs to be reconsidered in parallel, for instance, through a review of how partial safety factors are applied. This should be considered specifically in the context of composite cast-in-situ piles where interface adhesion is strongly dependent on the concrete casting and curing conditions.

5.3.2. Screw displacement pile design

The findings from instrumented tests on screw displacement piles show that current design methods tend to overestimate the contribution of the base resistance, but underestimate the shaft contribution. A best-fit to the instrumented data has indicated an α_s of 0.012 and α_p of 0.25, where α_p is determined with the adapted filter averaging method. Compared to a larger dataset of both uninstrumented and instrumented results, this best-fit method shows good agreement on average across all pile types, but the high variability suggests that CPT-based design of each type of screw displacement pile (Type 1, Type 2, Type 3 and Type 4, Figure 4.1) needs to be considered explicitly in design code, particularly with regards to installation-specific effects on their shaft resistance.

5.3.3. Friction fatigue

The shaft response of the driven precast piles at Amaliahaven was modelled well using Equation 2.3 and the Unified pile design method (Figure 2.15, Figure 2.16). The current design method in NEN 9997-1 assumes a constant α_s with depth for driven precast piles, leading to an overestimation of the shaft capacity of the pile—a potentially unsafe scenario.

Other research (Flynn and McCabe, 2016) has suggested that driven cast-in-situ piles (referred to in NEN 9997-1 as *vibropalen*) are also affected by friction fatigue, given the installation similarities between this pile type and driven precast piles. In this respect, a large amount of friction fatigue would have been expected in the driven cast-in-situ piles at Amaliahaven, yet the measurements gave no evidence of such a phenomenon (Figure 2.15, Figure 2.16). These results suggest that soil flow around the enlarged base plate and the withdrawal of the reusable casing are the governing factors in the shaft capacity of driven cast-in-situ, essentially removing any effect of friction fatigue.

Design methods therefore should include a depth-dependent term like Equation 2.3 to account for the effects of friction fatigue in driven precast piles.

5.3.4. Pile testing in NPR 7201

Pile testing in the Netherlands is generally performed in accordance with the NPR 7201 (2017) guidance document and in consultation with the NPR 7201 advisory committee. The guidance document provides a framework with which pile tests programmes can be designed and has been effective in developing a transparent and unified approach to pile testing across the country. Based on the work of this dissertation, some additional recommendations have been made for the guidance document:

- Removal of unload/reload cycles after each load step because of its detrimental effect on the pile shaft resistance, and thus affecting how the pile class factors are determined. Specific provisions should be made for load tests which aim to understand the cyclical response of piles.
- The advantages of distributed fibre optic sensing, particularly with its spatial resolution, should be reflected better within the standard, both in terms of the test quality designations (Class A1, Class A2 …) and the existing requirement to have sensors within one diameter from the pile head.
- The current creep criteria create excessive test durations, whilst providing little benefit in terms of pile test interpretation, particularly when the majority of the

pile capacity is derived from sand. Making the magnitude of the subsequent load increase dependent on the current creep rate, such as that proposed in Table 3.3, offers a means of capturing the full load-displacement curve whilst also giving comparable results to historical load tests.

- Incentivising open-access data and publishing findings from each test campaign would improve the scientific and societal value of performing pile load tests, as well as accelerating the Netherlands' reputation in foundation research and innovation.

5.4. Recommendations for future research

5.4.1. Structural capacity of piles

The structural integrity of the DCIS and screw injection piles dominated their overall performance, ultimately outweighing any uncertainties in the geotechnical design factors. The very dense sands of Amaliahaven led to debonding at the grout–steel interface of the screw injection piles and also may have caused the concrete deterioration at the bottom of the DCIS piles. At Delft, the soft impermeable layers affected the grout flow during installation, something which also ultimately affected the structural integrity of the grout body. A vital next step to this research is understanding the site-specificity of these failures, particularly with regards to soils with high confining stresses and where confined aquifers are present.

The installation procedure may have also initiated the structural failure. The water–cement ratio of screw injection piles, for instance, is an interplay between sustaining the fluidisation rate (that is, a high water–cement ratio) with a strong, grout shell (a low water–cement ratio). The water–cement ratios in this study ranged from 1.0 to 2.0. These ratios are typical of industry practice in the Netherlands, although it is generally considered a very fluid, weak grout mix, even when compared to the local guidelines for grout anchors (CUR, 2017). Structural failure in the Amaliahaven and Delft test piles suggests that the current water–cement prescriptions are not structurally sufficient. Nevertheless, future changes to these prescriptions need to consider the effect on installation performance, particularly in unique geological conditions.

Anticipating some of these structural flaws can be done by pile integrity testing, particularly where significant changes in the pile's cross-sectional area and stiffness may occur. Notwithstanding, sonic integrity testing did not detect structural abnormalities in the DCIS piles at Amaliahaven nor in the screw injection piles at Delft. A possible cause of this is the congested reinforcing of the DCIS piles and the slender steel tubes of the screw injection piles, both of which potentially inhibited the seismic waves travelling through the pile.

Thermal integrity tests are another potential solution (Mullins, 2010; Hopman and Hölscher, 2016; Sun et al., 2021). To assess whether anomalies in the pile shaft have formed, thermal integrity tests make use of the heat of hydration during concrete curing. Some recent research into thermal integrity testing (Hopman and Hölscher, 2016; Spruit et al., 2017; Rui et al., 2017) has used distributed fibre optic temperature sensing (Raman scattering) to improve the detection rate of structural flaws. The high spatial resolution of Raman sensing, combined with the low instrumentation footprint, is a significant benefit of the technique when compared to conventional integrity tests. Furthermore, with commercially

available data loggers now reaching more and more economical prices, this is becoming a more viable technique for practice.

5.4.2. Installation effects on screw displacement piles

The five design methods for screw displacement piles (Chapter 4) showed a high variation in how accurately they predicted the total capacity of Type 3 piles (such as De Waal or Omega piles). The instrumented records (Figure 4.6), along with a dependency between prediction accuracy and pile length (Figure 4.11), suggests that shaft resistance predictions could be improved. Nevertheless, the variability may express the complex mechanisms that govern the behaviour of Type 3 piles: a combined interplay between soil transport around the auger tip, soil displacement around the enlarged body, and re-equalisation in the confining stresses when the drilling tool is removed. The variation in confining stresses this may create would also imply a variance in α_s with depth.

The soil conditions, drilling tool geometry, and installation procedure all affect the confining stresses (Slatter, 2000; W. F. van Impe, 2001; Larisch, 2014). However, isolating each one of these factors was not possible with the current dataset, particularly given the variety of soil conditions and drilling tools. Type 3 piles instrumented with distributed fibre optic sensors would already help with understanding the behaviour of these piles, particularly if variations in drilling tool geometry and installation parameters could be achieved at the same site. Similarly, scaled laboratory tests or advanced numerical modelling techniques, such as discrete element modelling, would be hugely beneficial in understanding the different installation mechanisms.

Other questions still remain with screw displacement piles as a whole, particularly with regards to how installation parameters affect the geotechnical capacity (Admiraal et al., 2022; W. F. van Impe, 2001; NeSmith and NeSmith, 2006) and structural capacity (Teixeira et al., 2019) of these piles.

5.4.3. Serviceability limit state

The results in this dissertation have mainly considered the pile's response at large displacements, that is, the ultimate limit state (ULS). The serviceability limit state (SLS), on the contrary, considers low to intermediate displacements. At these displacements, pile response is usually modelled as a series of one-dimensional springs along the pile shaft (t-z curves) and underneath the pile base (q-z curves). These curves can be derived theoretically (Bateman et al., 2022; Crispin et al., 2018) or empirically (Bohn et al., 2017; Lehane, Li, and Bittar, 2020), and are often calibrated on instrumented records from static load tests and subsequently validated by the load–displacement response at the pile head.

Inevitably, SLS performance has been well assessed for driven precast and bored piles. However, only a small number of analyses have been performed on screw displacement piles (Allani and Huybrechts, 2020; Krasiński, 2012; Park et al., 2012) and driven cast-in-situ piles (Flynn, 2014). For instance, the base resistances of the screw injection piles at Amaliahaven and Delft suggests that their base response is largely controlled by the density and stiffness of the surrounding soil (Chapter 3.4.5). At Amaliahaven, where screw injection piles were tested adjacent to full-displacement driven precast piles, the screw injection piles mobilised their resistance at a much more gradual rate (Figure 2.14), suggesting that their base response differs substantially from a full-displacement pile. For further research,

both the instrumented database in Chapter 3 and the complete databases in Appendix A and Appendix B offers a good means of developing and validating new load-transfer methods for screw displacement piles, particularly in the context of the findings of this dissertation.

A

Database of Screw Displacement Piles

The complete screw displacement pile database is presented below, parts of which were used for the analyses in Chapter 3 and Chapter 4. All tests meet the following criteria:

- A cone penetration test was performed in the vicinity of the test pile, penetrating four pile diameters beyond the pile tip.
- All tests are maintained static load tests in compression or tension
- The full load-displacement response at the pile head was provided.

The database contains 129 pile tests in total, the majority of which are Type 3 and Type 4 piles. Most of the data was compiled from public literature and the tests at Amaliahaven, Delft and Werkendam has been collected first-hand by the author. The analysis of the tests from Oostwoud and Werkendam, performed in 2022 and 2023, has not been reported at the time of writing. The tests at Moerdijk, for which extracted records were available (Figure 4.4), also include seven additional piles which were subjected to rapid load tests, thus failing to meet the database criteria.

Records from the TU Delft and Deltares archive (indicated with an asterisk) are not publicly available but may be obtained upon request.

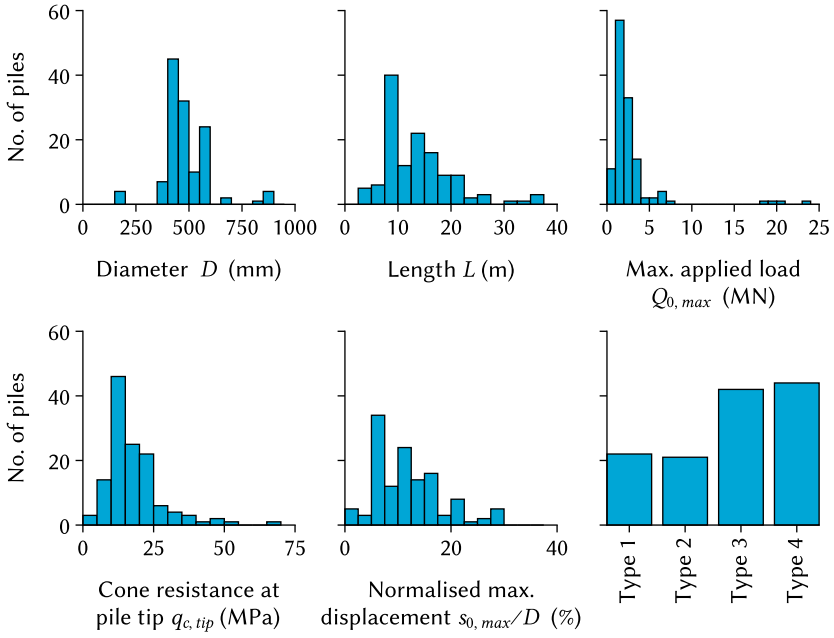

Figure A.1: Visual summary of the screw displacement pile database.

Table A.1: Database of static load tests on screw displacement piles with CPT data. The definition of d and D is given in Figure 4.1 and descriptions of each pile type is given in Chapter 4.2. Tests indicated with an asterisk (*) are from the TU Delft/Deltares archive and may be obtained upon request.

Site & Pile	d (mm)	D (mm)	L (m)	$q_{c,tip}$ (MPa)	$Q_{0,max}$ (MN)	$s_{0,max}/D$ (%)	Instrumented? (Y/N)	Reference
Type 1: Smooth shaft								
Almere SBP1	360	430	6.2	11	0.5	5	N	Schokking and IJnsen, 2014
Almere SBP2	360	430	6.3	10	0.6	5	N	Schokking and IJnsen, 2014
Almere SBP3	360	430	13.0	14	1.6	6	N	Schokking and IJnsen, 2014
Almere SBP4	360	430	13.1	12	1.7	8	N	Schokking and IJnsen, 2014
Almere SBP5	360	430	10.3	4	0.9	8	N	Schokking and IJnsen, 2014
Almere SBP6	360	430	10.2	3	1.0	6	N	Schokking and IJnsen, 2014
Beemster P2	70	150	2.9	17	0.2	28	Y	van der Geest et al., 2020
Beemster P3	70	150	2.9	37	0.1	28	Y	van der Geest et al., 2020
Beemster P6	70	150	2.9	35	0.1	25	Y	van der Geest et al., 2020
Beemster P7	70	150	2.9	33	0.1	29	Y	van der Geest et al., 2020
Bremen P2	440	560	8.5	10	1.8	5	N	de Cock, 2001
Limelette A1	380	450	9.6	20	3.1	14	Y	Maertens and Huybrechts, 2003
Limelette C1	390	450	9.7	22	1.6	6	Y	Maertens and Huybrechts, 2003
Renkum P1	355	560	26.4	22	2.4	29	N	Verstraelen et al., 2016
Seildeich P1	440	560	14.8	16	2.5	5	N	de Cock, 2001
Seildeich P2	440	560	13.8	16	3.0	5	N	de Cock, 2001
Terneuzen P02	460	560	20.0	13	6.0	10	Y	van Baars et al., 2018
Terneuzen P04	460	560	20.0	16	5.3	13	Y	van Baars et al., 2018
Terneuzen P06	460	560	19.9	15	4.4	14	Y	van Baars et al., 2018
Zimmerplatz P1	420	560	14.0	15	2.8	6	N	de Cock, 2001
Zuid-Oost Beemster P104	380	465	16.1	17	2.3	17	N	van Delft and van Dorp, 2010*
Zuid-Oost Beemster P105	380	465	16.2	17	2.3	15	N	van Delft and van Dorp, 2010*

Continued on next page …

Table A.1 (continued)

Site & Pile	d	D	L	$q_{c,tip}$	$Q_{0,max}$	$s_{0,max}/D$	Instrumented?	Reference
Type 2: Helical shaft								
Berlin P2	460	560	14.2	12	3.5	6	N	W. F. van Impe, 1988
Elblag P61	560	810	11.0	5	3.2	5	N	Gwizdała and Krasiński, 2005;
Gent I P1	460	510	13.05	8	2.8	9	N	W. F. van Impe, 1988
Gent I P2	460	510	13.5	10	3.1	13	N	W. F. van Impe, 1988
Gent II P6	460	510	12.5	28	2.5	5	N	de Beer, 1988
Gent II P10	460	510	2.5	28	2.3	3	N	de Beer, 1988
Limelette A2	360	510	9.2	21	3.1	6	Y	Maertens and Huybrechts, 2003
Limelette B3	360	510	9.4	23	3.6	13	Y	Maertens and Huybrechts, 2003
Limelette B4	360	510	9.4	23	3.6	13	Y	Maertens and Huybrechts, 2003
Limelette C2	360	510	9.1	22	2.7	5	Y	Maertens and Huybrechts, 2003
Oldenburg P1	510	560	9.5	22	2.3	5	N	de Cock, 2001
Oldenburg P2	510	560	7	8	1.7	5	N	de Cock, 2001
Oostwoud P27	340	410	14.2	14	1.3	14	Y	(to be reported)
Oostwoud P28	340	410	13.8	16	1.5	12	Y	(to be reported)
Werkendam P5	273	410	16.6	12	1.7	8	Y	(to be reported)
Werkendam P6	273	410	16.6	13	1.7	6	Y	(to be reported)
Werkendam P7	273	410	16.1	17	1.7	6	Y	(to be reported)
Werkendam P8	273	410	16.1	12	1.7	7	Y	(to be reported)
Zeeland O1	310	460	9.1	32	1.4	15	Y	APTS, 2022*
Zeeland O2	310	460	8.0	24	1.6	12	Y	APTS, 2022*
Zeeland O3	310	460	9.5	20	1.8	15	Y	APTS, 2022*
Type 3: Displacement body								
Amsterdam-Sloten P7	360	400	14.6	7	1.7	19	N	de Wit, 1999*
Amsterdam-Sloten P8	360	400	14.3	10	1.7	17	N	de Wit, 1999*
Amsterdam-Sloten P10	360	400	15.4	10	1.8	16	N	de Wit, 1999*
Bratislava TP1	n/a	410	17.9	75	2.0	9	Y	Stacho, 2018

Continued on next page …

Table A.1 (continued)

Site & Pile	d	D	L	$q_{c,tip}$	$Q_{0,max}$	$s_{0,max}/D$	Instrumented?	Reference
Bratislava TP2	n/a	410	15.9	70	2.0	6	Y	Stacho, 2018
Elblag P9	300	400	7.5	17	1.1	8	Y	Krasiński and Wiszniewski, 2021
Gdańsk P806	300	400	12.9	16	1.6	5	Y	Krasiński et al., 2023
Gdańsk P807	300	400	12.3	12	1.8	6	Y	Krasiński et al., 2023
Gdańsk P808	300	400	12.7	11	1.7	6	Y	Krasiński et al., 2023
Gdańsk P809	300	400	12.9	10	1.7	12	Y	Krasiński et al., 2023
Grottgera P600	300	400	11.0	13	0.9	10	Y	Krasiński, 2023
Grottgera P602	300	400	10.9	15	1.5	11	Y	Krasiński, 2023
Hamburg PA	310	510	10.4	13	3.2	8	N	Busch et al., 2013
Hamburg PB	n/a	440	8.4	15	2.2	13	N	Busch et al., 2013
Limelette A3	n/a	410	9.5	22	2.9	13	Y	Maertens and Huybrechts, 2003
Limelette A4	n/a	410	9.5	23	2.6	16	Y	Maertens and Huybrechts, 2003
Limelette C3	n/a	410	9.5	21	2.8	17	Y	Maertens and Huybrechts, 2003
Limelette C4	n/a	410	9.5	19	2.5	21	Y	Maertens and Huybrechts, 2003
Loenhout S2	n/a	410	9.5	14	1.2	14	Y	Theys et al., 2003
Lomme P1	273	360	8.5	25	1.7	14	Y	Bustamente and Gianeselli, 1997
Midden-Beemster P1	410	570	17.5	28	1.8	9	N	de Wit, 1994*
Midden-Beemster P5	410	670	17.0	37	1.8	6	N	de Wit, 1994*
Oostende P1	n/a	460	21.6	30	3.6	16	Y	P. O. van Impe et al., 2013
Oostwoud P1	273	360	16.0	17	1.6	16	Y	(to be reported)
Oostwoud P6	273	360	16.4	14	1.1	19	Y	(to be reported)
Oostwoud P12	273	360	16.5	9	1.4	38	Y	(to be reported)
Oostwoud P22	273	360	18.0	12	1.8	15	Y	(to be reported)
Playa Vista P42	n/a	457	14.9	16	2.4	5	N	Reader and Armstrong, 2005
Pruszcz Gdański b1	n/a	356	7.5	10	1.2	6	Y	Krasiński, 2011b
Pruszcz Gdański b2	n/a	356	7.1	12	1.0	5	Y	Krasiński, 2011b
Santa Cruz C2	350	450	9.5	9	2.4	28	Y	Fellenius et al., 2017
Soodi S1	406	560	12.7	12	1.8	6	N	Leetsaar and Korkiala Tanttu, 2023

Continued on next page …

Table A.1 (continued)

Site & Pile	d	D	L	$q_{c,tip}$	$Q_{0,max}$	$s_{0,max}/D$	Instrumented?	Reference
Soodi S4	n/a	440	12.5	12	1.9	5	N	Leetsaar and Korkiala Tanttu, 2023
Vilvoorde P3	410	410	14.0	45	2.1	5	Y	Bottiau, 1995
Vilvoorde P5	410	410	8.2	14	1.9	14	Y	Bottiau, 1995
Werkendam P1	273	410	17.4	10	2.4	11	Y	(to be reported)
Werkendam P2	273	410	17.9	5	2.4	8	Y	(to be reported)
Werkendam P3	273	410	17.4	11	2.3	9	Y	(to be reported)
Werkendam P4	273	410	17.9	9	2.2	10	Y	(to be reported)
Zulawy b1	n/a	400	10.2	17	0.9	5	Y	Krasiński, 2011a
Zulawy b2	n/a	400	10.4	25	0.9	3	Y	Krasiński, 2011a
Zulawy b3	n/a	400	10.3	24	0.7	4	Y	Krasiński, 2011a
Type 4: Screw injection								
Amaliahaven SI1	610	850	37.0	42	20.3	14	Y	Chapter 2
Amaliahaven SI2	610	850	37.1	45	23.3	16	Y	Chapter 2
Amaliahaven SI3	610	850	35.0	30	18.6	18	Y	Chapter 2
Amaliahaven SI4	610	850	34.1	50	19.0	15	Y	Chapter 2
Delft F1	355	470	20.0	11	2.7	21	Y	Chapter 3
Delft F2	355	470	19.2	13	2.6	20	Y	Chapter 3
Delft T1	382	470	19.9	11	2.6	15	Y	Chapter 3
Delft T2	382	470	20.3	9	2.3	21	Y	Chapter 3
Delft T3	382	470	20.9	12		21	Y	Chapter 3
Galecopper P1	457	570	31.5	12	7.5	2	Y	Hocombe et al., 2015
Galecopper P2	457	570	27.0	17	6.6	2	Y	Hocombe et al., 2015
Gent II P3	380	450	13.0	12	2.4	10	N	de Beer, 1988
Gent II P8	380	450	13.0	20	2.1	9	N	de Beer, 1988
Haren P1	540	660	16.4	16	4.8	8	Y	Bottiau and Huybrechts, 2019
Lemmer A1	355	470	9.5	24	1.0	10	N	Admiraal et al., 2022
Lemmer A2	355	470	9.5	13	1.0	10	N	Admiraal et al., 2022
Lemmer A3	355	470	9.5	22	1.1	10	N	Admiraal et al., 2022

Continued on next page …

Table A.1 (continued)

Site & Pile	d	D	L	$q_{c,tip}$	$Q_{0,max}$	$s_{0,max}/D$	Instrumented?	Reference
Lemmer B1	355	470	9.5	22	1.2	10	N	Admiraal et al., 2022
Lemmer B2	355	470	9.5	15	1.2	10	N	Admiraal et al., 2022
Lemmer B3	355	470	9.5	20	1.3	10	N	Admiraal et al., 2022
Lemmer C1	355	470	9.5	10	1.3	10	N	Admiraal et al., 2022
Lemmer C2	355	470	9.5	3	1.3	10	N	Admiraal et al., 2022
Lemmer C3	355	470	9.5	26	1.3	10	N	Admiraal et al., 2022
Lemmer D1	355	470	9.5	12	1.2	10	Y	Admiraal et al., 2022
Lemmer D2	355	470	9.5	13	1.2	10	Y	Admiraal et al., 2022
Lemmer D3	355	470	9.5	24	1.1	10	Y	Admiraal et al., 2022
Lemmer E1	355	470	9.5	22	1.1	10	N	Admiraal et al., 2022
Lemmer E2	355	470	9.5	6	1.3	10	N	Admiraal et al., 2022
Lemmer E3	355	470	9.5	8	1.3	10	N	Admiraal et al., 2022
Moerdijk P4	435	530	11.3	17	2.0	16	N	IFCO, 2003*
Renkum P2	355	560	26.4	20	3.6	21	N	Verstraeten et al., 1988
Rosmalen P1	219	400	8.0	13	1.6	22	N	Geerling et al., 1992*
Rosmalen P2	219	400	7.8	10	1.6	26	N	Geerling et al., 1992*
Rosmalen P3	273	400	7.4	9	1.6	21	Y	Geerling et al., 1992*
Rosmalen P4	273	400	7.9	11	1.8	23	N	Geerling et al., 1992*
Rosmalen P5	273	400	7.2	11	1.7	49	N	Geerling et al., 1992*
Rotterdam Centraal P1	406	560	18.0	33	2.9	5	N	Spruit et al., 2012
Rotterdam Centraal P5	406	560	15.0	5	2.6	3	N	Spruit et al., 2012
Terneuzen P01	460	560	21.3	13	5.9	4	Y	van Baars et al., 2018
Terneuzen P03	460	560	20.2	14	6.1	13	Y	van Baars et al., 2018
Terneuzen P05	460	560	20.2	15	6.4	15	Y	van Baars et al., 2018
Wijnhaven P2	406	560	24.0	19	3.0	6	Y	Grondmechanica Delft, 1987*
Wijnhaven P4	406	560	24.0	19	3.0	6	Y	Grondmechanica Delft, 1987*
Zwolle P1	450	560	11.0	10	3.0	6	N	de Cock, 2001

B

Database of Driven Cast-in-Situ Piles

The driven cast-in-situ pile database is presented below and extends on the database compiled by Flynn (2014) and Flynn and McCabe (2021). All tests meet the following criteria:

- A cone penetration test was performed in the vicinity of the test pile, penetrating four pile diameters beyond the pile tip.
- All tests are maintained static load tests in compression or tension
- The full load-displacement response at the pile head was provided.

The database contains 51 pile tests in total, including the 15 tests that were reported in Flynn (2014) and Flynn and McCabe (2021). The majority of the new tests come from the archive of TU Delft and Deltares and include variants of DCIS piles like *Vibrex*, *Vibro-Fundex* and *Vibro-SD*. Piles which use a concrete plug instead of a driving shoe, so-called *Franki* piles, are not included in the database.

Notably, the tests from Beneluxtunnel, Hengelo, de Gaag, Rijswijk and Zeist followed a traditional pile test procedure used in the Netherlands whereby three to five unload/reload cycles were performed after each and every load step. Crucially, this may affect the mobilised capacity and make it difficult to compare with other pile tests.

Records from the TU Delft and Deltares archive (indicated with an asterisk) are not publicly available but may be obtained upon request.

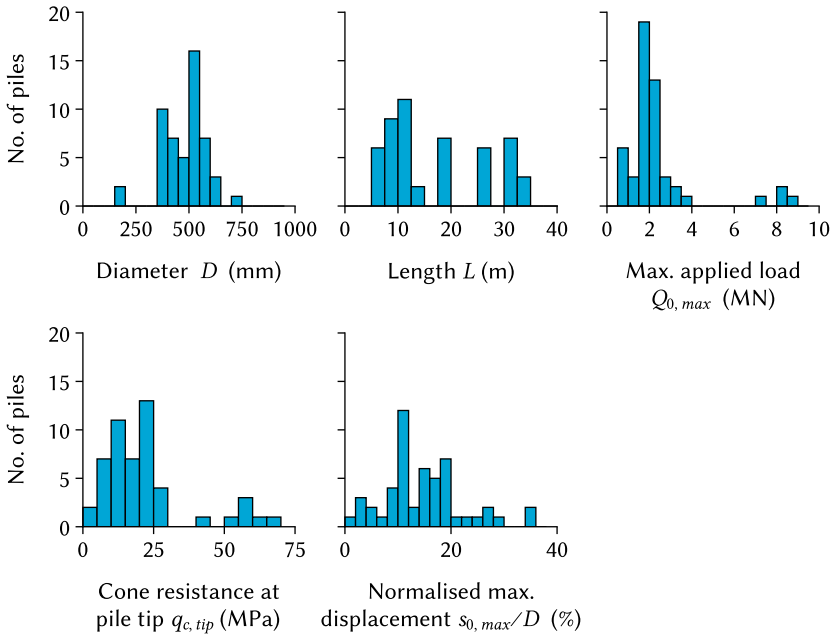

Figure B.1: Visual summary of the driven cast-in-situ pile database.

Table B.1: Database of static load tests on driven cast-in-situ piles with CPT data. The outer diameter of the reusable casing is represented by d and the diameter of the enlarged base plate by D. Tests indicated with an asterisk (*) are from the TU Delft/Deltares archive and may be obtained upon request.

Site & Pile	d (mm)	D (mm)	L (m)	$q_{c,tip}$ (MPa)	$Q_{0,max}$ (MN)	$s_{0,max}/D$ (%)	Instru-mented? (Y/N)	Reference
Alblasserdam T1	356	435	19.5	23	2.2	18	Y	Ligthart and Timmer, 2019*
Alblasserdam T2	356	435	19.5	18	2.2	18	Y	Ligthart and Timmer, 2019*
Alblasserdam T3	356	435	19.5	20	2.4	9	Y	Ligthart and Timmer, 2019*
Amaliahaven DCIS1	380	480	32.5	42	7.4	28	Y	Chapter 2
Amaliahaven DCIS2	380	480	32.5	68	8.8	16	Y	Chapter 2
Amaliahaven DCIS3	380	480	32.5	55	8.0	27	Y	Chapter 2
Amaliahaven DCIS4	380	480	32.5	55	8.4	21	Y	Chapter 2
Beneluxtunnel KH	457	520	26.0	20	0.8	2	N	van Noortwijk et al., 1994*
Beneluxtunnel LH	457	520	26.0	20	1.8	6	N	van Noortwijk et al., 1994*
Beneluxtunnel LN	457	520	26.0	20	2.0	3	Y	van Noortwijk et al., 1994*
Beneluxtunnel VH	508	550	26.0	20	0.5	1	N	van Noortwijk et al., 1994*
Beneluxtunnel VS	508	550	26.0	20	1.0	2	N	van Noortwijk et al., 1994*
Beneluxtunnel KN	508	550	26.0	20	1.8	5	N	van Noortwijk et al., 1994*
De Gaag P1	457	508	30.0	10	0.8	23	Y	Geerling and Janse, 1997*
De Gaag P2	457	508	30.0	22	0.5	14	Y	Geerling and Janse, 1997*
De Gaag P3	508	557	30.0	14	1.7	19	Y	Geerling and Janse, 1997*
De Gaag P4	508	557	30.0	22	2.7	19	Y	Geerling and Janse, 1997*
De Gaag P5	508	557	30.0	26	2.0	17	Y	Geerling and Janse, 1997*
De Gaag P7	457	508	30.0	25	1.6	16	Y	Geerling and Janse, 1997*
Groot-Bijgaarden P2	508	520	10.0	15	2.4	10	N	BGGG-GBMS, 1985
Groot-Bijgaarden P3	508	620	10.0	15	2.2	10	N	BGGG-GBMS, 1985
Groot-Bijgaarden P5	508	720	10.0	12	2.0	10	N	BGGG-GBMS, 1985
Haarlem P86	380	480	10.8	9	1.8	9	N	Woldringh, 1987*
Hengelo P1	457	520	9.6	12	1.5	16	N	Grondmechanica Delft, 1985*

Continued on next page ...

Table B.1 (continued)

Site & Pile	d	D	L	$q_{c,tip}$	$Q_{0,max}$	$s_{0,max}/D$	Instrumented?	Reference
Rijswijk P3	323	360	18.3	15	1.7	34	Y	Geerling and Janse, 1993*
Rijswijk P4	323	360	18.3	15	1.8	24	Y	Geerling and Janse, 1993*
Soodi S1	406	520	12.7	13	2.1	19	N	Leetsaar and Korkiala Tanttu, 2023
Soodi S2	406	520	11.3	2	2.0	34	N	Leetsaar and Korkiala Tanttu, 2023
Waalwijk P3	180	180	10.9	13	0.7	10	N	Klein, 2011*
Waalwijk P5	180	180	10.9	13	0.7	11	N	Klein, 2011*
Zeist P02	457	517	7.0	7	1.6	10	N	Heins, 1973
Zeist P03	457	517	7.0	7	1.6	15	N	Heins, 1973
Zeist P04	457	517	8.0	7	1.6	14	N	Heins, 1973
Zeist P05	457	517	8.0	7	1.8	13	N	Heins, 1973
Zeist P08	457	517	9.0	7	1.3	14	N	Heins, 1973
Zeist P11	457	517	9.0	7	1.8	13	N	Heins, 1973
Database from Flynn (2014) and Flynn et al. (2021)								
Dagenham D1	320	380	7.7	52	2.6	11	Y	Flynn, 2014
Erith E1	320	380	10.8	18	1.7	4	N	Flynn, 2014
Erith E3	320	380	11.1	25	2.0	11	Y	Flynn, 2014
Kallo K5	406	406	9.3	25	1.8	17	N	de Beer et al., 1979
Kallo K7	406	609	9.4	27	2.9	11	N	de Beer et al., 1979
Le Havre A4	430	430	10.5	62	1.7	19	N	Evers et al., 2003
Le Havre C1	410	430	10.5	59	1.9	15	Y	Evers et al., 2003
Mechelen KW11	508	550	18.5	14	3.8	26	Y	Verstraelen et al., 2016
Mechelen KW12	508	600	18.5	14	3.2	19	Y	Verstraelen et al., 2016
Pontarddulais P1	320	380	8.5	4	0.9	10	Y	Flynn, 2014
Ringsend TP20	408	425	12.5	13	3.3	9	N	Suckling, 2003
Ryton R1	320	380	6.0	15	1.7	11	Y	Flynn, 2014
Ryton R2	320	380	7.0	20	1.6	11	Y	Flynn, 2014
Ryton R3	320	380	5.5	14	2.2	9	Y	Flynn, 2014
Shotton S1	320	380	5.8	21	2.2	14	Y	Flynn, 2014

References

Admiraal, B. J., Aguilar, S. A., Van Dijk, S., & IJnsen, P. (2022). Influence of grout injection parameters on shaft bearing capacity of screw displacement piles. *Proceedings of the 11th International Conference on Stress Wave Theory and Design and Testing Methods for Deep Foundations*. https://doi.org/10.5281/zenodo.7139213

AFNOR. (2018). *NF P94-262/A1: Justification des ouvrages géotechniques - Normes d'application nationale de l'Eurocode 7 - Fondations profondes*.

Ahmadi, M. M., & Robertson, P. K. (2005). Thin-layer effects on the CPT qc measurement. *Canadian Geotechnical Journal*, *42*(5), 1302–1317. https://doi.org/10.1139/t05-036

Allani, M., & Huybrechts, N. (2020). Berekening van zettingen van verticaal belaste palen: Methods voor het afleiden van vervormingsparameters [magazine]. *Geotechniek*, *4*, 10–16.

American Petroleum Institute. (2011). *Geotechnical and foundation design considerations* (RP-2GEO). API. Washington DC, USA.

Anusic, I., Lehane, B. M., Eiksund, G. R., & Liingaard, M. A. (2019). Evaluation of installation effects on set-up of field displacement piles in sand. *Canadian Geotechnical Journal*, *56*(4), 461–472. https://doi.org/10.1139/cgj-2017-0730

APTS. (2022). *Rapportage statische belastingproef Klasse A1 op Olivierpalen® in Terneuzen* (G16206_RAP_40240_V_3). Terneuzen, The Netherlands.

Atkinson, J. H. (2000). Non-linear soil stiffness in routine design. *Géotechnique*, *50*(5), 487–508. https://doi.org/10.1680/geot.2000.50.5.487

Basu, P., Prezzi, M., & Basu, D. (2010). Drilled Displacement Piles – Current Practice and Design. *DFI Journal - The Journal of the Deep Foundations Institute*, *4*(1), 3–20. https://doi.org/10.1179/dfi.2010.001

Basu, P., Prezzi, M., & Salgado, R. (2014). Modeling of installation and quantification of shaft resistance of drilled-displacement piles in sand. *International Journal of Geomechanics*, *14*(2), 214–229. https://doi.org/10.1061/(ASCE)GM.1943-5622.0000303

Bateman, A. H., Crispin, J. J., Vardanega, P. J., & Mylonakis, G. E. (2022). Theoretical t-z curves for axially loaded piles. *Journal of Geotechnical and Geoenvironmental Engineering*, *148*(7), 04022052. https://doi.org/10.1061/(ASCE)GT.1943-5606.0002753

BGGG-GBMS. (1985). Belgian Geotechnical Volume. *Golden Jubilee of the International Society for Soil Mechanics and Foundation Engineering (ISSMFE)*.

Bittar, E. J., Lehane, B. M., Blake, A., Richards, D., White, D. J., Mahdavi, S., & Cerfontaine, B. (2023). CPT-based design method for helical piles in sand. *Canadian Geotechnical Journal*, *61*(1), 107–112. https://doi.org/10.1139/cgj-2022-0209

Bittar, E. J., Lehane, B. M., Boulanger, R. W., & DeJong, J. T. (2020). CPT filter to estimate the end bearing of closed-ended driven piles in layered sands. *Proceedings of the 4th International Symposium on Frontiers in Offshore Geotechnics*, 520–528.

Bittar, E. J., Tian, Y., & Lehane, B. M. (2022). Application of a new qc averaging approach for end bearing of driven piles in sand. *Cone Penetration Testing 2022*, 832–837. https://doi.org/10.1201/9781003308829-123

Bohn, C., Lopes dos Santos, A., & Frank, R. (2017). Development of axial pile load transfer curves based on instrumented load tests. *Journal of Geotechnical and Geoenvironmental Engineering*, *143*(1), 04016081. https://doi.org/10.1061/(ASCE)GT.1943-5606.0001579

Bottiau, M., & Cortvrindt, G. (1994). Recent experience with the Omega-Pile. *Proceedings of the 5th International Conference on Piling and Deep Foundations*, *13*, 3.11.0–3.11.7.

Bottiau, M., & Huybrechts, N. (2019). Recent advances in pile design, construction, monitoring and testing. *Proceedings of the 17th European Conference on Soil Mechanics and Geotechnical Engineering*. https://doi.org/10.32075/17ECSMGE-2019-1116

Bottiau, M. (1995). Comparative assessment of the bearing capacity out of CPT-results. *Proceedings CPT '95*, 399–406.

Bottiau, M. (2015). Current status, trends and future of deep foundations [magazine]. *DFI Deep Foundations*, 23–27. https://dfi.dcatalog.com/v/November-December-2015/?page=82

Boulanger, R. W., & DeJong, J. T. (2018). Inverse filtering procedure to correct cone penetration data for thin-layer and transition effects. *Proceedings of the 4th International Symposium on Cone Penetration Testing (CPT'18)*, 24–44.

Brown, D. A., Dapp, S. D., Thompson, R. W., & Lazarte, C. A. (2007, January 1). *Geotechnical Engineering Circular No. 8: Design and Construction of Continuous Flight Auger Piles* (Technical Report No. FHWA-HIF-07-03). Federal Highway Administration. Washington DC, USA. Retrieved March 22, 2024, from https://rosap.ntl.bts.gov/view/dot/41170

Busch, P., Grabe, J., & Gerressen, F. W. (2013). Influence of the installation process of full displacement bored piles on the subsoil. *Proceedings of the Conference on Baltic Piling Days 2012*, 157–163.

Bustamente, M., & Gianeselli, L. (1982). Pile bearing capacity prediction by means of static penetrometer CPT. *Proceedings of the Second European Symposium on Penetration Testing*, 493–500.

Bustamente, M., & Gianeselli, L. (1997). Portance d'un pieu De Waal, vissé moulé dans un sable sous nappe. *Bulletin des Laboratoires des Ponts et Chaussées*, (208), 107–115.

Bustamente, M., & Gianeselli, L. (1998). Installation parameters and capacity of screwed piles. *Proceedings of the 3rd International Geotechnical Seminar on Deep Foundations on Bored and Auger Piles (BAP III)*, 95–108.

Cerfontaine, B., Brown, M. J., Knappett, J. A., Davidson, C., Sharif, Y. U., Huisman, M., Ottolini, M., & Ball, J. D. (2023). Control of screw pile installation to optimise performance for offshore energy applications. *Géotechnique*, *73*(3), 234–249. https://doi.org/10.1680/jgeot.21.00118

Chai, F. (2024). *Pile base resistance prediction in multilayered soil systems based on direct CPT methods* [Doctoral dissertation, University of New South Wales].

Chai, F., Liu, B., Xue, J., & Duffy, K. (2025). Assessing direct CPT-based methods for predicting pile base resistance using coupled DEM-FDM simulations. *Computers and Geotechnics*, *183*, 107230. https://doi.org/10.1016/j.compgeo.2025.107230

Chin, F. (1970). Estimation of the ultimate load of piles from tests not carried to failure. *Proc. 2nd Southeast Asian Conference on Soil Engineering, Singapore, 1970*.

Crispin, J. J., Leahy, C. P., & Mylonakis, G. (2018). Winkler model for axially loaded piles in inhomogeneous soil. *Géotechnique Letters*, *8*(4), 290–297. https://doi.org/10.1680/jgele.18.00062

CUR. (2017). *Ankerpalen* (CUR-publicatie 236). Delft, The Netherlands.

de Beer, E. E. (1971). Méthodes de déduction de la capacité portante d'un pieu à partir des résultats des essais de pénétration. *Annales des Travaux Publics de Belgique*, *1971–2*, 191–268.

de Beer, E. E. (1988). Different behaviour of bored and driven piles. *Proc. 1st International Seminar on Deep Foundations on Bored and Auger Piles (BAP I)*, 47–82.

de Beer, E. E., Lousberg, E., de Jonghe, A., Carpentier, R., & Wallays, M. (1979). Analysis of the results of loading tests performed on displacement piles of different types and sizes penetrating at a relatively small depth into a very dense sand layer. *Recent Developments in the Design and Construction of Piles*, 199–211. https://doi.org/10.1680/rditdacop.00827.0022

de Boorder, M. (2019). *Development of a new CPT averaging technique and review of existing CPT based methods for the calculation of total pile capacity* [M.Sc. Thesis]. TU Delft. http://resolver.tudelft.nl/uuid:2b2587e5-aa76-458b-af41-f21cd35d58d9

de Boorder, M., de Lange, D. A., & Gavin, K. G. (2022). An alternative CPT averaging procedure to estimate pile base capacity. *Proceedings from the 11th International Conference on Stress Wave Theory and Design and Testing Methods for Deep Foundations*. https://doi.org/10.5281/zenodo.7142197

de Cock, F. A. (2001). A database approach to overview pile loading tests on displacement screw piles in Western Europe – 1970–2000. *Proceedings of the Symposium on Screw Piles*, 89–125.

de Cock, F. A. (2008). Sense and sensitivity of pile load-deformation behaviour. *5th International Symposium on Deep Foundations on Bored and Auger Piles (BAP V)*, 23–44.

de Cock, F. A., & Imbo, R. P. (1994). Atlas screw pile: A vibration-free, full displacement, cast-in-situ pile. *Transportation Research Record*, (1447), 49–62.

de Gijt, J. G., & Broeken, M. (2013). *Quay Walls* (2nd Edition). CRC Press.

de Klijn-Chevalerias, M., & Javed, S. (2017). The Dutch approach for assessing and reducing environmental impacts of building materials. *Building and Environment*, *111*, 147–159. https://doi.org/10.1016/j.buildenv.2016.11.003

de Lange, D. A. (2018). *CPT in thinly layered soils: Validation tests and analysis for multi thin layer correction* (No. 1209862–006). Nederlandse Aardolie Maatschappij. https://nam-onderzoeksrapporten.data-app.nl/reports/download/groningen/en/3a1f937a-799a-4921-a64f-eac65acf14f7

de Wit, T. (1994). *Proefbelasting op in de grond gevormde verdringingsschroefpalen (DPA-palen) Vroom/HBF te Midden-Beemster* (AE-02157). Sassenheim, The Netherlands.

de Wit, T. (1999). *Rapport betreffende proefbelasting op verdringingsschroefpalen (DPA-palen) van Vroom Funderingstechnieken/HBF te Amsterdam-Sloten* (AB-05466). Geomet. Alphen aan de Rijn, The Netherlands.

Doan, L. V., & Lehane, B. M. (2021). CPT-based design method for axial capacities of drilled shafts and auger cast-in-place piles. *Journal of Geotechnical and Geoenvironmental Engineering*, *147*(8), 04021077. https://doi.org/10.1061/(ASCE)GT.1943-5606.0002542

Duffy, K. J. (2020). *Report on pile test results at Maasvlakte II: Driven Precast Piles*. TU Delft. Delft, The Netherlands. https://research.tudelft.nl/en/publications/report-on-pile-test-results-at-maasvlakte-ii-driven-precast-piles

Duffy, K. J. (2021a). *Report on pile test results at Maasvlakte II: Screw injection piles*. TU Delft. Delft, The Netherlands. https://research.tudelft.nl/en/publications/report-on-pile-test-results-at-maasvlakte-ii-screw-injection-pile

Duffy, K. J. (2021b). *Report on pile test results at Maasvlakte II: Vibro piles*. TU Delft. Delft, The Netherlands. https://research.tudelft.nl/en/publications/report-on-pile-test-results-at-maasvlakte-ii-vibro-piles

Duffy, K. J. (2024). *Delft screw injection pile tests: Factual report*. TU Delft. Delft, The Netherlands. https://research.tudelft.nl/en/publications/delft-screw-injection-pile-tests-factual-report

Duffy, K. J., Gavin, K. G., de Lange, D. A., & Korff, M. (2024). Base resistance of screw displacement piles in sand. *Journal of Geotechnical and Geoenvironmental Engineering*, *150*(8), 04024070. https://doi.org/10.1061/JGGEFK/GTENG-12340

Duffy, K. J., Gavin, K. G., de Lange, D. A., & Korff, M. (2022). Residual stress measurement of driven precast piles using distributed fibre optic sensors. *Proceedings from the 11th International Conference on Stress Wave Theory and Design and Testing Methods for Deep Foundations*. https://doi.org/10.5281/zenodo.7146663

Duffy, K. J., Gavin, K. G., Korff, M., de Lange, D. A., & Roubos, A. A. (2024). Influence of installation method on the axial capacity of piles in very dense sand. *Journal of Geotechnical and Geoenvironmental Engineering*, *150*(6). https://doi.org/10.1061/JGGEFK/GTENG-12026

Evers, G., Hass, G., Frossard, A., Bustamente, M., Borel, S., & Skinner, H. (2003). Comparative performances of continuous flight auger and driven cast in place piles in sands. *Proceedings of the 4th International Geotechnical Seminar on Deep Foundations on Bored and Auger Piles*, 138–144.

Fellenius, B. H. (2001). From strain measurements to load in an instrumented pile [magazine]. *Geotechnical News Magazine*, *19*(1), 35–38.

Fellenius, B. H. (2002). Determining the resistance distribution in piles. Part 2: Method for determining the residual load [magazine]. *Geotechnical News Magazine*, *20*(3), 25–29.

Fellenius, B. H., Terceros, M. H., & Massarch, R. K. (2017). Bolivian experimental site for testing. *Proceedings of the 3rd Bolivian International Conference on Deep Foundations—Volume 2*, *2*, 3–30.

Figueroa, G., Marinucci, A., & Lemnitzer, A. (2022). Axial load capacity predictions of drilled displacement piles with SPT- and CPT-based direct methods. *DFI Journal - The Journal of the Deep Foundations Institute*, *16*(2). https://doi.org/10.37308/DFIJnl.20220512.262

Fleming, W. G. K. (1992). A new method for single pile settlement prediction and analysis. *Géotechnique*, *42*(3), 411–425. https://doi.org/10.1680/geot.1992.42.3.411

Fleming, W. G. K., Weltman, A., Elson, K., & Randolph, M. F. (2008). *Piling Engineering* (3rd Edition). Taylor & Francis.

Fleming, W., & Thorburn, S. (1983). Recent piling advances, state of the art report. *Proceedings of the International Conference on Advances in Piling and Ground Treatment for Foundations,*

Flynn, K. N. (2014). *Experimental investigations of driven cast-in-situ piles* [Doctoral dissertation, NUI Galway].

Flynn, K. N., & McCabe, B. A. (2016). Shaft resistance of driven cast-in-situ piles in sand. *Canadian Geotechnical Journal*, *53*(1), 49–59. https://doi.org/10.1139/cgj-2015-0032

Flynn, K. N., & McCabe, B. A. (2021). Applicability of CPT capacity prediction methods to driven cast-in-situ piles in granular soil. *Journal of Geotechnical and Geoenvironmental Engineering*, *147*(2), 04020170. https://doi.org/10.1061/(ASCE)GT.1943-5606.0002445

Flynn, K. N., & McCabe, B. A. (2022). Instrumented concrete pile tests – part 1: A review of instrumentation and procedures. *Proceedings of the Institution of Civil Engineers - Geotechnical Engineering*, *175*(1), 86–111. https://doi.org/10.1680/jgeen.21.00126

Flynn, K. N., McCabe, B. A., & Egan, D. (2012). Residual load development in cast-in-situ piles – a review and new case history. *Proceedings of the 9th International Conference on Testing and Design Methods for Deep Foundations*, 765–773.

Frank, R. (2017). Some aspects of research and practice for pile design in France. *Innovative Infrastructure Solutions*, *2*(1), 32. https://doi.org/10.1007/s41062-017-0085-4

Ganju, E., Han, F., Prezzi, M., & Salgado, R. (2020). Static capacity of closed-ended pipe pile driven in gravelly sand. *Journal of Geotechnical and Geoenvironmental Engineering*, *146*(4), 04020008. https://doi.org/10.1061/(ASCE)GT.1943-5606.0002215

Gavin, K. G., Cadogan, D., & Casey, P. (2009). Shaft capacity of continuous flight auger piles in sand. *Journal of Geotechnical and Geoenvironmental Engineering*, *135*(6), 790–798. https://doi.org/10.1061/(ASCE)GT.1943-5606.0000073

Gavin, K. G., Cadogan, D., Tolooiyan, A., & Casey, P. (2013). The base resistance of non-displacement piles in sand. Part I: Field tests. *Proceedings of the Institution of Civil Engineers - Geotechnical Engineering*, *166*(6), 540–548. https://doi.org/10.1680/geng.11.00100

Gavin, K. G., Kovacevic, M. S., & Igoe, D. (2021). A review of CPT based axial pile design in the Netherlands. *Underground Space*, *6*(1), 85–99. https://doi.org/10.1016/j.undsp.2019.09.004

Gavin, K. G., & Lehane, B. M. (2007). Base load – displacement response of piles in sand. *Canadian Geotechnical Journal*, *44*(9), 1053–1063. https://doi.org/10.1139/T07-048

Gavin, K. G., & O'Kelly, B. C. (2007). Effect of friction fatigue on pile capacity in dense sand. *Journal of Geotechnical and Geoenvironmental Engineering*, *133*(1), 63–71. https://doi.org/10.1061/(ASCE)1090-0241(2007)133:1(63)

Geerling, J., & Janse, E. (1993). *Proefbelastingen op twee typen gronderverdringende funderingspalen* (CO-330890/56). Grondmechanica Delft. Delft, The Netherlands.

Geerling, J., & Janse, E. (1997). *Trekpalenonderzoek locatie de Gaag proefbelastingen op 9 palen* (CO-351310/195). Grondmechanica Delft. Delft, The Netherlands.

Geerling, J., Janse, E., & Kruzinga, J. (1992). *Proefbelastingen op schroefinjectiepalen te Rosmalen* (CO-329720). Grondmechanica Delft. 1992.

Grondmechanica Delft. (1985). *RW-1/spoortlijn te Henglo. Trekproeven op 1 Vibro- en 1 Ringvibrator-paal* (CO 274810). Delft, The Netherlands.

Grondmechanica Delft. (1987). *Spoorwegtunnel te Rotterdam. Trekproeven.* (81-117H). Delft, The Netherlands.

Gwizdała, K., & Krasiński, A. (2005). Experience gained at the application of Atlas piles in Poland. *Proceedings of the 10th International Conference on Piling and Deep Foundations*, 460–464.

Heins, W. F. (1973). Trekproeven op volgens het vibro-systeem in de grond gevormde palen van geringe lengte te Zeist. *LGM Mededelingen*, *15*(3), 65–102.

Hemel, M.-J. (2023). *Amsterdam quays under pressure: Modelling and testing of historic canal walls* [Doctoral dissertation, Delft University of Technology]. https://repository.tudelft.nl/record/uuid:102edff8-8960-4633-830c-369aef8e279f

Hijma, M. P. (2019). *From river valley to estuary: The early-mid Holocene transgression of the Rhine-Meuse valley, The Netherlands* [Doctoral dissertation, Utrecht University].

Hijma, M. P., Cohen, K. M., Roebroeks, W., Westerhoff, W. E., & Busschers, F. S. (2012). Pleistocene Rhine–Thames landscapes: Geological background for hominin occupation of the southern North Sea region. *Journal of Quaternary Science*, *27*(1), 17–39. https://doi.org/10.1002/jqs.1549

Hocombe, T., Moore, P., te Boekhorst, C., Gittens, R., & den Blanken, S. (2015). Screw grout injection piled foundations for major bridge strengthening in Utrecht. *Proceedings of the XVI European Conference on Soil Mechanics and Geotechnical Engineering, ECSMGE 2015*, 289–294. https://doi.org/10.1680/ecsmge.60678.vol2.022

Hopman, V., & Hölscher, P. (2016). *Opzet testlocatie voor in de grond gevormde palen* (No. 1209345–002). Deltares. Delft, The Netherlands. https://www.cob.nl/wp-content/uploads/2018/01/1209345-002_Testlocatie-in-de-grond-gevormde-palen.pdf

Huybrechts, N. (2001). Test campaign at Sint-Katelijne-Waver and installation techniques of screw piles. *Screw Piles - Installation and Design in Stiff Clay*, 159–212.

Huybrechts, N., De Vos, M., Bottiau, M., & Maertens, L. (2016). Design of piles—Belgian practice. *Proceedings of ISSMGE - ETC 3 International Symposium on Design of Piles in Europe*, 7–44.

Huybrechts, N., & Whenham, V. (2003). Pile testing campaign on the Limelette test site & installation techniques of screw piles. *Proceedings of the Second Symposium on Screw Piles*, 71–130.

IFCO. (2003). *Uitvoering en resultaten statische proefbelasting op een Terr-econ paal aan de Vlasweg te Moerdijk* (R02dm017). Waddinxveen, The Netherlands.

Imbo, R. P. (1984). The Atlas screw pile: An improved foundation technique for the vibration free execution of piles with larger capacity. *Proceedings of the 6th Budapest Conference on Soil Mechanics and Foundation Engineering*, 363–372.

Jardine, R. J. (2020). Geotechnics, energy and climate change: The 56th Rankine Lecture. *Géotechnique*, *70*(1), 3–59. https://doi.org/10.1680/jgeot.18.RL.001

Jardine, R. J., Chow, F., Overy, R., & Standing, J. (2005, January). *ICP design methods for driven piles in sands and clays*. Thomas Telford. https://doi.org/10.1680/idmfdpisac.32729.fm

Jardine, R. J., Zhu, B. T., Foray, P., & Yang, Z. X. (2013). Measurement of stresses around closed-ended displacement piles in sand. *Géotechnique*, *63*(1), 1–17. https://doi.org/10.1680/geot.9.P.137

Jeffrey, J. (2012). *Investigating the performance of continuous helical displacement piles* [Doctoral dissertation, University of Dundee].

JGJ. (2008). *Technical code for building pile foundations*. Ministry of Housing and Urban-Rural Development of the People's Republic of China.

Kania, J., Sorensen, K., & Fellenius, B. H. (2020). Application of distributed fibre optic cables in piles. *Geotechnical Engineering Journal of the SEAGS & AGSSEA*, *51*(3), 1–9.

Kechavarzi, C., Pelecanos, L., de Battista, N., & Soga, K. (2019). Distributed fibre optic sensing for monitoring reinforced concrete piles. *Geotechnical Engineering Journal of the SEAGS & AGSSEA*, *50*(2), 43–51.

Kementzetzidis, E. (2023). *Cyclic behaviour of laterally loaded (mono)piles in sand: With emphasis on pile driving effects* [Doctoral dissertation, Delft University of Technology]. https://doi.org/10.4233/uuid:36b8a133-2a5a-49b3-9701-f75f102bbe3d

Kempfert, H.-G., & Becker, P. (2010). Axial pile resistance of different pile types based on empirical values. *Deep Foundations and Geotechnical In Situ Testing*, 149–154. https://doi.org/10.1061/41106(379)18

Klar, A., Bennett, P. J., Soga, K., Mair, R. J., Tester, P., Fernie, R., St John, H. D., & Torp-Peterson, G. (2006). Distributed strain measurement for pile foundations. *Proceedings of the Institution of Civil Engineers - Geotechnical Engineering*, *159*(3), 135–144. https://doi.org/10.1680/geng.2006.159.3.135

Klein, I. (2011). *Rapport betreffende proefbelasting op Vibro-SD palen van Vroom Funderingstechnieken te Waalwijk* (AA12333-2). Geomet. Alphen aan de Rijn, The Netherlands.

Knappett, J. A., Caucis, K., Brown, M. J., Jeffrey, J. R., & Ball, J. D. (2016). CHD pile performance: Part II – numerical modelling. *Proceedings of the Institution of Civil Engineers - Geotechnical Engineering*, *169*(5), 436–454. https://doi.org/10.1680/jgeen.15.00132

Konstadinou, M., Stathopoulou, E., Luger, D., Elkadi, A. S., & Meijer, G. (2023). Driveability back-analyses of onshore vibratory and vibrojetting installation tests on tubular piles. *Proceedings of the 9th International SUT Offshore Site Investigation and Geotechnics Conference*, 784–791. https://doi.org/10.3723/NSKP9707

Korff, M., Hemel, M.-J., & Peters, D. J. (2022). Collapse of the Grimburgwal, a historic quay in Amsterdam, the Netherlands. *Proceedings of the Institution of Civil Engineers - Forensic Engineering*, 1–10. https://doi.org/10.1680/jfoen.21.00018

Krasiński, A. (2011a). Advanced field investigations of screw piles and columns. *Archives of Civil Engineering*, *2*(1), 45–57. https://doi.org/10.2478/v.10169-011-0005.5

Krasiński, A. (2011b). Badania terenowe przemieszczeniowych pali i kolumn wkręcanych typu SDP i SDC. *Roads and Bridges - Drogi i Mosty*, (1–2), 21–58. Retrieved June 27, 2023, from https : / / mostwiedzy . pl / pl / publication / badania - terenowe - przemieszczeniowych-pali-i-kolumn-wkrecanych-typu-sdp-i-sdc,118128-1

Krasiński, A. (2012). Proposal for calculating the bearing capacity of screw displacement piles in non-cohesive soils based on CPT results. *Studia Geotechnica et Mechanica*, *34*(4), 51–51. https://doi.org/10.5277/sgm041204

Krasiński, A. (2023). Estimation of screw displacement pile-bearing capacity based on drilling resistances. *Studia Geotechnica et Mechanica*, *45*(S1), 1–11. https://doi.org/10.2478/sgem-2023-0014

Krasiński, A., Słabek, A., Więcławski, P., Wiszniewski, M., Kusio, T., & Tisler, W. (2023). Results of the "DPDT-Auger" research project on screw displacement piles. *Architecture, Civil Engineering, Environment*, (3), 89–99. https://doi.org/10.2478/acee-2023-0036

Krasiński, A., & Wiszniewski, M. (2021). Identification of residual force in static load tests on instrumented screw displacement piles. *Studia Geotechnica et Mechanica*, *43*(4), 438–451. https://doi.org/10.2478/sgem-2021-0025

Kulhawy, F. H., & Mayne, P. W. (1990, August 1). *Manual on estimating soil properties for foundation design* (EPRI-EL-6800). Electric Power Research Inst., Palo Alto, CA (USA); Cornell Univ., Ithaca, NY (USA). Geotechnical Engineering Group. Retrieved November 10, 2018, from https://www.osti.gov/biblio/6653074-manual-estimating-soil-properties-foundation-design

Lacasse, S., Nadim, F., Andersen, K. H., Knudsen, S., Eidsvig, U. K., Yetginer, G. L., Guttormsen, T., & Eide, A. (2013). Reliability of API, NGI, ICP and Fugro axial pile capacity calculation methods. *Proceedings of the Offshore Technology Conference*. https://doi.org/10.4043/24063-MS

Lam, C., Jefferis, S. A., Suckling, T. P., & Troughton, V. M. (2015). Effects of polymer and bentonite support fluids on the performance of bored piles. *Soils and Foundations*, *55*(6), 1487–1500. https://doi.org/10.1016/j.sandf.2015.10.013

Larisch, M. (2014). *Behaviour of stiff, fine-grained soil during the installation of screw auger displacement piles* [Doctoral dissertation, The University of Queensland].

Leetsaar, L., & Korkiala Tanttu, L. (2023). Deterministic and probabilistic analyses of the bearing capacity of screw cast in situ displacement piles in silty soils as measured by CPT and SDT. *The Baltic Journal of Road and Bridge Engineering*, *18*(2), 99–127. https://doi.org/10.7250/bjrbe.2023-18.600

Lehane, B. M., Jardine, R. J., Bond, A. J., & Frank, R. (1993). Mechanisms of shaft friction in sand from instrumented pile tests. *Journal of Geotechnical Engineering*, *119*(1), 19–35. https://doi.org/10.1061/(ASCE)0733-9410(1993)119:1(19)

Lehane, B. M., Li, L., & Bittar, E. J. (2020). Cone penetration test-based load-transfer formulations for driven piles in sand. *Géotechnique Letters*, *10*(4), 568–574. https://doi.org/10.1680/jgele.20.00096

Lehane, B. M., Lim, J. K., Carotenuto, P., Nadim, F., Lacasse, S., Jardine, R. J., & van Dijk, B. (2017). Characteristics of unified databases for driven piles. *Offshore Site Investigation Geotechnics 8th International Conference Proceedings*, *1*, 162–194. https://doi.org/10.3723/OSIG17.162

Lehane, B. M., Liu, Z., Bittar, E. J., Nadim, F., Lacasse, S., Jardine, R. J., Carotenuto, P., Rattley, M., Jeanjean, P., Gavin, K. G., Gilbert, R., Bergan-Haavik, J., & Morgan, N. (2020). A new 'unified' CPT-based axial pile capacity design method for driven piles in sand. *Proceedings of the 4th International Symposium on Frontiers in Offshore Geotechnics*, 462–477.

Lehane, B. M., Schneider, J., & Xu, X. (2005). *A review of design methods for offshore driven piles in siliceous sand* (GEO 05358). University of Western Australia. Perth, Australia.

Li, Q., Stuedlein, A. W., & Marinucci, A. (2017). Axial load transfer of drilled shaft foundations with and without steel casing. *DFI Journal - The Journal of the Deep Foundations Institute*, *11*(1), 13–29. https://doi.org/10.1080/19375247.2017.1403074

Ligthart, S., & Timmer, P. (2019). *Proefbelasting Alblasserdam* (No. 23738). Vroom Funderingstechnieken. Oosthuizen, The Netherlands.

Maertens, J., & Huybrechts, N. (2003). Results of the static pile load tests at the Limelette test site. *Proceedings of the 2nd Symposium on Screw Piles*, 167–214.

Meyerhof, G. G. (1959). Compaction of sands and bearing capacity of piles. *Journal of the Soil Mechanics and Foundations Division*, *85*(6), 1–29. https://doi.org/10.1061/JSFEAQ.0000231

Moshfeghi, S., & Eslami, A. (2019). Reliability-based assessment of drilled displacement piles bearing capacity using CPT records. *Marine Georesources & Geotechnology*, *37*(1), 67–80. https://doi.org/10.1080/1064119X.2018.1448493

Mullins, G. (2010). Thermal integrity profiling of drilled shafts. *DFI Journal - The Journal of the Deep Foundations Institute*, *4*(2), 54–64.

NBN. (2022). *Norm NBN EN 1997-1 ANB:2022*. Bureau voor Normalisatie.

NEN. (2017a, November 1). *NCS 7201: Zelfverklaring 'Proefbelasting van funderingspalen' behorend bij NPR 7201*.

NEN. (2017b, November 1). *NEN 9997-1+C2:2017*. Nederlands Normalisatie-Instituut.

NeSmith, W. M. (2002). Design and installation of pressure-grouted, drilled displacement piles. *Proceedings of the Ninth International Conference on Piling and Deep Foundations*.

NeSmith, W. M., & NeSmith, W. M. (2006). Application of data acquired during drilled displacement pile installation. *GeoCongress 2006: Geotechnical Engineering in the Information Technology Age*, 1–6. https://doi.org/10.1061/40803(187)177

Niazi, F. S., & Mayne, P. W. (2016). CPTu-based enhanced UniCone method for pile capacity. *Engineering Geology*, *212*, 21–34. https://doi.org/10.1016/j.enggeo.2016.07.010

NPR 7201. (2017). *NPR 7201:2017 - Geotechniek - Bepaling van het axiaal draagvermogen van funderingspalen door middel van proefbelastingen*.

O'Neill, M. W. (1991). Construction practices and defects in drilled shafts. *Transportation Research Record*, *1331*, 6–14. https://onlinepubs.trb.org/Onlinepubs/trr/1991/1331/1331-002.pdf

Pagella, G., Mirra, M., Ravenshorst, G., Gard, W., & van de Kuilen, J.-W. (2024). Characterization of the remaining material and mechanical properties of historic wooden foundation piles in Amsterdam. *Construction and Building Materials*, *450*, 138616. https://doi.org/10.1016/j.conbuildmat.2024.138616

Paik, K., Salgado, R., Lee, J., & Kim, B. (2003). Behavior of open- and closed-ended piles driven Into sands. *Journal of Geotechnical and Geoenvironmental Engineering*, *129*(4), 296–306. https://doi.org/10.1061/(ASCE)1090-0241(2003)129:4(296)

Park, S., Roberts, L. A., & Misra, A. (2012). Design Methodology for Axially Loaded Auger Cast-in-Place and Drilled Displacement Piles. *Journal of Geotechnical and Geoen-*

vironmental Engineering, *138*(12), 1431–1441. https://doi.org/10.1061/(ASCE)GT.1943-5606.0000727

Poulos, H. G., Carter, J. P., & Small, J. C. (2001). Foundations and retaining structures - Research and practice. *Proceedings of the 15th International Conference on Soil Mechanics and Geotechnical Engineering (ICSMGE)*, 2527–2606.

Prendergast, L. J., Gandina, P., & Gavin, K. G. (2020). Factors influencing the prediction of pile driveability using CPT-based approaches. *Energies*, *13*(12), 3128–3147. https://doi.org/10.3390/en13123128

Pucker, T., & Grabe, J. (2012). Numerical simulation of the installation process of full displacement piles. *Computers and Geotechnics*, *45*, 93–106. https://doi.org/10.1016/j.compgeo.2012.05.006

Pujadas-Gispert, E., Sanjuan-Delmás, D., de la Fuente, A., Moonen, S. P. G., & Josa, A. (2020). Environmental analysis of concrete deep foundations: Influence of prefabrication, concrete strength, and design codes. *Journal of Cleaner Production*, *244*, 118751. https://doi.org/10.1016/j.jclepro.2019.118751

Quinten, T., Ioannou, C., Askarinejad, A., Cabrera, M., & Gavin, K. G. (2023). A centrifuge study into the installation response of steel, open-ended, tubular piles, dynamically driven using prolonged impulses. *Symposium on Energy Geotechnics 2023*, 1–2. https://doi.org/10.59490/seg.2023.618

Randolph, M. F. (2003). Science and empiricism in pile foundation design. *Géotechnique*, *53*(10), 847–875. https://doi.org/10.1680/geot.2003.53.10.847

Reader, M. D., & Armstrong, T. W. (2005). Extensive pile testing of auger pressure grouted displacement (APGD) piles. *Proceedings of the 30th DFI Annual Conference on Deep Foundations*, 15.

Reinders, K., van Seters, A., & Korff, M. (2016). Design of piles according to Eurocode 7 – Dutch practice. *Proceedings of the ISSMGE - ETC 3 International Symposium on Design of Piles in Europe*.

Rijsdijk, K. F., Passchier, S., Weerts, H. J. T., Laban, C., Leeuwen, R. J. W. van, & Ebbing, J. H. J. (2005). Revised Upper Cenozoic stratigraphy of the Dutch sector of the North Sea Basin: Towards an integrated lithostratigraphic, seismostratigraphic and allostratigraphic approach. *Netherlands Journal of Geosciences*, *84*(2), 129–146. https://doi.org/10.1017/S0016774600023015

Roubos, A. A., de Lange, D. A., Duffy, K. J., van der Wal, E., & Gavin, K. G. (2024). Towards sustainable port infrastructure by performing full-scale pile load tests. *Proceedings of the 35th PIANC World Congress*.

Roubos, A. A. (2019). *Enhancing reliability-based assessments of quay walls* [Doctoral dissertation, Delft University of Technology]. https://doi.org/10.4233/uuid:40632b7a-970e-433d-9b4e-ff2d2249b156

Rui, Y., Kechavarzi, C., O'Leary, F., Barker, C., Nicholson, D., & Soga, K. (2017). Integrity testing of pile cover using distributed fibre optic sensing. *Sensors*, *17*(12), 2949. https://doi.org/10.3390/s17122949

Sandanayake, M., Zhang, G., & Setunge, S. (2016). Environmental emissions at foundation construction stage of buildings – Two case studies. *Building and Environment*, *95*, 189–198. https://doi.org/10.1016/j.buildenv.2015.09.002

SBR. (2010). *Handboek Funderingen - Deel B* (CRW NF 575.10).

Schokker, J., Bakker, M. A. J., Dubelaar, C. W., Dambrink, R. M., & Harting, R. (2015). 3D subsurface modelling reveals the shallow geology of Amsterdam. *Netherlands Journal of Geosciences*, *94*(4), 399–417. https://doi.org/10.1017/njg.2015.22

Schokking, F., & IJnsen, P. (2014). Onderzoek installatie en belasting van grondverdringende schroefpalen, Almere-Poort [magazine]. *Geotechniek*, 10–17.

Sharif, Y. U. (2024). *The Effects of Rotary Installation on the Axial Capacity of Displacement Piles in Sand* [Doctoral dissertation, University of Dundee]. Retrieved February 24, 2025, from https://discovery.dundee.ac.uk/en/studentTheses/the-effects-of-rotary-installation-on-the-axial-capacity-of-displ

Sharif, Y. U., Brown, M. J., Cerfontaine, B., Davidson, C., Ciantia, M. O., Knappett, J. A., Ball, J. D., Brennan, A., Augarde, C., Coombs, W., Blake, A., Richards, D., White, D., Huisman, M., & Ottolini, M. (2021). Effects of screw pile installation on installation requirements and in-service performance using the discrete element method. *Canadian Geotechnical Journal*, *58*(9), 1334–1350. https://doi.org/10.1139/cgj-2020-0241

Shi, D., Yang, Y., Deng, Y., & Xue, J. (2019). DEM modelling of screw pile penetration in loose granular assemblies considering the effect of drilling velocity ratio. *Granular Matter*, *21*(3), 74. https://doi.org/10.1007/s10035-019-0933-3

Siegel, T. C., & McGillivray, A. (2009). Interpreted residual load in an augered cast-in-place pile. *Proceedings of the 34th Annual Conference on Deep Foundations*, 173–182.

Siegel, T., Day, T., Turner, B., & Faust, P. (2019). Measured end resistance of CFA and drilled displacement piles in San Francisco Area alluvial clay. *Journal of the Deep Foundations Institute*, *12*(3), 186–189.

Slatter, J. (2000). *The Fundamental Behaviour of Displacement Screw Piling Augers* [Doctoral dissertation, Monash University].

Spruit, R., Hannink, G., & van Zanten, D. (2012). Tubex-groutinjectiepalen proefbelast voor Metrostation CS in Rotterdam. *Geotechniek*, 28–32.

Spruit, R., van Tol, F., Broere, W., Doornenbal, P., & Hopman, V. (2017). Distributed temperature sensing applied during diaphragm wall construction. *Canadian Geotechnical Journal*, *54*(2), 219–233. https://doi.org/10.1139/cgj-2014-0522

Stacho, J. (2018). The design of drilled displacement system piles using the cavity expansion theory. *Acta Geotechnica Slovenica*, *15*(2), 81–91. https://doi.org/10.18690/actageotechslov.15.2.81-91.2018

Stoevelaar, R., van Lottum, H., & Rietdijk, J. (2014). *Axiaal draagvermogen van palen* (Rapport 229). CUR. Gouda, The Netherlands.

Stuedlein, A. W., Reddy, S. C., & Evans, T. M. (2014). Interpretation of augered cast in place pile capacity using static loading tests. *DFI Journal - The Journal of the Deep Foundations Institute*, *8*(1), 39–47. https://doi.org/10.1179/1937525514Y.0000000003

Suckling, T. P. (2003). Driven cast insitu piles, the CPT and SPT—two case studies [magazine]. *Ground Engineering*, 28–32.

Suleiman, M. T., Ni, L., Davis, C., Lin, H., & Xiao, S. (2016). Installation effects of controlled modulus column ground improvement piles on surrounding soil. *Journal of Geotechnical and Geoenvironmental Engineering*, *142*(1), 04015059. https://doi.org/10.1061/(ASCE)GT.1943-5606.0001384

Sun, Q., Elshafie, M., Barker, C., Fisher, A., Schooling, J., & Rui, Y. (2021). Thermal integrity testing of cast in situ piles: An alternative interpretation approach. *Structural Health Monitoring*, *20*(5), 2493–2512. https://doi.org/10.1177/1475921720960042

te Kamp, W. (1977). Sonderen en funderingen op palen in zand. *Sondeer Symposium 1977*, 119–133.

Tehrani, F. S., Arshad, M. I., Prezzi, M., & Salgado, R. (2018). Physical modeling of cone penetration in layered sand. *Journal of Geotechnical and Geoenvironmental Engineering*, *144*(1), 04017101. https://doi.org/10.1061/(ASCE)GT.1943-5606.0001809

Teixeira, A., Noordam, A., & de Lange, D. A. (2019). Towards a pile quality prediction for screw displacement piles using Bayesian networks. In A. G. Correia, J. Tinoco, P. Cortez, & L. Lamas (Eds.), *Information Technology in Geo-Engineering* (pp. 540–550). Springer International Publishing. https://doi.org/10.1007/978-3-030-32029-4_47

ter Steege, F. (2022). *Screw and screw-injection piles: Classification of the load-settlement response and improving the design process* [MSc Thesis]. TU Delft. https://repository.tudelft.nl/record/uuid:ad6d726e-c5f5-41b2-a295-576b350b8e6e

Theys, F., Maertens, J., & Maekelberg, W. (2003). Practical experience with screw piles used for the high-speed railway in Belgium. *Proceedings of the Second Symposium on Screw Piles*, 235–271.

Tovar-Valencia, R. D., Galvis-Castro, A., Salgado, R., & Prezzi, M. (2021). Effect of base geometry on the resistance of model piles in sand. *Journal of Geotechnical and Geoenvironmental Engineering*, *147*(3), 04020180. https://doi.org/10.1061/(ASCE)GT.1943-5606.0002472

United Nations Environment Programme. (2024). *Global status report for buildings and construction*. United Nations Environment Programme (UNEP) and Global Alliance for Buildings and Construction (GlobalABC). Nairobi, Kenya. https://doi.org/10.59117/20.500.11822/45095.

van Baars, S., Rica, S., de Nijs, G. A., de Nijs, G. J. J., & Riemens, H. J. (2018). Dutch field tests validating the bearing capacity of Fundex piles. *Proceedings of the 4th International Symposium on Cone Penetration Testing (CPT'18)*, 101–107.

van Delft, M. C. H., & van Dorp, R. F. (2010). *Proefbelasting VSD-palen te Zuid-Oost Beemster*. IFCO. Waddinxveen, The Netherlands.

van Impe, P. O., van Impe, W. F., & Seminck, L. (2013). Discussion of an instrumented screw pile load test and connected pile group load settlement behavior. *Journal of Geo-Engineering Sciences*, *1*(1), 13–36. https://doi.org/10.3233/JGS-130011

van Impe, W. F. (1988). Considerations on auger pile design. *Proc. 1st International Seminar on Deep Foundations on Bored and Auger Piles (BAP I)*, 193–218.

van Impe, W. F. (1996). Experiences with a new type of displacement screw pile. *Proceedings of the Sixth International Conference and Exhibition on Piling and Deep Foundations*, 1.1.1–1.1.9.

van Impe, W. F. (2001). Considerations on the influence of screw pile installation parameters on the overall pile behaviour. *Proceedings of the Symposium on Screw Piles*, 127–149.

van Mierlo, W., & Koppejan, A. (1952). Lengte en draagvermogen van heipalen [magazine]. *Bouw*, *3*.

van Noortwijk, D., Everts, H. J., & Janse, E. (1994). *Onderzoek trekpalen tweede Beneluxtunnel* (CO-350830/8). Grondmechanica Delft. Delft, The Netherlands.

van Seters, A. (2016). General Report – Calculation methods based on direct derivation from in situ tests. *ISSMGE - ETC 3 International Symposium on Design of Piles in Europe*, 31–45.

van Tol, A. F., Stoevelaar, R., Bezuijen, A., Jansen, H. L., & Hannink, G. (2013). Compressive resistance of piles, an update. *Proc. 18th International Conference on Soil Mechanics and Geotechnical Engineering (ICMSGE)*, *3*, 2885–2888.

van Weele, A., & Lencioni, B. (1999). Het mislukken van een paalfundering is duur, maar leerzaam [magazine]. *Geotechniek*, *1*.

van der Geest, A. J., Admiraal, B. J., & IJnsen, P. (2020). Schaalproeven op draagvermogen grondverdringende (schroef)palen [magazine]. *Geotechniek*, 7–16.

van der Linden, T. I., de Lange, D. A., & Korff, M. (2018). Cone penetration testing in thinly inter-layered soils. *Proceedings of the Institution of Civil Engineers - Geotechnical Engineering*, *171*(3), 215–231. https://doi.org/10.1680/jgeen.17.00061

Varaskin, S., Hamidi, B., Huybrechts, N., & Denies, N. (2016). Ground improvement vs pile foundations. *ISSMGE - ETC3 International Symposium on Design of Piles in Europe*.

Verheyde, F. A., & Baguelin, F. (2019). Pile design using CPT results: The LPC method. *13th Australia New Zealand Conference on Geomechanics*, 421–426.

Verstraelen, J., Maekelberg, W., & Medaets, M. (2016). Recent experiences with static pile load testing on real job sites. *ISSMGE - ETC 3 International Symposium on Design of Piles in Europe*, 63–85.

Verstraeten, A. J., Doornbos, S., & Dupont, E. (1988). Tubex-grout-injected piles for the Parenco paper mill in Renkum. *Proc. 1st International Seminar on Deep Foundations on Bored and Auger Piles (BAP I)*, 377–384.

Vesic, A. S. (1965). Ultimate loads and settlements of deep foundations in sand. *Proceedings of the Symposium on Bearing Capacity and Settlement of Foundations*, 53–68.

Vos, P. C., Bunnik, F. P. M., Cohen, K. M., & Cremer, H. (2015). A staged geogenetic approach to underwater archaeological prospection in the Port of Rotterdam (Yangtzehaven, Maasvlakte, The Netherlands): A geological and palaeoenvironmental case study for local mapping of Mesolithic lowland landscapes. *Quaternary International*, *367*, 4–31. https://doi.org/10.1016/j.quaint.2014.11.056

White, D. J., & Bolton, M. D. (2005). Comparing CPT and pile base resistance in sand. *Proceedings of the Institution of Civil Engineers - Geotechnical Engineering*, *158*(1), 3–14. https://doi.org/10.1680/geng.2005.158.1.3

White, D. J., & Lehane, B. M. (2004). Friction fatigue on displacement piles in sand. *Géotechnique*, *54*(10), 645–658. https://doi.org/10.1680/geot.2004.54.10.645

Woldringh, R. F. (1987). *Mettingen verricht aan de Fluidatiepalen volgens het systeem van Parera Huizen van Bewaring te Haarlem*. Toegepast Onderzoek Waterstaat.

WTCB. (2020). *Richtlijnen voor de toepassing van de Eurocode 7 in België volgens de NBN EN 1997-1 ANB* (Rapport nr. 20). WTCB. Brussels, Belgium.

Xu, X., & Lehane, B. M. (2008). Pile and penetrometer end bearing resistance in two-layered soil profiles. *Géotechnique*, *58*(3), 187–197. https://doi.org/10.1680/geot.2008.58.3.187

Xu, X., Schneider, J. A., & Lehane, B. M. (2008). Cone penetration test (CPT) methods for end-bearing assessment of open- and closed-ended driven piles in siliceous sand. *Canadian Geotechnical Journal*, *45*(8), 1130–1141. https://doi.org/10.1139/T08-035

Yost, K. M., Yerro, A., Green, R. A., Martin, E., & Cooper, J. (2022). MPM modeling of cone penetrometer testing for multiple thin-layer effects in complex soil stratigraphy. *Journal of Geotechnical and Geoenvironmental Engineering*, *148*(2), 04021189. https://doi.org/10.1061/(ASCE)GT.1943-5606.0002730

Nomenclature

Acronyms

AR	Advancement ratio
AFNOR	*Association Française de Normalisation* (French Standardisation Association)
API	American Petroleum Institute
BOFDA	Brillouin Optical Frequency Domain Analysis
CFA	Continuous flight auger
CMC	Controlled Modulus Column
COV	Coefficient of variation
DCIS	Driven cast-in-situ (also known as *vibro* piles)
DFOS	Distributed fibre optic sensing
DP	Driven precast
DPDT	Displacement Pile Drilling Tool
FBG	Fibre Bragg Gratings
FDP	Full displacement pile
FHWA	Federal Highway Administration
GU	Ground Unit
InPAD	Investigation of the Axial Capacity of Piles in Sand
ISO	International Organisation for Standardisation
LCPC	Laboratoire Central des Ponts et Chaussées
NBN	*Bureau voor Normalisatie/Bureau de Normalisation* (Belgian Standards Body)
NEN	*Nederlands Normalisatie Instituut* (Dutch Institute for Standardisation)
NVAF	*Nederlandse Vereniging Aannemers Funderingswerken* (Dutch Association for Foundation Contractors)
SDC	Soil Displacing Column

SDP	Soil Displacing Pile
SI	Screw injection
SLS	Serviceability Limit State
TKI	*Het Topconsortium voor Kennis en Innovatie* (Top Consortia for Knowledge and Innovation)
ULS	Ultimate Limit State

Greek symbols

α_p	Pile class factor for determining the pile base resistance
α_s	Pile class factor for determining the pile shaft resistance
σ'_{v0}	In-situ vertical effective stress
ε	Strain

Latin symbols

Δz_h	Vertical pile displacement for one full pile rotation
A_{base}	Cross-sectional area at the pile base
D	Outermost diameter of the pile
d	Diameter of the removable casing
D_{eq}	Pile equivalent diameter
D_{meas}	Measured diameter of an extracted pile
f_s	CPT friction sleeve resistance
h	Distance from the pile base
L	Pile length
L_p	Pile penetration into load-bearing sand layer.
p_a	Atmospheric pressure
p_h	Helical pitch
Q_0	Load applied on top of the pile
q_b	Pile base resistance
q_c	CPT cone tip resistance

q_s Pile shaft resistance

$Q_{0,0.1D}$ Load on the pile head at a pile base displacement of 10 % of the pile diameter D

$Q_{0,1inch}$ Load on the pile head at a pile head displacement of 1 inch

$Q_{0,max}$ Maximum load applied on the pile head

$q_{b,0.1D}$ Pile base resistance at a base displacement of $0.1D$

$q_{b,lim}$ Limiting base resistance

$q_{c,4D/8D}$ $q_{c,avg}$ determined using the Dutch 4D/8D method

$q_{c,avg}$ Weighted average of cone resistances for predicting the pile base capacity

$q_{c,filter}$ $q_{c,avg}$ determined using the adapted filter method

$q_{c,LCPC}$ $q_{c,avg}$ determined using the LCPC ±1.5D method

$q_{c,tip}$ CPT cone resistance at the pile tip

Q_{meas} Measured load on the pile head at failure

Q_{pred} Predicted load on the pile head at failure

$Q_{pulldown}$ Pulldown force

$q_{s,avg}$ Average shaft resistance across a soil layer

$q_{s,lim}$ Limiting shaft resistance

s_0 Displacement of pile head

s_b Displacement of the pile base

T Temperature

u_2 CPT porewater pressure

w_s Correction factor in the FHWA design method for the pile shaft resistance, depending on soil gradation and angularity

w_t Correction factor in the FHWA design method for the pile base resistance, depending on soil gradation and angularity

Curriculum Vitæ

Kevin Duffy

15-06-1995 Born in Drogheda, Ireland.

Education

2019–2025 Ph.D. Candidate in Geotechnical Engineering,
Department of Civil Engineering & Geosciences,
Delft University of Technology
Thesis: Axial capacity of piles in sand: a field investigation using distributed fibre optic sensing
Promotor: Prof. dr. K.G. Gavin
Copromotor: Dr. ir. M. Korff

2017–2019 MSc in Civil, Structural & Environmental Engineering
University College Dublin, Ireland

2013–2017 BSc in Civil, Structural & Environmental Engineering
University College Dublin, Ireland

2007–2013 St Mary's Diocesan School, Drogheda, Ireland

Professional Experience

2021–current Geotechnical Engineer
InGEO Consulting, Delft, The Netherlands

2018–2018 Geotechnical Engineer
Fugro, The Hague, The Netherlands

2017–2017 Trainee Engineer
Per Aarsleff A/S, Aarhus, Denmark

Awards

2022	Best Paper Competition for Young Professionals *11th International Conference on Stress Wave Theory and Design and Testing Methods for Deep Foundations*
2022	Nominee Elmo DiBiagio Young Engineers Award *11th International Symposium on Field Monitoring in Geomechanics*
2020	Irish Young Geotechnical Engineer Award
2019	Roughan O'Donovan Award for Best Masters Thesis

List of Publications

Journal Papers

1. **Duffy, K.J.**, Gavin K.G., Korff, M., de Lange, D.A., Roubos, A.A. (2024). Influence of installation method on the axial capacity of piles in very dense sand. *Journal of Geotechnical and Geoenvironmental Engineering*, 150(6), 04024043.

2. **Duffy, K.J.**, Gavin K.G., Korff, M., de Lange, D.A. (2024) Base resistance of screw displacement piles in sand. *Journal of Geotechnical and Geoenvironmental Engineering*, 150(8), 04024070.

3. Chai, F., Xue, J., Liu, B., **Duffy, K.J.**, (2025) Assessing direct CPT-based methods for predicting pile base resistance using coupled DEM-FDM simulations. *Computers and Geotechnics*, 183, 107230.

4. **Duffy, K.J.**, Gavin K.G. (2025) CPT-based prediction of screw displacement pile capacity in granular soils. *Proceedings of the Institution of Civil Engineers - Geotechnical Engineering*. (under review).

5. Lai F., **Duffy, K.J.**, Gavin, K.G., Lu, D., Roubos, A.A. (2025) Integration of field monitoring and numerical modelling to evaluate the construction performance of deep-sea quay walls. *Journal of Geotechnical and Geoenvironmental Engineering*. (under review).

Conference Papers

1. Chai, F., Xue, J., **Duffy, K.J.** (2024). Database analysis of averaging methods for driven pile base resistance prediction. In *Proceedings of the 3rd International Conference on Press-in Engineering 2024*. Singapore.

2. **Duffy, K.J.** (2024). Improving axial pile design through full-scale field testing and fibre optic sensing. In *Proceedings of the 28th European Young Geotechnical Engineers Conference (EYGEC)*. Demir Kapija, North Macedonia.

3. **Duffy, K.J.**, Gavin, K.G, Lai, F. (2024). Maximising a foundation's lifetime through monitoring: a case study from the port of Rotterdam. In *Proceedings of Foundation Reuse Conference*. Amsterdam, The Netherlands.

4. Roubos, A.A., de Lange, D.A., **Duffy, K.J.**, van der Wal, E., Gavin, K.G. (2024). Towards sustainable port infrastructure by performing full-scale pile load tests. In *Proceedings of 35th PIANC World Congress*. Cape Town, South Africa.

5. **Duffy, K.J.**, Gavin K.G., Korff, M., de Lange, D.A., (2023). Application of axial load tests in the Netherlands to offshore pile design. In *Proceedings of 9th International Offshore Site Investigation and Geotechnics Conference (OSIG)*. London, United Kingdom.

6. Chai, F., Xue, J., Fang-Bao, T., **Duffy, K.J.**, Gavin K.G. (2023). Influence of a thin weak layer on closed-ended pile behavior in sand. In *Proceedings of the 8th International Symposium on Geotechnical Safety and Risk (ISGSR)*. Newcastle, Australia.

7. **Duffy, K.J.**, Gavin K.G., Korff, M., de Lange, D.A., (2022). Residual stress measurement of driven precast piles using distributed fibre optic sensors. In *Proceedings from the 11th International Conference on Stress Wave Theory and Design and Testing Methods for Deep Foundations (SW22).* Rotterdam, The Netherlands.
8. **Duffy, K.J.**, Gavin K.G., Askarinejad, A., Korff, M., de Lange, D.A., Roubos, A.A. (2022). Field testing of axially loaded piles in dense sand. In *Proceedings of the 20th International Conference on Soil Mechanics and Geotechnical Engineering.* Sydney, Australia.
9. de Lange, D.A., **Duffy, K.J.**, Chai, F., Gavin K.G., (2021). Towards a new pile design code. In *Proceedings of Geotechniekdag 2021.* Amersfoort, the Netherlands.

Magazine Articles

1. Roubos, A.A., de Lange, D.A., **Duffy, K.J.**, Jaspers Focks, D.-J., Gavin, K.G. (2025). Towards sustainable port infrastructure by performing full-scale pile load tests. *Geotechniek Special Edition on Foundation Decarbonization and Reuse.*
2. **Duffy, K.J.**, de Lange, D.A., Gavin, K.G. (2025). The InPAD project: an investigation into the axial capacity of piles in sand. *Geotechniek*, 29(1).


TUDelft